WALK-AWAY AUTOMATION OF IN-VITRO PATCH-CLAMP ELECTROPHYSIOLOGY

A Dissertation
Presented to
The Academic Faculty

by

Ilya Kolb

In Partial Fulfillment
of the Requirements for the Degree
Doctor of Philosophy in Biomedical Engineering

Georgia Institute of Technology
Emory University
December 2017

WALK-AWAY AUTOMATION OF IN-VITRO PATCH-CLAMP ELECTROPHYSIOLOGY

Approved by:

Dr. Craig Forest, Advisor
George W. Woodruff School of Mechanical Engineering
Georgia Institute of Technology

Dr. Andrew Jenkins
Department of Pharmacology
Emory University School of Medicine

Dr. Christopher J. Rozell
School of Electrical and Computer Engineering
Georgia Institute of Technology

Dr. Tim Jarsky
Allen Institute for Brain Science

Dr. Annabelle Singer
Wallace H. Coulter Department of Biomedical Engineering
Georgia Institute of Technology

Date Approved: October 4, 2017

ACKNOWLEDGEMENTS

A side effect of spending the better part of each day studying the brain is that eventually, unavoidably, you turn the microscope on your own mind and begin examining it. What I am seeing now is how difficult it is for this particular mind to summarize the entire Ph.D. and draw conclusions. It has been a long journey throughout which I have experienced disappointment and jubilation, failure and success, hopelessness and inspiration. Nevertheless, regret was never on the spectrum of emotions I felt during this experience, and I finish my Ph.D. training with more enthusiasm, energy, and motivation than when I started it. This project would never see the light of day without the amazing people with whom I have had the pleasure of working and who have contributed greatly to this endeavor. I would like to acknowledge them here.

I first want to thank Dr. Craig Forest, an outstanding advisor and mentor. In the Precision Biosystems Laboratory, Craig has diligently crafted a unique environment of excellence, mutual support, integrity, and friendship. In his mentorship, Craig is fair, logical, and always open to hearing a student's point of view. I have learned a tremendous amount from him. His support and advice were critical to my success.

I would like to thank my committee members who devoted their time and mental energy to ensure that this project succeeds. Dr. Annabelle Singer, Dr. Andrew Jenkins, Dr. Tim Jarsky, and Dr. Chris Rozell have not only steered the scientific direction of this project but have all served as mentors and role models.

The wonderful members of the group that is the Precision Biosystems Laboratory (fastest lab at Georgia Tech!) deserve more gratitude than I can express. Lab members Dr. Suhasa Kodandaramaiah, Dr. Melissa Li, Dr. Chris Phaneuf, Dr. Caitlin Austin, and Dr. Greg Holst were instrumental in helping me in the beginning stages of my research. Current lab members Bo Yang, Tim Lee, Scott Thourson, Corey Landry, Colby Lewallen and Mighten Yip have helped me with advice as well as experimental assistance. Special thanks go to William Stoy, co-worker and true friend, with whom I've shared too many adventures and fond memories to enumerate.

I would like to thank the undergraduate students in the lab who entrusted me to guide them into the perilous world of research and who have greatly contributed to this work: Leonard Tsai, Erin Rousseau, Dhara Patel, Amanda Felouzis, Michael Wang, Laura Heller, and Sofia Switzer.

I have been lucky enough to collaborate with some of the best neuroscientists and neuroengineers in the world: Dr. Hongkui Zeng, Dr. Christof Koch, Dr. Steve Traynelis, Dr. Adam Shai, Dr. Ed Boyden, Dr. Reid Harrison, Dr. Alex Chubykin, Dr. Marlene Cohen and Dr. Douglas Ruff. I am honored to call them colleagues. In addition, Olivia Moody, Dr. Jing Zhang, and John Lee have provided their expertise and assistance in several critical parts of this work.

I would like to acknowledge my funding sources from the National Institute of Health, particularly the Computational Neuroscience Training Grant as well as the Allen Institute for Brain Science.

The support of my close friends has been invaluable: Sitara Sankar, Peter Borden, Dwight Chambers, Kyle Blum, Alex Ortiz, and others have made the Ph.D. experience one that I will always remember fondly.

Finally, I would like to thank my parents, Ivan and Natalia, and my grandparents, Ella, Eduard, Gallina, and Arkadiy. They always believed in me and whether they know it or not, taught me to believe in myself. This work would be impossible without their love and support.

TABLE OF CONTENTS

LIST OF TABLES

LIST OF FIGURES

cell, dissociated cells are pulled to a planar surface with many (tens to hundreds of) micro-apertures in individual wells, allowing the simultaneous high-throughput patch-clamp recordings.

LIST OF SYMBOLS AND ABBREVIATIONS

DIC	Differential Interference Contrast
aCSF	Artificial Cerebro-Spinal Fluid
DAQ	Data Acquistion System
IG	Image-Guided
HEK293	Human Embryonic Kidney cells
GABA	Gamma-Aminobutyric acid
$GABA_AR$	Gamma-Aminobutyric acid Receptor Type A
R_{GS}	Gigaseal resistance
T_{GS}	Time to form gigaseal
R_a	Access resistance
SEM	Scanning Electron Microscope
ESI-MS	Electrospray Ionization Mass Spectroscopy
PBS	Phosphate Buffered Saline
LAS	Linear Alkylbenzene Sulfonate
EC_{50}	Half-maximal effective concentration
GUI	Graphical User Interface
VI	Visual area I
OR	Odds ratio
CI	Confidence Interval

SUMMARY

The complexity of the brain makes it a difficult target for systematized study. This is evidenced by the fact that to date, no unified taxonomy of cell type or connectivity pattern has emerged in the field of neuroscience. The ability to perform a complete census of cell types and connections in the brain would be a major step towards understanding the brain and treating its disorders.

A gold-standard technique for performing neuronal classification is patch-clamp recording, which allows single-cell profiling of neuronal morphology, electrical activity, genetic expression, and connectivity patterns; however the technique is highly manual and laborious, making it unsuitable for large-scale studies that would be needed for neuronal classification efforts. A system that performs multiple recordings independently of human intervention, in a "walk-away" automated fashion, would be transformative. This work presents three techniques that enable full automation of the patch-clamp recording process. The first technique is the integration of pipette pressure control with trajectory planning which allows for reliable targeting of cells in brain slices. The second technique is automated pipette cleaning, which circumvents the need for a trained user to swap out pipettes between each patch-clamp trial. The third technique is machine vision which replaces a human operator in the final, most delicate aspects of patch-clamp recording. These techniques were combined to create a robotic system, called the "patcherBot", enabling automated patch-clamp recording of 10 cells consecutively with no human intervention.

The patcherBot was deployed to perform image-guided patch-clamp recording in adherent cells and neurons in brain slices. With one pipette, the system exhibits ~45 minutes of unattended operation, approximately an order of magnitude longer than previous automation efforts. The whole-cell success rate in both preparations was comparable to that of trained human operators (58 to 77%). The patcherBot was also modified to control two patch-clamp pipettes, which approximately doubled the throughput and enabled the study of inter-neuronal connections. Since unlike a human operator, the algorithm can control multiple pipettes simultaneously, adding more pipettes to the system could enable the patcherBot to surpass even the most skilled human operators and increase throughput. This system could thus serve as a tool for large-scale data collection for neuronal classification studies.

CHAPTER 1. INTRODUCTION

1.1 Motivation

A comprehensive understanding of brain function is one of the greatest scientific goals of modern times. The reasons for our interest in understanding the brain range from purely pragmatic to highly philosophical. On the pragmatic side, a mechanistic understanding of neurological dysfunction could greatly inform medical treatments of brain disorders. While neuroscientists are making inroads into understanding mechanisms of diseases such as Alzheimer's and Parkinson's (Gradinaru et al., 2009; Grady et al., 2003; Greicius et al., 2004; McIntyre and Hahn, 2010), an understanding of other neuropathologies such as schizophrenia, post-traumatic stress disorder, and major depressive disorder remain elusive. This is because psychiatric disorders likely involve nuanced, de-localized, circuit-level perturbations in brain connectivity and function (Etkin et al., 2009; Shin et al., 2006), making them difficult to study (see (Deisseroth, 2012; Sohal, 2012) for a review).

Another pragmatic benefit of understanding the brain is the ability to ultimately recreate portions of its complex structure *in silico*. Human brains currently vastly outperform computational algorithms in various tasks, such as speech recognition, vision processing, and conceptual grouping. For example, even young children can pick out the two related words in the set of words {"rain", "music", "umbrella", "book"}, yet for a computer algorithm, this task would be challenging. The words "rain" and "umbrella" share no neither a prefix nor root word, and sound nothing alike; and yet our brains effortlessly pick

them out based on their semantic relationship. Can computers be programmed to emulate human brains? Ideas for "brain-inspired" computational algorithms have their roots in the 1940s but have only found practical application in the 1980s when pioneers like JJ Hopfield demonstrated that simple artificial neural networks can be used to perform a variety of classification tasks (Hopfield, 1982). Recently, the advent of deep learning and availability of rich, annotated training datasets for neural networks has spurred a revolution in the field. Artificial neural networks are now a staple in e-commerce, handwriting recognition, image processing, self-driving cars, and other commercial avenues (LeCun et al., 2015). Conceptually simple 1- to 8-layer neural networks, containing from 512 to 1024 artificial neurons already exhibit remarkable speech recognition capability (Mohamed et al., 2012). Yet that still pales in comparison to the human cortex that has over 20 billion neurons, wired together with an immensely complex architecture. Utilizing connectivity motifs from real brains to inform the design of artificial neural networks could open the door to even more sophisticated, low-power, generalized artificial intelligence systems.

The last broad motivation to study the brain is less pragmatic but not less important than the previous examples: namely, the brain in some ways represents a "final frontier" of all biological sciences. That is, a comprehensive understanding of consciousness provides the ultimate insight into what it means to be human. Formidable efforts have gone into forming coherent and useful definitions of consciousness (Crick and Koch, 1990; Tononi, 2004); however, few would argue that more scientific discoveries are needed to define and grapple with the problem.

Phrases such as "understanding the brain" tend to serve as a call to action, an important impetus for scientific and technological progress in neuroscience. However a question that

is not often addressed is: what does an understanding of the brain look like? And how do we know when we get there? One way to answer these questions is to consider what an understanding of other biological systems "looks like" and extrapolate to the brain. As an example, we can take the biologically vital, yet, on first approximation, simple, cardiovascular system. Decades of research have led to a comprehensive equation-based understanding of many cardiovascular concepts. For instance, the cardiac output (in L/min) of the heart is defined as:

$$CO = SV * HR$$

where SV is stroke volume (volume of blood ejected from the heart per heartbeat, L/beat) and HR is the heart rate (beats/min). In this regard, thinking of the cardiovascular system as set of pipes with a pump can get us far: engineering principles of pressure, flow and viscosity have been readily applied to the cardiovascular system. Further, the degree of pharmaceutical and surgical interventions that can be performed to fix a heart is a testament to our thorough understanding of the system. From blood thinners, cholesterol-lowering drugs, to heart transplants, pacemakers, and cardiac bypass machines, the interventions at the disposal of a modern cardiologist and cardiothoracic surgeon are awe-inspiring.

It is clear that we do not have a commensurate level of understanding of the brain. Rather, much of our understanding is incomplete and correlative, not mechanistic. What would it look like if we knew as little about the heart as we know about the brain? It would not be surprising to find journal articles with titles such as "Blood vessels in the right arm contract during exercise", and "Baroreceptors are involved in decreasing blood pressure". On the other hand, what does a more mechanistic level of understanding look like in the brain? A

key part is the ability to reduce complexity in the system by creating accurate sufficiently-detailed models, much like the pump being a model for the heart. Such simplifications open the door to using concepts from physics and engineering to make complex problems tractable. While great strides have been made in creating computational models of brain activity, few truly unifying models have yet emerged (Markram et al., 2015). The importance of models lies in their predictive properties. Models of brain regions should predict neuronal activity characteristics, and behavioral outcomes. These models can, in turn, begin to inform treatments for brain disorders. The vision for a complete understanding of the brain involves using specific patient-tailored models to devise personal treatments for complex disorders.

1.2 Reductionist approach

With the vision of what it means to understand the brain, the question arises, what is the "best" way to study the brain to bring us closer to that understanding? Historically, neuroscientists have taken a variety of approaches. I will focus on a "reductionist" approach, which postulates that a complex system can be understood by studying its constituent parts (Kandel, 2001). In modern neuroscience, the neuron is often regarded as an atomic computational unit, as made famous by the neuron doctrine (Shepherd, 2015). Decades of research into neuronal diversity have confirmed that the theory of neuron as the simplest, indivisible unit is no more than a convenient fantasy (Larkum and Zhu, 2002; London and Häusser, 2005; Yuste and Denk, 1995). Nevertheless, on the scale of the entire

brain, the study of individual neurons, their morphology, genetic contents, and connectivity, as part of a reductionist approach is a good starting point.

How valuable is the reductionist approach and can it lead to scientific breakthroughs? We can point to dozens of ground-breaking discoveries in biology as evidence towards the affirmative. As an example, the role of DNA was elucidated by first analyzing the molecule and then forming hypotheses about its role in complex phenomena such as protein synthesis and heritability. Indeed, the concept of a nucleotide as a basic unit of genetic information is a simplification; nevertheless, the study of millions of these nucleotides has led to fundamental biological and medical discoveries. In a similar vein, the discovery of "place cells" in the hippocampus (O'Keefe and Nadel, 1978) has allowed the formulation of hypotheses about learning and memory that would otherwise be impossible. It is conceivable then to extend this idea to the entire brain, reasoning that its organization and function can ultimately be gleaned by a thorough examination of individual neurons.

Several high-profile multi-million dollar initiatives have undertaken this approach to study the brain. For example, the Blue Brain Project, started in 2005, undertook the challenge of creating the highest-fidelity computational model of a mouse cortical column to date (Markram, 2006). More than a decade later, the group indeed revealed a computational model of more than 30,000 individual neurons in a small (0.3 mm^3) piece of mouse brain tissue (Markram et al., 2015). In an effort of similar magnitude, the Allen Institute for Brain Science has set out to profile tens of thousands of neurons on a single-cell level with the goal of grouping neurons among electrophysiological, morphological, and genetic axes, as well as defining connectivity patterns in the brain (Allen Institute for Brain Science, 2015; Tasic et al., 2016).

Nevertheless, there is debate as to whether the reductionist approach is a valuable one. In a now-famous correspondence entitled "*Can a biologist fix a radio? – Or, what I learned while studying apoptosis"*, Lazebnik satirized the field of cancer biology by imagining a scenario in which biologists must fix a radio with no understanding of how it works, and only a set of basic experimental techniques at their disposal (Lazebnik, 2002). The results are predictably humorous:

> "How would we begin? First, we would secure funds to obtain a large supply of identical functioning radios in order to dissect and compare them to the one that is broken. We would eventually find how to open the radios and will find objects of various shape, color, and size […] Eventually, all components will be cataloged, connections between them will be described, and the consequences of removing each component or their combinations will be documented. This will be the time when the question, previously obscured by the excitement of productive research, would have to be asked: Can the information that we accumulated help us to repair the radio? It will turn out that sometimes it can, such as if a cylindrical object that is red in a working radio is black and smells like burnt paint in the broken radio. Replacing the burned object with a red object will likely repair the radio […] However, if the radio has tunable components, such as those found in my old radio […] and in all live cells and organisms, the outcome will not be so promising. Indeed, the radio may not work because several components are not tuned properly, which is not reflected in their appearance or their connections. What is the probability that this radio will be fixed by our biologists? I might be overly

pessimistic, but a textbook example of the monkey that can, in principle, type a Burns poem comes to mind."

The analogy is pertinent to the reductionist approach to neuroscience in the following way: even if we can eventually catalog the shapes, electrical properties, and all other relevant parameters of neurons, will we achieve sufficient understanding of the brain to fix it? To address this question, Jonas and Kording performed a thought experiment in which they ask whether a standard microprocessor can be "understood" using conventional experimental methodologies in neuroscience (Jonas and Kording, 2017). Using this naïve approach, the authors attempt to arrive at a comprehensive, useful picture of information processing in the microprocessor (Figure 1). The goal of the study was to find out whether present neuroscience techniques can ever produce a satisfactory explanation of the brain. Disappointingly, even after stacking the deck substantially in their favor, including possessing a complete transistor-level wiring diagram, and voltage time series trace for every wire, the authors found that the techniques they used were insufficient to recreate a meaningful information flow-based diagram of the microprocessor (Figure 1a). Instead, the authors argue, these techniques produce maps more reminiscent of Figure 1b, which, while impressive in scope, falls short of conveying a straightforward description of processing at each stage. In this way, the authors question whether the end-goal of the reductionist approach, namely, a single-cell resolution activity map and connectivity diagram will even be useful to neuroscience. Given that such an approach is likely to take years of research, millions of dollars of investments, and thousands of man-hours, it is worthwhile to consider whether the goal is worth it.

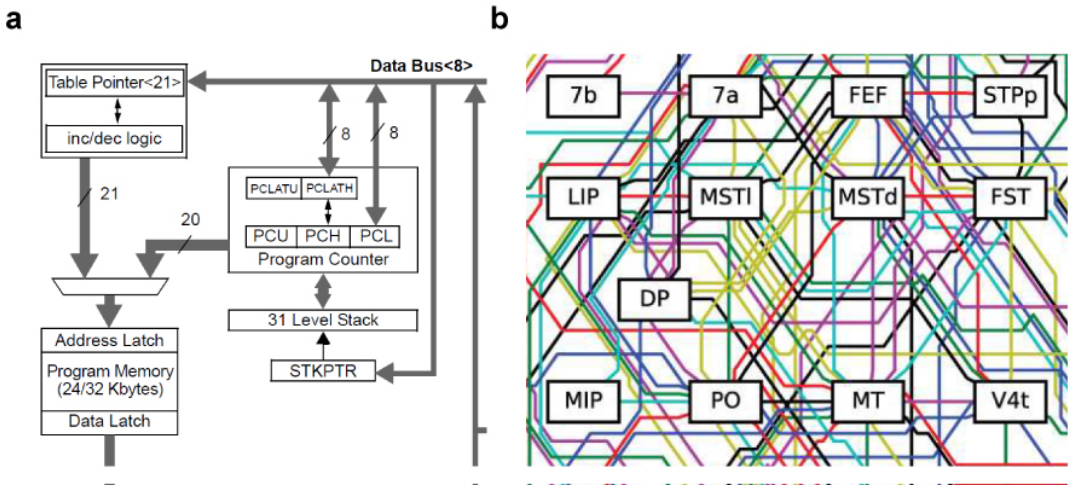

Figure 1: Comparison of connectivity diagram excerpts of a microprocessor (PIC18F2455) and the primate visual system (Felleman and Van Essen, 1991).

These concerns can be addressed by first acknowledging that single-neuron profiling of the brain is a necessary step, but not an end goal (Zeng and Sanes, 2017). That is, the single-cell resolution map should be treated as an enabling tool for further discoveries. Several concrete examples of what a single-cell resolution map of the brain would bring can be provided. First, a single-cell genetic profile would allow for extremely targeted drug and gene therapy interventions. This would be a major improvement over current drug treatments which often simply bathe the entire brain in a drug, likely contributing to the many side effects of drugs. Further, this approach could enable highly customizable studies of brain circuits in model animals: for example, using optogenetics (Boyden et al., 2005) to silence the activity of a very specific subset of cells could reduce the complexity of the entire intact system, making it possible to study independent "modules" in the brain.

Second, only extensive electrophysiological and morphological reconstructions of brain circuits could reveal the basic computational units (the equivalents of logic gates and memory buffers in the microprocessor) in the brain. Understanding these computational units could be critical to conceptualizing information pathways on a mechanistic level. Third, single-cell resolution maps in healthy and diseased or injured brains would reveal important properties about brain dysfunction and potentially provide therapeutic targets. Therefore the reductionist approach, while painstaking, is a necessary step to dramatically improved scientific studies as well as therapeutics.

1.3 Review of techniques

Several techniques are currently available to study the brain on this microscopic single-cell level. Three types of techniques will be discussed below: imaging, extracellular recoding, and intracellular recording. The techniques, and several advantages and disadvantages are outlined in Figure 2 and Table 1.

Single-cell imaging techniques have historically focused on detecting intracellular Ca^{2+} transients that occur as a result of action potential firing. This was accomplished first by bulk-loading brain tissue with acetoxymethyl (AM) esters such as Fura-2 (Smetters et al., 1999), and subsequently creating genetically encoded Calcium indicators (gCaMPs) (Akerboom et al., 2012; Tian et al., 2009). Other dyes have been designed to be direct voltage transducers (for review, see (Chemla and Chavane, 2010; Ebner and Chen, 1995)). The combination of Calcium-sensitive dyes with two-photon imaging has allowed large-scale studies of neuronal networks (Ohki et al., 2005). However, even with the advent of

new high-fidelity indicators (Chen et al., 2013; Dana et al., 2016), they are indirect transducers of electrical activity, and thus typically cannot resolve single action potentials or sub-threshold cellular activity (Vogelstein et al., 2010).

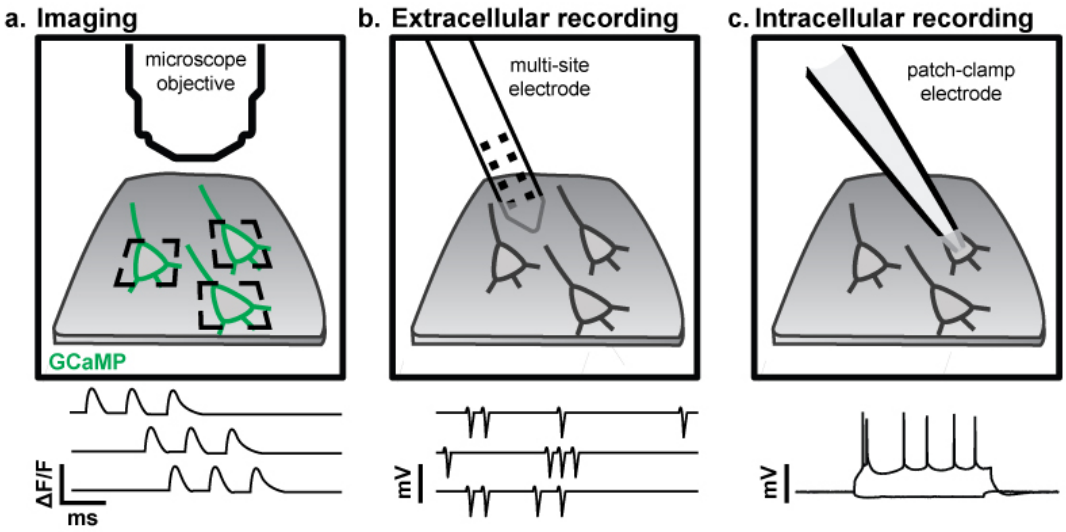

Figure 2: Comparison of three brain recording techniques with sufficient resolution to resolve single-cell electrical activity. Top panels show technique, bottom panels show sample signals. a. Single-cell imaging of genetically encoded fluorescent probes such as GCaMP. Signal from multiple neurons are measured as a change in fluorescence divided by basal fluorescence (ΔF/F) over time. b. Extracellular recording using a multi-site electrode. Signals from multiple neurons are recoded as voltage spikes. c. Intracellular recording using a patch-clamp electrode. One electrode records from one cell but the signal-to-noise ratio is very high, allowing the observation of sub-threshold activity.

Table 1: Advantages and disadvantages of single-cell recording techniques

	Imaging Figure 2a	**Extracellular recording Figure 2b**	**Intracellular recording Figure 2c**
Description	Single-cell imaging of fluorescent dyes or genetically encoded fluorescent proteins	Probes (typically silicon-based) inserted into the brain to record multi-unit activity	Glass micropipettes used to record from single cells
Advantages	Can be minimally invasive High-throughput (dozens of neurons simultaneously)	Medium to high-throughput (dozens to hundreds of neurons simultaneously)	High-resolution electrical activity Single-cell morphology, connectivity
Disadvantages	Photobleaching, requires toxic dyes or genetic modifications. Depth-limited (typically: ~400 μm, 1 mm with newest advances	Does not allow identification of recorded neuron	Low-throughput (typically <12 cells per day)

An alternative to imaging is using extracellular microelectrode probes to record the electrical activity of one or more neurons in vivo or in a brain tissue slice (Gray et al., 1995). This is a very common technique in electrophysiology, which has been growing with the advent of novel electrode types that exhibit improved bio-compatibility and contain more/higher-density channels (Scholvin et al., 2016). However, given that the brain tissue acts as a non-homogenous volume conductor, it is often difficult to discriminate the activity of several neighboring neurons, leading to uncertainties in the origins of the recorded signals (Harris et al., 2001, 2002). The lack of physical contact between the probe and the target cell also limits the types of investigations that can be performed.

Intracellular recording has been an instrumental technique in uncovering fundamental biophysical properties of electrically active cells. A key breakthrough in 1949 was the idea to pull hollow glass capillaries to a sharp (< 1μm) tip, fill the capillary with an electrically-conductive fluid, and pierce single muscle cells (Ling and Gerard, 1949). The pulled glass served two purposes: first it was sharp enough to penetrate cell membrane and second it was a nearly-perfect electrical insulator, which increased the signal-to-noise ratio of the recording. A physical probe inside the cell of interest gives the experimenter the ability to record and control the current and/or voltage of the cell. Using this technique or variants of it, many instrumental studies have been performed. For example, our modern understanding of the action potential stems from the work of Hodgkin and Huxley (Hodgkin and Huxley, 1952), who in 1949 used intracellular recording to perform voltage clamp experiments, leading to the first computational models of the neuronal action potential.

1.3.1 Patch-clamp recording

Intracellular recording was further revolutionized in 1976 by Neher and Sakmann (Hamill et al., 1981; Neher and Sakmann, 1976) who invented patch-clamp recording. They found that using a glass micropipette to form a physical seal with a small patch of membrane on a target cell, the electrical activity of the cell could be recorded with high temporal and voltage resolution, fully avoiding interfering signals from other neurons (Figure 3). The sensitivity of patch-clamp recording has uniquely permitted the recording of signals as small as the current in an individual ion channel (Hoshi et al., 1990) and synapse (Edwards et al., 1990). Whole-cell patch-clamp recording, a variant of the technique in which the patch of membrane is ruptured to obtain access to the cell cytosol has been used to characterize synaptic plasticity (Jaffe and Johnston, 1990), study sub-cellular compartments (Larkum and Zhu, 2002), and elucidate connectivity among nearby neurons (Markram et al., 1997).

The integrity of the sampled tissue must be maintained as much as possible to reliably capture the single-cell properties and connectivity patterns of neurons. The most faithful representations of neuronal activity can be obtained by performing *in-vivo* recordings from awake animals (Margrie et al., 2002). Unfortunately, brain motion, difficulty in visualization, and space constraints make large-scale in-vivo studies prohibitively time-consuming (e.g. 1 cell / 100 attempts). Recording from anesthetized animals is slightly more fruitful (10-30 cells / 100 attempts, see (Kodandaramaiah et al., 2012)). However, much higher success rates (50-90 cells / 100 attempts) can be reached if the brain is

explanted, kept alive, and sliced into thin (300-400 μm) sections (Edwards et al., 1989; Stuart et al., 1993). These slices are then anchored down to be observed under a transmitted-light microscope, thus eliminating motion and visualization issues, which contributes to the high success rate. On the other hand, the slicing process inevitably destroys the dendritic arbors and axons of neurons near the slice surface which may skew connection probabilities (Stepanyants et al., 2009); however, the magnitude of that effect is debated (Jiang et al., 2016). Presently, the brain slice preparation remains a gold-standard technique for assessing cell type and connectivity.

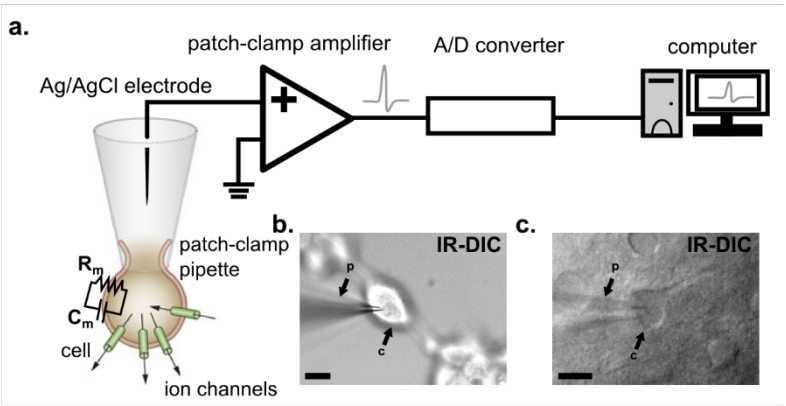

Figure 3: Whole-cell patch-clamp recording. a. A glass patch-clamp pipette is navigated to a cell membrane. A physical seal between the pipette tip and a small patch of cell membrane is established. This patch is pneumatically ruptured, creating a whole-cell configuration in which the aggregate activity of ion channels as well as passive properties of the cell such as its membrane resistance (R_m) and capacitance (C_m) can be measured. Electrical activity is recorded with an Ag/AgCl electrode, amplified, digitized, and processed on the computer. Image modified from (Ashcroft and Rorsman, 2013). Infrared differential interference contrast (DIC) image of patch-clamp recording with a pipette "p" of (b) a cultured HEK293 cell and (c) a neuron in a mouse brain slice. Cells are labeled with "c". Scale bar: 10 μm in b and c.

A typical sequence of steps in a whole-cell electrophysiology experiment in brain slices is as follows:

1) Visually identify a target cell suitable for patch-clamp recording using differential interference optics (DIC) under high magnification (e.g. 40x) in the brain region of interest. A cell can be picked based on the presence of a fluorescent marker, distinguishing morphological characteristics, and/or the perceived health of its cell membrane.
2) Find the patch-clamp pipette under the high-magnification objective and apply positive pressure to the pipette by mouth or with a syringe.
3) Descend pressurized pipette to within ~10 μm to target cell. If this is done in tissue (not culture), pipette should move in tissue parallel to its axis to prevent tissue deformation.
4) Approach target cell slowly while monitoring the position of the cell and the pipette tip, the internal pressure in the pipette and the electrical resistance.
5) Form a gigaseal with the cell by releasing positive pressure and applying slight suction. Apply a holding voltage of -70 mV before break-in.
6) Break-in to the cell by applying brief suction pulses to the pipette and monitoring the response to the membrane test. Detect successful break-in by observing low holding current at -70 mV and capacitive transients in response to square wave voltage pulses.
7) Upon successful break-in, a whole-cell recording is established.

8) After the whole-cell recording is terminated, the pipette must be replaced to start a new recording on another cell.

These steps are outlined graphically in Figure 4.

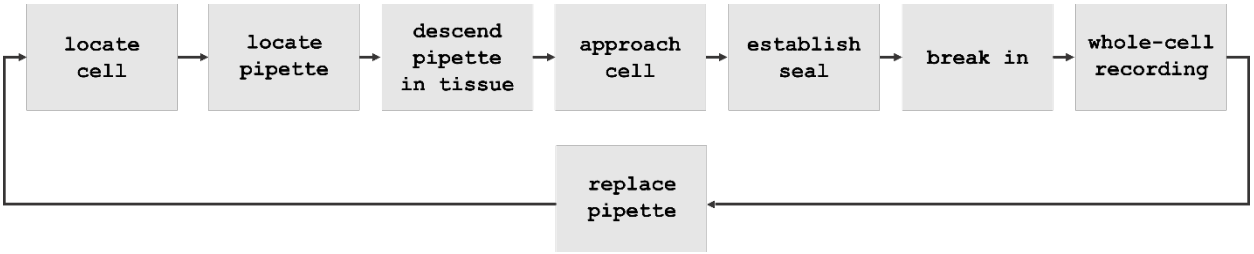

Figure 4: Graphical representation of a patch-clamp sequence in brain slices or cultured cells.

1.3.2 Limitations of patch-clamp recording

The immense diversity of neuronal cell types in the brain and their sparse connections create a tremendous demand for large sets of single-cell data that current patch-clamp systems cannot fulfill. Cell type classification of neurons remains a "holy grail" of neuroscience. Identifying classes of neurons is difficult because of their inherent within-group electrophysiological, morphological, and genetic variability, which leads to very "blurry" separation lines between groups. Thus it becomes necessary to use large datasets that enable the creation of sufficiently-defined borders between cell types. A notable attempt to do so is the recent effort by the Allen Institute for Brain Science (AIBS) aimed at creating a catalog of cells in the mouse primary visual cortex (VI). This ambitious multi-

year project is set to profile thousands of neurons using patch-clamping; however, with the current throughput limitations of the technique, it is not clear if these efforts can be replicated in other brain regions or by any other lab or institution in the future.

The sparse connections between neurons are fundamentally important to brain function but are difficult to study in large numbers. Inter-neuronal connections form the foundation of learning and memory and faulty connectivity patterns give rise to neurological disorders (Kempton MJ et al., 2011; Minshew and Williams, 2007). Despite the importance of these connections, there is a dearth of large-scale single-cell connectivity studies, owing to the compounded difficulty of patch-clamping multiple neurons simultaneously as well as the inherently low inter-neuronal connection probabilities. The low inter-neuronal connection probability (20% for neighboring cells but <5% for cells >300 μm apart in the cortex (Perin et al., 2011)) makes it necessary to patch hundreds to thousands of cells to obtain the necessary statistical power to define a neural connectivity diagram in just one part of the brain, necessitating years of uninterrupted effort by many highly skilled scientists. For example, studies of brain regions with low (~2%) connection probabilities will yield only ~39 connections in ~2,000 dual-patch recordings (Thomson et al., 1993). Recent advances in micromanipulator stability and electronic multiplexing have enabled eight and twelve simultaneous patches (Perin and Markram, 2013; Wang et al., 2015) which increases the number of connections that can be sampled simultaneously. This increase in throughput has led to impressive studies with the number of total patches numbering in the thousands, e.g. >8,000 (Jiang et al., 2013), > 2,500 (Lefort et al., 2009), >1,000 (Perin et al., 2011), >11,000 (Lee et al., 2014), >2,000 (Jiang et al., 2015). However, those studies still require hundreds of experiments and the high-channel patch-clamp technique still requires

tremendous skill, dexterity and experience to set up and use, and is thus far from a "benchtop" tool for analyzing neuronal connectivity. For hundreds of patch-clamp recording labs worldwide, the low throughput and difficulty of the technique are major barriers to collecting the massive amounts of data necessary for elucidating cell types and synaptic connectivity.

In stark contrast to the thousands of data points necessary to sufficiently identify a cell type or profile a synaptic connection, only a handful of cells (typically, <12 (Milligan et al., 2009)) are patched in a single day by an experimenter. This is primarily a result of two factors: first, neurons in brain slices die over the course of the experiment; 12+ hours after slicing the brain, it is thought that most neurons visible under DIC are unsuitable for patch-clamping (Aitken et al., 1995). Second, the highly manual nature of patch-clamp experiment which requires extensive attention, skill, and dexterity is physically and psychologically taxing on the investigator. Given the highly repetitive yet demanding nature of the task, human exhaustion is often a limiting factor and the main cause of the low throughput of the technique. Thus, when large datasets are necessary, many advantages of patch-clamp recording are offset by its low throughput.

1.3.3 Automation of patch-clamp recording

Several automation technologies have emerged to alleviate some of the manual tasks in patch-clamping. Fully-automated systems have been developed for patching onto dissociated cells (Fertig et al., 2002). These planar patch-clamp devices automatically capture cells suspended in solution into an etched cavity which replaces the conventional

patch-clamp pipette. While these systems are widely used in pharmacology due to their high throughput (Dunlop et al., 2008; Wood et al., 2004), they are not suitable for substrate-adhered (non-dissociated) cells or cells in sliced brain tissue, making them impractical for studying neurons in culture or brain slice.

For conventional (pipette-based) experiments, several hardware and software technologies have been crucial to reducing the complexity and increasing the throughput of each trial. On the hardware side, commercially-available motorized actuators and XY translation stages have enabled precise, motorized manipulation of a pipette to a target cell. Once a cell is approached, automated pipette pressure control via an "Autopatcher" device, developed in our lab, enables one to automatically form a gigaseal with the target neuron and break-in to reach the whole-cell configuration (Kodandaramaiah et al., 2012). Recently, the Autopatcher algorithm was modified to automatically perform two-photon targeted patch-clamp recording (Annecchino et al., 2017; Suk et al., 2017).

Various software packages take advantage of the motorized and automated hardware to automate portions of the patch-clamp trial. The LinLab and PatchVision software packages (Scientifica Ltd.) allow users to move pipette actuators to pre-defined positions, keep pipettes in view while moving the sample, and customize the function of stage and manipulator control devices. Free, open-source software packages such as Micro-Manager (Edelstein et al., 2014), Ephus (Suter et al., 2010) and Acq4 (Campagnola et al., 2014) effectively combine multiple acquisition and manipulation devices to create a unified user interface for patch-clamp recording and photostimulation. While these software packages automate electrophysiology experiments after a whole-cell configuration has been reached, they do not automate the patch-clamp procedure itself. A custom multi-electrode patch-

clamp system was developed that automated multi-pipette positioning and seal formation with up to 12 pipettes (Perin and Markram, 2013).

The hardware and software developments mentioned above have sped up experiments and enabled more convenient user interaction with scientific equipment but do not completely automate a full in-vitro microscope-guided patch-clamp experiment. That is, for all the mentioned solutions, a skilled and experienced user is still required to (1) manually navigate the pipette to the target cell and (2) replace pipettes after each patch-clamp attempt. Thus, existing technologies do not automate microscope-guided patch-clamp recording to the level of an autonomous, independently functioning system. While there are concerns that an automated system will not match the flexibility and experience of a trained user (Wang et al., 2015), few would argue that high-throughput patch-clamp data collection will be possible without major automation efforts.

An automated image-guided patch-clamp system would circumvent the need for a skilled user to continuously operate the system, enabling, for the first time, long-term unsupervised operation. The subsequent chapters will describe the three innovations that were necessary to create such a system. First, Chapter 2 will focus on the integration of pipette trajectory planning with pressure control in a single computer-assisted interface, named Autopatcher IG (Image-guided). The software package combines the previously-published Autopatcher algorithm (Kodandaramaiah et al., 2012) with pipette trajectory planning to enable visually-guided targeting. Chapter 3 will discuss the pipette cleaning technique which enables the reuse of patch-clamp pipettes. Chapter 4 will introduce the “patcherBot”, a robotic system that combines the techniques of the previous chapters with a machine vision

algorithm to create a walk-away, image-guided patch-clamp recording system. The technical concepts covered in each chapter are summarized graphically in Figure 5.

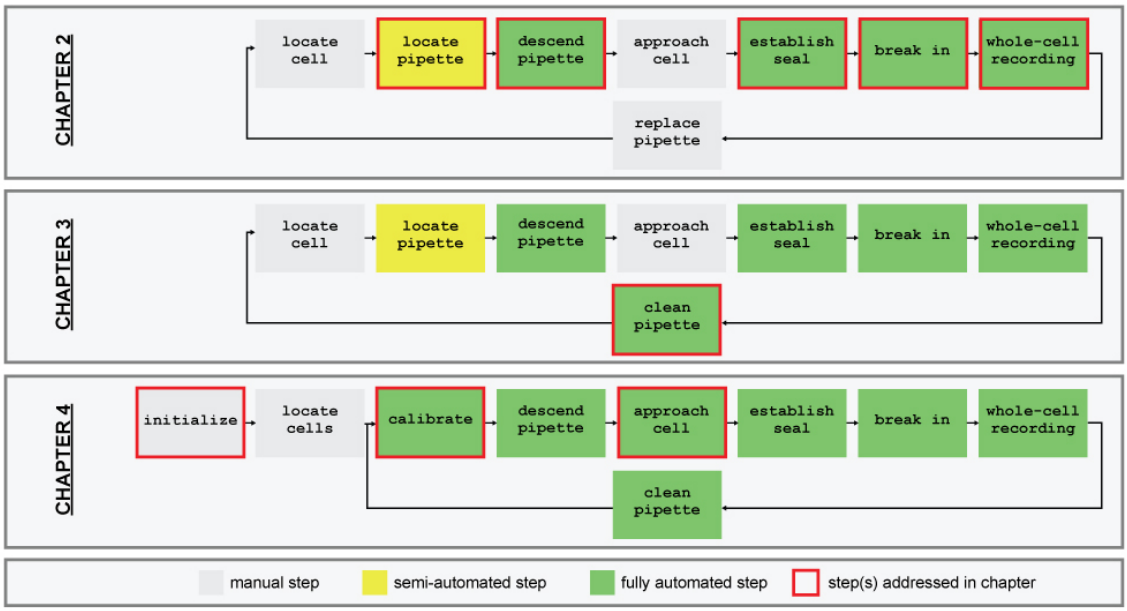

Figure 5: Description of thesis chapters in block diagram form.

CHAPTER 2. INTEGRATION OF AUTOPATCHING AND PIPETTE TRAJECTORY PLANNING

Portions of this chapter have previously been published (Wu et al., 2016).

2.1 Introduction

There is a growing demand for large datasets of patch-clamp recordings. For example, large-scale cell type classification of neurons based on electrophysiology and morphology as well as the study of their synaptic connections are some of the highest-priority goals in modern neuroscience (Alivisatos 2012, Alivisatos 2013, Insel, Landis et al. 2013, Kandel, Markram et al. 2013). However, patch-clamp recording of a large number of neurons has limitations: it is a challenging, laborious technique, akin to an art form, requiring a skilled and highly trained investigator. It is also low-throughput; unlike two-photon excitation microscopes and high-channel extracellular probes which can record the activity of hundreds of neurons simultaneously (Dombeck, Khabbaz et al. 2007, Berenyi, Somogyvari et al. 2014), even the most skilled and experienced patch-clamp investigators can record from only a few neurons per day.

Due to its low throughput, a typical patch-clamp experiment is highly repetitive, making it error-prone for the investigator. For example, when advancing the micropipette towards the target cell, errors such as advancing the pipette too far into the tissue, breaking the pipette tip and improperly setting the pipette pressure are common among novices and occasional among experienced users. The delicate pneumatic pressure changes applied to

the pipette necessary to form a whole-cell configuration are typically done by mouth or with syringe (Boulton, Baker et al. 1995, Walz 2007), making them difficult to replicate among labs and even among different investigators in the same lab. There is also a plethora of undocumented heuristics that are challenging to master and vary from lab to lab. This is especially an issue when large datasets collected by various laboratories for a single study must be directly comparable (Tripathy, Burton et al. 2015).

We have previously developed and tested the "Autopatcher": a robot for automated patch-clamp recording (Kodandaramaiah, Franzesi et al. 2012). The Autopatcher was designed to perform "blind" patch-clamp recordings; that is, using only electrical resistance, not visual information, as an indicator of cell proximity (Kodandaramaiah et al., 2016). However, often, targeting cells based on visual cues such as the shape or fluorescence of a cell is required (Komai, Denk et al. 2006, Lefort, Tomm et al. 2009).

We have developed the Autopatcher IG ("Image-Guided"), a software package that automates the "locate pipette", "descend pipette in tissue", "establish seal", "break in" and "whole-cell recording" parts of the patch-clamp process (Figure 5). The automation of these states reduces user intervention during the experiment and increases throughput. This is accomplished by automation of pipette trajectory planning and execution, pneumatic pressure control, electrophysiological measurements, and data logging. We validate the performance of the Autopatcher IG by performing patch-clamp recordings of 39 cells in mouse brain slices. The Autopatcher IG is available open-source on www.autopatcher.org.

2.2 Methods

2.2.1 Hardware

The Autopatcher IG utilizes off-the-shelf patch-clamp electrophysiology hardware with minor modifications. The hardware setup is based on an upright microscope outfitted with DIC optics. Brain slices are visualized using low-magnification (4×) and high-magnification (40×) water-immersion objectives that can be exchanged manually using a swinging nosepiece or automatically using a motorized carriage. Image guidance is accomplished by interfacing with a charge-coupled device (CCD) camera (Rolera EMC2). The Autopatcher IG relies on motorized three-axis control of the microscope stage and the patch-clamp pipette manipulator (Scientifica SliceScope Pro 1000; Scientifica Ltd.). A pipette holder is connected to the headstage of a patch-clamp amplifier (Multiclamp 700B). The headstage is mounted on the pipette manipulator. A data acquisition board (e.g., Digidata 1550A; Molecular Devices) relays the electrical signal from the amplifier to the computer for processing and storage. Other complete patch-clamp systems or custom-built solutions can be implemented with additional driver programming (Figure 6 a,b). The only non-standard piece of electrophysiology hardware that is necessary for the Autopatcher IG is a computer-controlled pneumatic pressure control unit. We have adopted the software to utilize a commercially available patch-clamp pressure control system (Autopatcher pressure control box, Neuromatic Devices, Atlanta, USA).

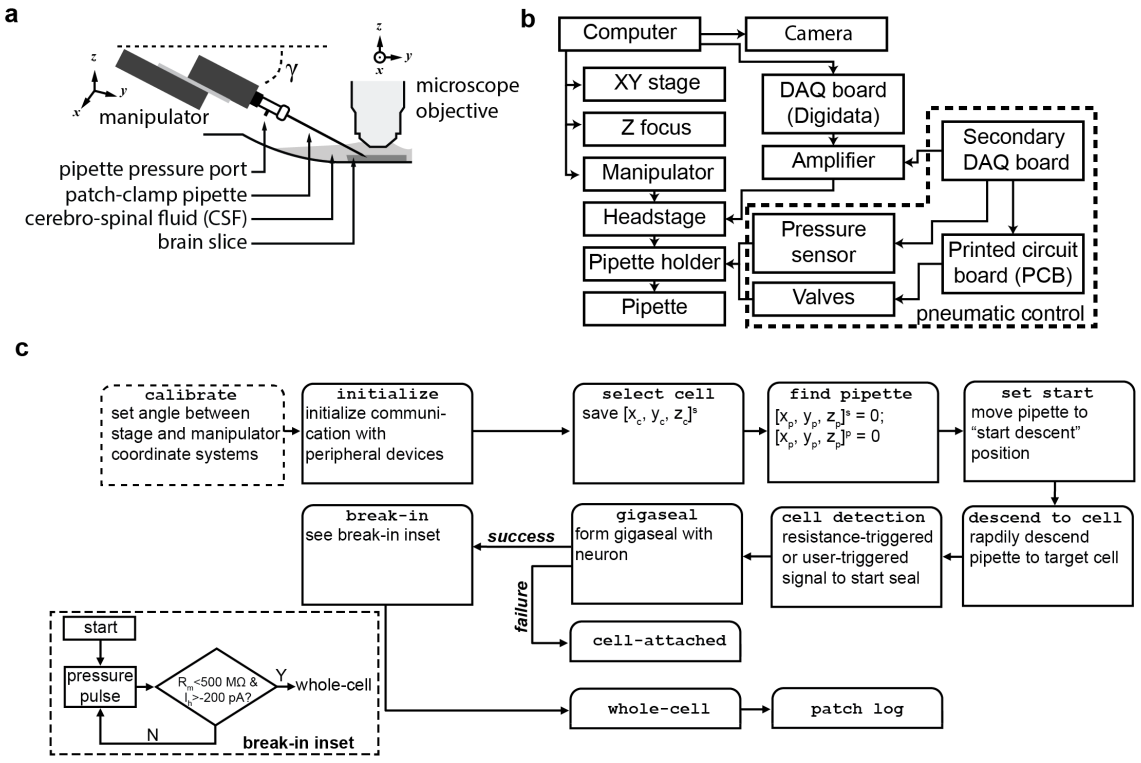

Figure 6: Experimental, hardware and software setup of the Autopatcher IG a. Experimental setup. Brain tissue in artificial cerebro-spinal fluid (aCSF) and the patch-clamp pipette are visualized using differential interference contrast (DIC) microscopy. The manipulator angle **γ** and the coordinate systems of the manipulator and stage are used to perform trajectory calculations to navigate the pipette to the target cell. The coordinate system of the stage differs from that of the manipulator by an arbitrary angle (**θ**, refer to text) in the XY plane. b. System-level schematic of the hardware setup. Standard patch-clamp electrophysiology equipment is used in conjunction with a pneumatic pressure control unit. c. Finite state machine architecture of the software. Inset (bottom left) shows the detailed break-in procedure. See Section 2.2.3 for details about the execution of the software.

2.2.2 Software architecture

The Autopatcher IG is organized as a state machine with 12 distinct states (Figure 6c). Transitions between states are accomplished either automatically or after processing user input such as a button click. The architecture of the software implements device driver abstraction – that is, if a user needs to implement a different camera, manipulator or pressure control system than what is currently supported, few changes to the code need to be made beyond replacement of low-level device commands.

2.2.3 Calibration procedure

A preliminary step to using the Autopatcher IG is calibration, performed once upon initial setup and any time the configuration of the hardware has changed. First, the user is prompted to set a "HOME" location: a set of stage and manipulator coordinates for which the pipette is in the microscope's field of view. From this HOME location, a calibration is performed which relates the coordinate system of the manipulator to that of the microscope stage. To perform the calibration, the operator switches to the high-magnification objective and moves the pipette to three pre-defined points in space.

The calibration procedure is performed as follows:

1. User brings the pipette to center of screen. Pipette (p) and stage (s) coordinate systems are zeroed:

$$\begin{bmatrix} x_p \\ y_p \\ z_p \end{bmatrix}^p = \begin{bmatrix} x_s \\ y_s \\ z_s \end{bmatrix}^s = \begin{bmatrix} 0 \\ 0 \\ 0 \end{bmatrix}$$

The p and s superscripts indicate the coordinate systems of the pipette manipulator and the stage, respectively.

2. Stage is moved in the x direction to the first calibration point: $\begin{bmatrix} X \\ 0 \\ 0 \end{bmatrix}^s$ where X is a user-defined calibration distance. User brings the pipette to center of screen again. Pipette coordinates are saved as $\begin{bmatrix} x_{p1} \\ y_{p1} \\ z_{p1} \end{bmatrix}^p$. The first calibration angle is calculated: $\theta_1 = \text{atan}\left(\frac{y_{p1}}{x_{p1}}\right)$.

3. Stage is moved in the y direction to the second calibration point: $\begin{bmatrix} X \\ Y \\ 0 \end{bmatrix}$. User brings the pipette to center of screen again. Pipette coordinates are saved as $\begin{bmatrix} x_{p2} \\ y_{p2} \\ z_{p2} \end{bmatrix}^p$. Second calibration angle is calculated: $\theta_2 = \text{atan}\left(\frac{y_{p2}-y_{p1}}{x_{p2}-x_{p1}}\right)$.

4. Best approximation of the angle between the pipette and stage coordinate systems calculated as average of θ_1 and θ_2: $\theta = \frac{\theta_1+\theta_2}{2}$.

We used $X = Y = 1$ mm to give a sufficiently accurate estimate of θ. After θ is determined, any x-y position from the pipette manipulator's coordinate system is transformed to that of the stage using: $\begin{bmatrix} x \\ y \end{bmatrix}^p = \mathbf{R}(\theta)\begin{bmatrix} x \\ y \end{bmatrix}^s$ where $\mathbf{R}(\theta)$ is the rotation matrix calculated using the angle θ. A re-calibration is necessary only when a part of the setup has been altered – that

is, if the angle between the stage and manipulator has changed. After the calibration is complete, the angle θ is saved to a settings file. The main Autopatcher IG program then uses θ to calculate the approach trajectory of the pipette towards the cell. Previously saved calibration values can also be loaded.

2.2.4 Steps in the patch-clamp trial

The patch-clamp trial begins by initializing communication with peripheral devices – the motorized actuators, pneumatic pressure control unit, camera, and data acquisition boards. After initialization, the user is prompted to select a target cell. The coordinates of the cell are saved in terms of the stage's coordinate system as $\begin{bmatrix} x_c \\ y_c \\ z_c \end{bmatrix}^s$. Next, the software brings the pipette and the stage to the HOME location defined in the calibration step. Depending on the trial-to-trial variability of pulled pipette sizes and other actuation inaccuracies, the pipette may appear slightly off-center and/or out of focus. To account for this, the user is asked to make a small correction to bring the pipette to the crosshair in the center of the camera window. Importantly, using pulled pipettes of approximately the same length for each trial will reduce the time it takes to find them under the microscope. The manipulator and stage coordinates are set to zero.

The trajectory that the pipette must take to reach the cell is calculated using the coordinate transform performed in the calibration step. We have found that "on-axis" pipette descent, or descent in which the pipette enters tissue along its shaft axis results in a higher percentage of stable whole-cell configurations than vertical descent (along the z-axis) into

tissue; however, the user may choose between the two options. The position from which the pipette should begin its descent is determined as follows:

1. Cell position in x and y in the pipette's coordinate system is found: $\begin{bmatrix} x_c \\ y_c \end{bmatrix}^p = \mathbf{R^T}(\theta) \begin{bmatrix} x_c \\ y_c \end{bmatrix}^s$ where the $^{\mathbf{T}}$ superscript indicates the transpose of the matrix. Due to the zeroing of coordinate systems in the calibration step, $z_c^p = z_c^s$.

2. If "on-axis" motion is chosen, the position from which pipette descent starts is $\begin{bmatrix} x_c + \frac{z_{safety}}{\operatorname{atan}\gamma} \\ y_c \\ z_c + z_{safety} \end{bmatrix}^p$ where z_{safety} is a safety factor (2 mm by default) that is set to ensure the pipette does not touch the slice surface before starting the descent, and γ is the angle of the pipette relative to horizontal (Fig 2A). If vertical descent is chosen, the position from which the pipette descent starts is $\begin{bmatrix} x_c \\ y_c \\ z_c + z_{safety} \end{bmatrix}^p$, that is, directly above the target cell.

The pipette rapidly descends either along its axis or vertically to within 10 μm of the target cell. The descent is done under positive pressure (200 mBar) to avoid clogging of the tip and to "clean" the surface of the cell with fluid, which improves gigaseal quality (Boulton, Baker et al. 1995, Walz 2007). The pressure is subsequently quickly switched to 50 mBar to avoid prolonged exposure of the cell to intracellular solution containing a high concentration of potassium, which is detrimental to its health (Smith, Bradley et al. 2006, Kudo, Nozari et al. 2008, Cauli and Hamel 2010). Once the pipette is in close proximity to the target cell, the software awaits a signal to initiate the gigasealing algorithm. The user

manually adjust pipette position if necessary, and presses “OK” to initiate the gigasealing algorithm.

The gigasealing algorithm is a temporal sequence of pipette pressure changes largely similar to that developed in (Kodandaramaiah, Franzesi et al. 2012). Briefly, the algorithm switches to 0 mBar pressure for 8 s, and then to suction (-50 mBar) for 40 s, or until a gigaseal is obtained. We have found that these default parameters result in a large percentage of successful gigaseals; however, it is possible for the user to alter the times at which different pressures are applied and how much pressure is applied using the GUI.

After the software determines that a gigaseal has been successfully established, the break-in algorithm is initiated (Figure 6c, inset). The algorithm applies progressively higher-suction and/or longer pressure pulses to break in and reach a whole-cell patch-clamp configuration. After each pressure pulse, the Autopatcher IG checks the user-set thresholds of resistance and holding current to detect if whole-cell access has been established, as is typically done manually (Boulton, Baker et al. 1995, Walz 2007). If the membrane resistance is below a certain threshold (indicating that the gigaseal has been ruptured) and the holding current at -70 mV is above a threshold (indicating that the cell is healthy and has not been lost during the break-in process), the algorithm concludes that the whole-cell patch-clamp trial has been successful. We have chosen a resistance cutoff of 500 MΩ and a current cutoff of -200 pA; however, these values can be adjusted based on cell type and the perceived health of the brain slice.

A successful break-in results in the “whole-cell” state in the algorithm while a failure to reach a gigaseal or break in results in the “cell-attached” or juxtacellular state. When the

algorithm reaches the "whole-state" state, control of the amplifier is optionally traded from the secondary DAQ board to the primary DAQ board such as a Digidata 1550A. This allows the operator to proceed with whole-cell electrophysiology using familiar software such as Clampex (Molecular Devices). As a final step of the algorithm, all data associated with the trial is recorded and stored in a "patch log". The patch log stores the resistance and pressure of the pipette over time, low-magnification and high-magnification images of the cell, the depth of the target cell in the slice and other relevant parameters. All metadata are saved in time-stamped folders, making them easily accessible for tracking success rate over time, finding optimal parameters and algorithms for specific preparations or cell types, and automatically organizing data into an easily manageable folder structures. The LabVIEW GUI (Figure 7) is provided as a compiled executable and as user-editable source code. An introductory software usage guide to using this GUI to patch-clamp in practice is provided in Appendix A.

2.2.5 In-vitro testing

The system was tested on tissue from young mice as well as from adult mice to evaluate the performance of the automated algorithm in two different experimental preparations. All animal procedures were approved by the Committee on Animal Care at the Allen Institute for Brain Science. Acute brain slices were prepared from adult (P50-P180) C57BL/J6 mice using the protective recovery method described in detail elsewhere (Ting, Daigle et al. 2014).

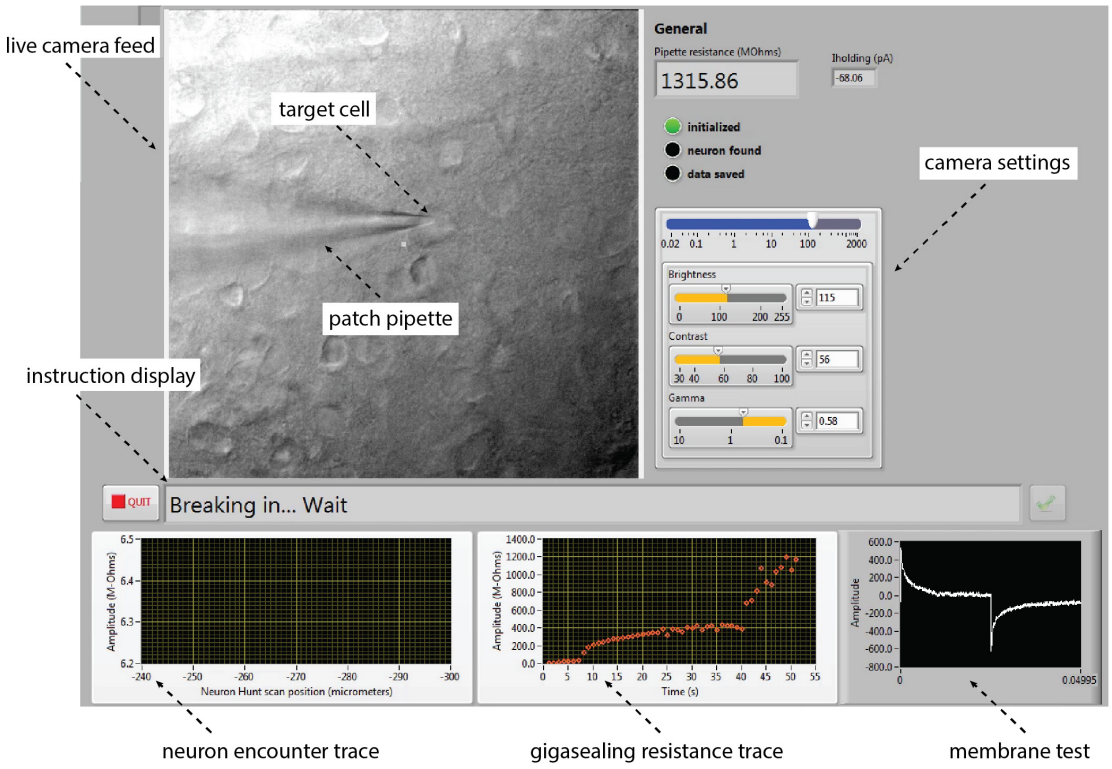

Figure 7: Graphical user interface (GUI). LabVIEW-based GUI shows the algorithm during break-in. A live camera feed shows the positions of the patch pipette and target cell. A neuron encounter trace shows resistance as a function of pipette position if the resistance-triggered cell detection option is used. In this trial, the user-triggered cell detection option was used. The gigasealing resistance trace shows pipette resistance as a function of time after gigasealing has been initiated. In this trial, user-triggered cell detection was used with the parameters in Table 1. The membrane test panel shows the membrane currents in response to a test pulse (+10 mV) immediately after a successful break-in. The break-in algorithm will detect a decreased membrane resistance and holding current close to zero, thus exiting with a successful whole-cell recording.

Briefly, animals were heavily anesthetized with isofluorane and perfused trans-cardially with NMDG solution containing (in mM): 93 N-methyl-D-glucamine (NMDG), 2.5 KCl,

1.2 NaH2PO4, 30 NaHCO3, 20 HEPES, 25 Glucose, 5 Na-ascorbate, 3 Na-pyruvate, 10 MgSO4.7H2O, 0.5 CaCl2.2H2O (pH titrated to 7.3-7.4, osmolarity: 300-310). Mice were quickly decapitated, the brain was extracted, embedded in 2% agarose and cut into 300 μm coronal slices using a VF200 compresstome (Precisionary Instruments) in the cutting solution. The slices were incubated at 34 ºC in the cutting solution for 10-12 minutes. They were then transferred to a recovery solution containing (in mM) 92 NaCl, 2.5 KCl, 1.2 NaH2PO4, 30 NaHCO3, 20 HEPES, 25 Glucose, 5 Na-ascorbate, 2 Thiourea, 3 Na-pyruvate, 2 MgSO4.7H2O, 2 CaCl2.2H2O (pH: 7.3-7.4, osmolarity: 300-310) for at least 60 minutes prior to beginning recording. Recordings were performed at room temperature (25 ºC) in an open bath chamber (RC-29, Warner Instruments) with standard recording solution containing (in mM): 124 NaCl, 2.5 KCl 1.2 NaH2PO4, 24 NaHCO3, 5 HEPES, 12.5 Glucose, 2 MgSO4.7H2O, 2 CaCl.2H2O. The liquid junction potential was not corrected.

Patch-clamp electrodes were pulled from filamented borosilicate glass tubes (BF150-86-10, Sutter Instruments) using a P-97 micropipette puller (Sutter Instruments) to a resistance of 3.5-7.9 MΩ. Internal solution contained (in mM): 20 KCl, 100 Na-gluconate, 10 HEPES, 4 MgATP, 0.3 Na_2GTP, 7 phosphocreatine-Tris, and 0.2% biocytin with pH adjusted to 7.4 and osmolarity adjusted to 300 mOsm. In some experiments, 4% w/v Alexa Fluor 594 (A-10438, Life Technologies) or Lucifer Yellow (L-453, Life Technologies) were added to the intracellular solution to visualize patch-clamped cells under fluorescent optics. Cell characteristics were obtained 5 min after a successful break-in using Clampex. The

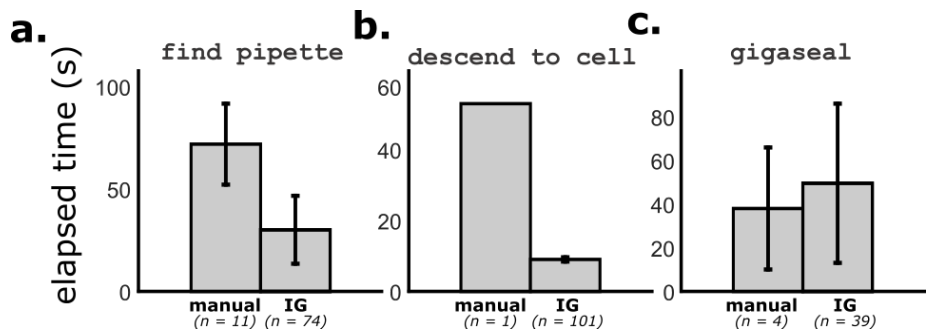

Figure 8: Benchmarking Autopatcher IG throughput against manual throughput. a. The time to find the pipette under the microscope objective was reduced due to the automation of the "find pipette" state. b. The time to descend to the cell was reduced using the pipette trajectory planning algorithm. c. The time to form a gigaseal was not significantly different between manual and Autopatcher IG trials.

algorithm was considered to yield a successful whole-cell recording if $R_a < 80$ MΩ and I_{hold} at -70 mV > -200 pA. All data are reported as mean ± s.e.m.

2.3 Results

2.3.1 Assisted patch-clamp electrophysiology in mouse visual cortex

The algorithm resulted in a stable whole-cell recording in 39 of 95 trials (41% success rate). In trials where the gigasealing step was initiated (n = 84/95, 88%), a gigaseal was established in the majority of cases (n = 60/84, 71%, R_{Gseal} = 1.39 ± 0.06 GΩ). In both preparations, where the algorithm failed to establish a gigaseal it was manually aborted. Importantly, when the algorithm failed to initially establish a gigaseal or to break-in using pre-defined parameters, switching to a manual control of the GUI to apply additional pulses of negative pressure would often lead to a successful whole-cell recording. In both

preparations, failures were typically caused by clogging of the pipette (manifested by increased pipette resistance) during approach, an inability to establish a gigaseal, or poor cell characteristics (which may be caused by incorrect selection of a putative "healthy-looking" cell, a limitation shared with manual patching).

The automated provided by Autopatcher IG decreased the time to perform several parts of the patch-clamp process, enabling higher throughput than manual attempts. Autopatcher IG significantly decreased the time it takes to find the pipette under the objective ($P=3.9\times10^{-11}$, Figure 8a) and descend the pipette to the target cell ($P=1.4\times10^{-186}$, Figure 8b, Student's unpaired t-test), as compared to manual operation. The time to form a gigaseal with the cell was not significantly different between manual and Autopatcher IG trials (P=0.54, Figure 8c). This suggests that the Autopatcher IG automated gigasealing algorithm is sufficiently robust to mimic the fine manual pressure application of trained users.

Electrophysiology and morphology data obtained using the Autopatcher IG were similar to those obtained manually by other groups (Walz 2007). Representative images show the electrophysiological properties of four neurons and their morphology under DIC (Figure 9). The neurons exhibited typical electrophysiological recording characteristics (Figure 10) such as capacitance (102.9 ± 6.2 pF), holding current at -70 mV (-12.0 ± 4.0 pA), and access resistance (19.0 ± 1.1 MΩ) similar to those reported by skilled manual patch-clamp investigators (Kobayashi and Takahashi 1993, Borst, Helmchen et al. 1995, Debanne, Boudkkazi et al. 2008, Anderson, Huguenard et al. 2010, Cho, Jang et al. 2010).

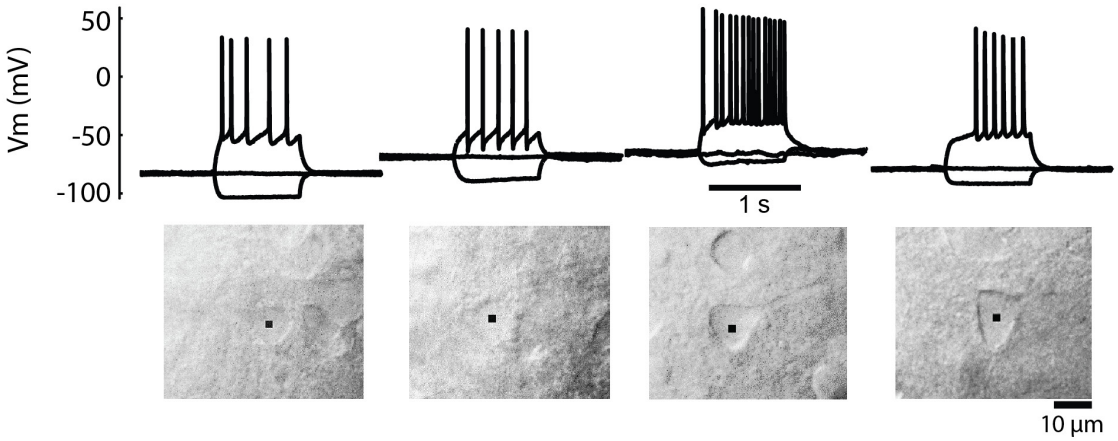

Figure 9: Representative electrophysiology and morphology of neurons patched using Autopatcher IG. The differences in spike patterns illustrate various putative electrophysiological cell types.

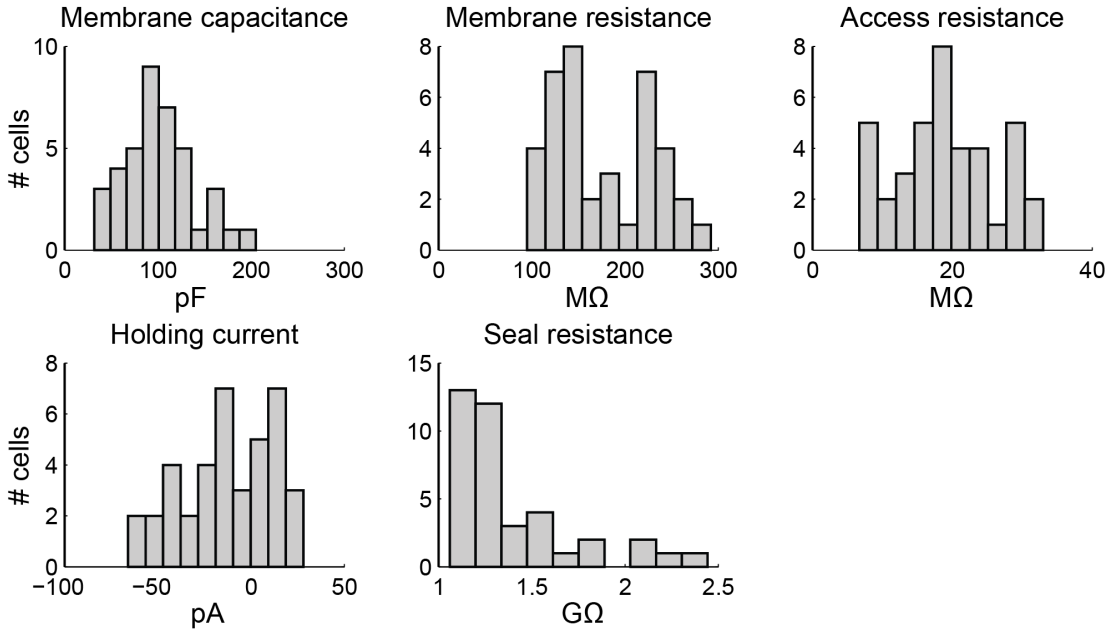

Figure 10: Cell characteristics of neurons patch-clamped using the Autopatcher IG. Neurons exhibited recording characteristics similar to those in literature where the patch-clamp recordings were obtained manually (see section 2.3.1).

2.3.2 Patch log

The automatically-recorded patch log is a collection of images, measurements, and parameters that fully describe a successful or unsuccessful whole-cell patch-clamp trial. These metadata are stored in an individual folder for each trial and can be mined to reveal relevant information about patch-clamp attempts such as the timing of specific steps, pressures during gigasealing, success rates, and other characteristics of the trial. As an example of the usefulness of the patch log, we used resistance measurements during the gigasealing state to train and validate a classifier that can accurately predict the formation of a gigaseal within a few seconds of cell detection. We trained a naïve Bayes classifier (Bishop 2006) on 8 seconds of 1 Hz resistance measurements taken during the gigasealing step from a subset of patch-clamp trials (training data). We then validated the classifier on test data to predict whether each trial in the test data set would result in a gigaseal. The naïve classifier correctly predicted the formation of a gigaseal in 81 ± 11.2% of test trials and correctly predicted that the gigaseal will not form in 67 ± 18.4% of test trials (n=20 classifications run, 60% of trials, or approximately 50, used for training, 40%, or approximately 33, for testing). This technique is potentially useful for automatically and rapidly determining whether a gigaseal will eventually form after cell detection and can be used to speed up experiments.

2.4 Discussion

We have developed an image-guided patch-clamp electrophysiology software package, the Autopatcher IG, which, as far as we are aware, is the first one to automate multiple steps of the whole-cell patch-clamp experiment *in vitro*. We took steps to ensure that the software is suitable for a broad range of hardware configurations and user programming preferences. First, the Autopatcher IG can run on virtually any computer-controlled patch-clamp recording rig, augmented only by a pneumatic pressure control unit. Second, the abstracted structure of the code allows for simple driver programming for presently unsupported devices. On the other hand, the experimenter needs to have no programming experience to use the software with the commercially-available electrophysiology workstation we have tested.

We have successfully tested the Autopatcher IG with cortical slices from adult animals, yielding high success rates and demonstrating the usability of the software in two different experimental preparations. Statistics such as the overall success rate (percentage of patch-clamp attempts that resulted in whole-cell recordings) and time expended on each trial were tracked using the patch log.

The Autopatcher IG is intended to serve as a framework for quantifying and standardizing patch-clamp recording trials. The ability to algorithmically control all relevant peripheral devices from a single interface makes it possible to document and standardize existing "best practices" in obtaining whole-cell recordings (Boulton, Baker et al. 1995, Walz 2007). Integrated algorithmic control also makes it possible to explore and quantify new ways of obtaining whole-cell recordings. For instance, a millisecond-timescale closed-loop

pipette pressure control system could potentially outperform even a trained human in quickly establishing a gigaseal and breaking into a cell delicately. In the future, these algorithms can then be refined and optimized in a systematic fashion.

The selection of a suitable target cell is still a difficult user-dependent task that is currently not handled by the Autopatcher IG; however, further developments will automate and refine this process. The age of the animal, duration of the experiment, area of the brain, and even minute experimental details can have dramatic effects on the "health" of neurons and thus their ability to form stable gigaseals and whole-cell configurations (Boulton, Baker et al. 1995, Walz 2007). In future versions of the software, we will develop machine vision algorithms to reliably identify and track healthy cell bodies under DIC optics (Alexopoulos, Erickson et al. 2002) in order to achieve completely autonomous robotic patch-clamp experimentation. Further, targeting cells of a specific genetic type is currently only possible by manually identifying cell-type specific fluorescent markers on a cell. However, the combination of high-resolution fluorescent imaging and machine vision techniques could eventually enable the Autopatcher IG to automatically target and patch-clamp neurons based on their genetic cell type.

CHAPTER 3. CLEANING PATCH-CLAMP PIPETTES FOR IMMEDIATE REUSE

Note: portions of this chapter have previously been published (Kolb et al., 2016)

3.1 Introduction

Patch-clamp recording is a gold-standard single-cell electrophysiology technique that has been widely used to discover foundational biophysical properties of excitable cells (Hamill et al., 1981). In neuroscience, the superior sensitivity and resolution of patch-clamp recording has made it an indispensable tool for discovering the tenants of ion channel activity (Neher and Sakmann, 1976), synaptic integration (Edwards et al., 1990), plasticity (Bi and Poo, 1998) and network connectivity (Song et al., 2005) in a variety of experimental preparations from cultured cells to living brain tissue.

There is a growing demand for large-scale measurements of brain activity on a single-cell level (Alivisatos et al., 2012). Patch-clamp is well-suited for such studies because it can sample electrical, morphological and genetic properties of single cells and even sub-cellular compartments (Pfeffer et al., 2013; Stuart et al., 1993); however, the technique is not readily scalable. Thousands of neurons and connections must be sampled to reach conclusions about cell types and connectivity patterns in just one part of the brain (Allen Institute for Brain Science, 2015; Jiang et al., 2015; Lefort et al., 2009; Song et al., 2005). While recent engineering advancements (Wang et al., 2015) have made strides towards automating and scaling the patch-clamp technique, even to the point where a cell can be patched automatically (Kodandaramaiah et al., 2012), or up to twelve cells can be patched

simultaneously (Perin and Markram, 2013), the highly manual nature of the technique severely limits the throughput of patch-clamp and makes large-scale studies burdensome. While planar patch-clamp systems are high-throughput, they are unsuitable for investigations of adhered cultures or living tissue (Fertig et al., 2002). Thus there is significant interest in automation and scalability of pipette-based patch-clamp recording (Kodandaramaiah et al., 2013; Shen, 2016).

To achieve a successful recording, the patch-clamp pipette must have a clean tip to form a high-resistance (≥ 1 GΩ) junction (or gigaseal) with the cell membrane. In his Nobel Prize lecture, Edwin Neher remarked that "a gigaseal could be obtained reproducibly when suction was combined with some simple measures to provide for clean surfaces, such as using a fresh pipette for each approach and using filtered solutions" (Neher, 1992). However, the need for an operator to replace the pipette for each approach is a major limitation in the following types of experiments. First, when large single- or multi-patch datasets must be collected, automation is highly desirable but cannot be achieved when pipette replacement after every trial is necessary. Second, when performing in vivo patch-clamp studies of sleep, audition (Wehr and Zador, 2003), olfaction (Cang and Isaacson, 2003), or social interaction (Lenschow and Brecht, 2015), human operator involvement could be highly disruptive, yet unavoidable if pipettes must be replaced after every trial. Third, some promising studies are impractical at large scales because pipettes are not easily replaceable, for instance if they are coated (Ishikawa et al., 2010; Levis and Rae, 1993), custom-manufactured (Goodman and Lockery, 2000; Malboubi et al., 2010), or filled with precious molecules such as synthetic peptides, novel therapeutics, human patient samples or nucleic acid constructs (Rye et al., 2012).

We have discovered a simple, fast, and automated method for cleaning glass pipette electrodes that enables their immediate reuse. Reasoning that cleaning glass pipettes is not fundamentally different from cleaning other laboratory glassware, we found that immersing the tip into Alconox (Alconox Inc), a commercially-available detergent, at 2% w/v (20 mg/ml), for 60 seconds, permits multiple reuses in cell cultures, tissue slices, and in vivo. This discovery allows circumvents the need for the manual "replace pipette" step in the patch-clamp procedure, in favor of the automated "clean pipette" step (Figure 5).

3.2 Methods

3.2.1 Pipette cleaning method

We made minor modifications to standard *in vitro* and *in vivo* electrophysiology rigs to enable them to be used for pipette cleaning. We manufactured an electrophysiology recording chamber with two wells for the cleaning and rinse solutions. A variant of this chamber without the main recording well was manufactured for use *in vivo*. We programmed either a custom-built or commercially-available (Autopatch 1500, Neuromatic Devices) pressure control box to deliver timed pressure pulses to the pipette during the cleaning and rinsing steps. For pipette cleaning, we chose the maximum intake and expel pressures (-300 mBar, +1,000 mBar) that could be produced by our regulators (intake: 990-005203-005, Parker; expel: 990-005101-015, Parker). Different pressure regulators can also be used. We also programmed standard 3-axis micromanipulators to move the pipette automatically between the experimental preparation location and the two

baths. Finally, we created a graphical user interface (GUI) in LabVIEW (National Instruments) that starts the automatic cleaning procedure with a button click.

3.2.2 HEK293T cell preparation

Human embryonic kidney (HEK293T) cells (American Type Culture Collection, Manassas, VA) were maintained at 37°C and 5% CO2 in Eagle Minimum Essential Medium (MEM) supplemented with 5% FBS, 40μM L-glutamine, 100 U/ml penicillin and 0.1 mM streptomycin. Cells were passaged regularly and split when they reached 70% confluency. Cells used for in vitro electrophysiology experiments were grown on glass coverslips (12x12mm, No.2, VWR). For the pharmacology experiments, HEK293T cells were transfected with α1β2γ2 $GABA_A$ receptors and GFP (Green Fluorescent Protein) using X-tremeGENE (Roche Diagnostics). Patch-clamp experiments were performed 24-72 hours post-transfection in aCSF consisting of (in mM): 161 NaCl, 10 HEPES, 6 D-Glucose, 3 KCl, 1 $MgCl_2$, 1.5 $CaCl_2$ (pH: 7.4). The internal pipette solution consisted of (in mM): 120 KCl, 2 $MgCl_2$, 10 EGTA, 10 HEPES (pH: 7.2-7.3, osmolarity: 290-300 mOsm).

3.2.3 Primary neuron culture

Primary cortical neuronal cultures from E18 Sprague Dawley rat embryos were purchased from Brainbits, LLC preplated on glass coverslips at 16000 cells/cm^2. Cortical tissues were triturated with a Pasteur pipette, and then were plated onto 12-mm glass coverslips coated

with poly-D-lysine. Culture media (NbActiv4, Brainbits, LLC) consisted of Neurobasal/B27 supplemented with creatine, estrogen, and cholesterol. Neurons were maintained at 37°C in a humidified incubator gassed with 95% air and 5% CO_2. Patch-clamp experiments were performed at 8-12 days *in vitro* (DIVs) in aCSF consisting of (in mM): 126 NaCl, 3 KCl, 2 $CaCl_2$, 1.5 $MgSO_4$, 1 NaH_2PO_4, 25 $NaHCO_3$, 25 D-glucose, saturated with 95% O2 and 5% CO2 (pH 7.4). Internal solution consisted of (in mM): 100 K-gluconate, 30 KCl, 10 HEPES, 2 $MgSO_4$, 0.5 EGTA and 3 Mg-ATP (pH 7.4).

3.2.4 Brain slice preparation

All animal procedures were in accordance with the US National Institutes of Health Guide for the Care and Use of Laboratory Animals and were approved by the Institutional Animal Care and Use Committee at the Georgia Institute of Technology. Acute brain slices were prepared from male C57/BL6 mice (aged P30-P60) using the protective recovery method described in detail elsewhere (Ting et al., 2014). Animals were heavily anesthetized with isofluorane and perfused trans-cardially with NMDG solution containing (in mM): 93 N-methyl-D-glucamine (NMDG), 2.5 KCl, 1.2 NaH_2PO_4, 30 $NaHCO_3$, 20 HEPES, 25 Glucose, 5 Na-ascorbate, 3 Na-pyruvate, 10 $MgSO_4.7H_2O$, 0.5 $CaCl_2.2H_2O$ (pH: 7.3-7.4, osmolarity: 300-310 mOsm). Mice were quickly decapitated, the brain was extracted, embedded in 2% agarose and cut into 300 μm coronal slices. The slices were incubated at 34° C in the cutting solution for 10-12 minutes and subsequently transferred to a recovery solution containing (in mM) 92 NaCl, 2.5 KCl, 1.2 NaH_2PO_4, 30 $NaHCO_3$, 20 HEPES, 25 Glucose, 5 Na-ascorbate, 2 Thiourea, 3 Na-pyruvate, 2 $MgSO_4.7H_2O$, 2 $CaCl_2.2H_2O$ (pH:

7.3-7.4, osmolarity: 300-310 mOsm) for at least 60 minutes prior to recording. The recording aCSF consisted of (in mM): 124 NaCl, 2.5 KCl, 1.2 NaH_2PO_4, 24 $NaHCO_3$, 5 HEPES, 12.5 Glucose, 2 $MgSO_4.7H_2O$, 2 $CaCl.2H_2O$. The internal pipette solution consisted of (in mM): 135 K-Gluconate, 10 HEPES, 4 KCl, 1 EGTA, 0.3 Na-GTP, 4 Mg-ATP, 10 Na_2-phosphocreatine, 0.2 % w/v biocytin (pH: 7.2-7.3, osmolarity: 290-300 mOsm).

3.2.5 In vitro patch-clamp recording

Recordings in HEK cells, cultured neurons and brain slices were performed using standard *in vitro* electrophysiology systems (either SliceScope Pro 1000, Scientifica Ltd. or Axiovert 200, Zeiss). Borosilicate pipettes were pulled on a horizontal puller (P-97, Sutter Instruments) to a resistance 4-8 MΩ. Signals were acquired using Multiclamp 700B (Molecular Devices), and digitized at 10 kHz using a data acquisition board (NI USB-6221, National Instruments or Digidata 1322A, Molecular Devices). The data were saved to a computer using either a custom program written in LabVIEW or pClamp 9 (Molecular Devices).

For pharmacology experiments, drugs were applied using a rapid solution changer (RSC-160, BioLogics Science Instruments) connected to a 10-channel infusion pump (KD Scientific Inc) and controlled by pClamp 9. GABA concentration-response assays were performed by exposing each whole-cell patch to 8 increasing concentrations of GABA (0.3, 1, 3, 10, 30, 100, 300 and 1,000 μM) for 2 s with an 8 s washout between concentrations. Whole-cell currents were recorded in voltage clamp mode at -60mV, digitized at 200 Hz

and filtered at 100 Hz. Peak current responses to the concentrations were fit to the Hill equation:

$$I = I_{pk} \frac{[GABA]^h}{[GABA]^h + EC_{50}^h}$$

where I is the peak current, I_{pk} is the maximal evoked current, EC_{50} is the half-maximal response concentration, and h is the Hill coefficient. Adding Alconox to the internal solution did not appreciably change the pH or the osmolarity of the solution (ΔpH=0.02, ΔOsm=8 mOsm).

For cell quality measurements, seal resistance was recorded at 10 Hz from the moment of positive pressure release on a target cell, and until the gigaseal (defined as R ≥ 1GΩ) was held for at least 1 min. Seal resistance traces were smoothed with a 2.5 s moving average filter. The resistance at the end of the 1 min time interval was considered to be the ultimate gigaseal resistance (R_{GS}). The time to reach the gigaseal (T_{GS}) was calculated as the time elapsed between R = 20 MΩ and R = 1 GΩ if the gigaseal was successful; otherwise, T_{GS} was undefined and not included in analysis. In HEK cells and brain slices, access resistance (R_a) was measured in voltage clamp mode after pipette capacitance compensation, using a custom-written LabVIEW algorithm. In brain slices, a whole-cell was considered successful when the holding current was ≥ -250 pA, and access resistance was stable.

3.2.6 In vivo Autopatching

Methodology to perform automated in-vivo whole-cell patch-clamp electrophysiology has been previously described (Kodandaramaiah et al., 2016). Briefly, 3 male C57/BL6 mice (aged P30-P60) were anesthetized and maintained using isoflurane with a vaporizer (Datex-Ohmeda Isotec 5) at 1% concentration and checked periodically for response to toe-pinch. Mice were affixed in a stereotaxic apparatus (Kopf) and a head plate implant attached, followed by opening of a craniotomy 1 mm wide above the barrel cortex (centered 0.83 mm posterior and 3.0 mm lateral to bregma) using previously described protocols (Margrie et al., 2002). Once opened, the craniotomy was superfused with sterile saline throughout the experiment to keep the tissue moist. The anesthetized animals were then head-fixed using a custom holder composed of optical posts and plate clamps (Eksma Optics 830-0055). Pipettes, internal solution, amplification and digitization were the same as in the *in vitro* preparation.

3.2.7 Scanning Electron Microscopy

To prepare pipettes for SEM imaging, the internal solution was first drained using a micropipette (Eppendorf epTIPS, 20 μL). Pipettes were then tip-filled with DI water for 60 s by applying a strong vacuum (-300 mBar) in order to dilute any remaining internal solution at the tip and prevent the formation of salt crystals that would compromise image quality. Pipettes were then placed tip-down in a dessicator and left to dry overnight. They were then mounted to a custom-made sample holder and imaged with a Hitachi SU8230 SEM.

3.2.8 ESI-MS

Preparation of samples for ESI-MS was performed no more than 2 days prior to analysis. Standard patch pipettes were filled with 20 μL de-ionized (DI) water and cleaned using the standard cleaning procedure either once or ten times consecutively. In order to minimize potential noise in the intensity signal due to cellular debris, these pipettes were not used for patch-clamp recordings. In some cases, 67 μg/mL Alconox was added to the pipette internal solution. Pipette tips were carefully broken and all fluid was collected into microcentrifuge tubes (Safe-Lock, Eppendorf) under positive pressure (200 mBar). To find the detection limit, we created concentration standards by dissolving Alconox in DI water at 17.4, 174, 1,174 and 11,740 ng/mL. The pipette fluid and the Alconox standards were then transferred to individual vials (Waters Technologies) for analysis.

ESI-MS analysis was performed using Micromass Quattro LC in negative-ion mode. For each vial, the sample was infused at a rate of 10 μL/min and mixed with 50:50 water:acetonitrile with 10 mM ammonium acetate. The cone and capillary voltages were varied to get the best intensity for the [M-H]- ion, and then the collision voltage was varied to get the highest intensity for the product ion.

3.2.9 Histology and imaging

Immunohistochemistry and imaging was performed as previously described (Wu et al., 2016). Briefly, brain slices were fixed in 4% (w/vol) paraformaldehyde for 2-10 hours and subsequently transferred to phosphate-buffered saline (PBS). The slices were first

incubated for 30 min at room temperature in a blocking solution of 5% (vol/vol) normal goat serum, 0.5% (vol/vol) Triton X-100, diluted in PBS. The slices were then incubated (2 hrs) in the staining solution consisting of 1 μg/mL streptavidin-Alexa 594, 0.5% (vol/vol) Triton X-100 in PBS. After washing with PBS, the slices were mounted on charged glass slides, sealed with nail polish, and imaged using a confocal microscope (Zeiss) with 10× and 40× magnification.

3.3 Results

3.3.1 Cleaning patch-clamp pipettes

Patch-clamp pipettes are typically considered to be single-use due to the membrane residue that builds up on the pipette walls (Figure 11a); our pipette cleaning technique can be used to clean that debris. After a recording attempt in an experimental preparation, pipette cleaning is accomplished in three steps. First (Figure 11b, step i), the pipette is moved to a bath containing a cleaning agent. We reasoned that a cleaning agent could be pneumatically taken up into the pipette tip in order to remove adherent cellular debris resulting from a previous patch-clamp trial. The height of a typical lipid 'bleb' that forms in the pipette tip during a gigaseal is 30-60 μm (Milton and Caldwell, 1990). When applying a high vacuum (-300 mBar) to the pipette, fluid is taken up at a rate of ~760 pL/s based on pipette inner diameter of 1 μm (Sánchez et al., 2008). To reach a height of 60 μm in the pipette, 6.2 pL of fluid must be taken up, which would theoretically require approximately 8.2 ms; however, to account for tubing compliance and to ensure the cleaning agent reaches the bleb height at a high concentration, we initially apply the vacuum for 4s, which draws up

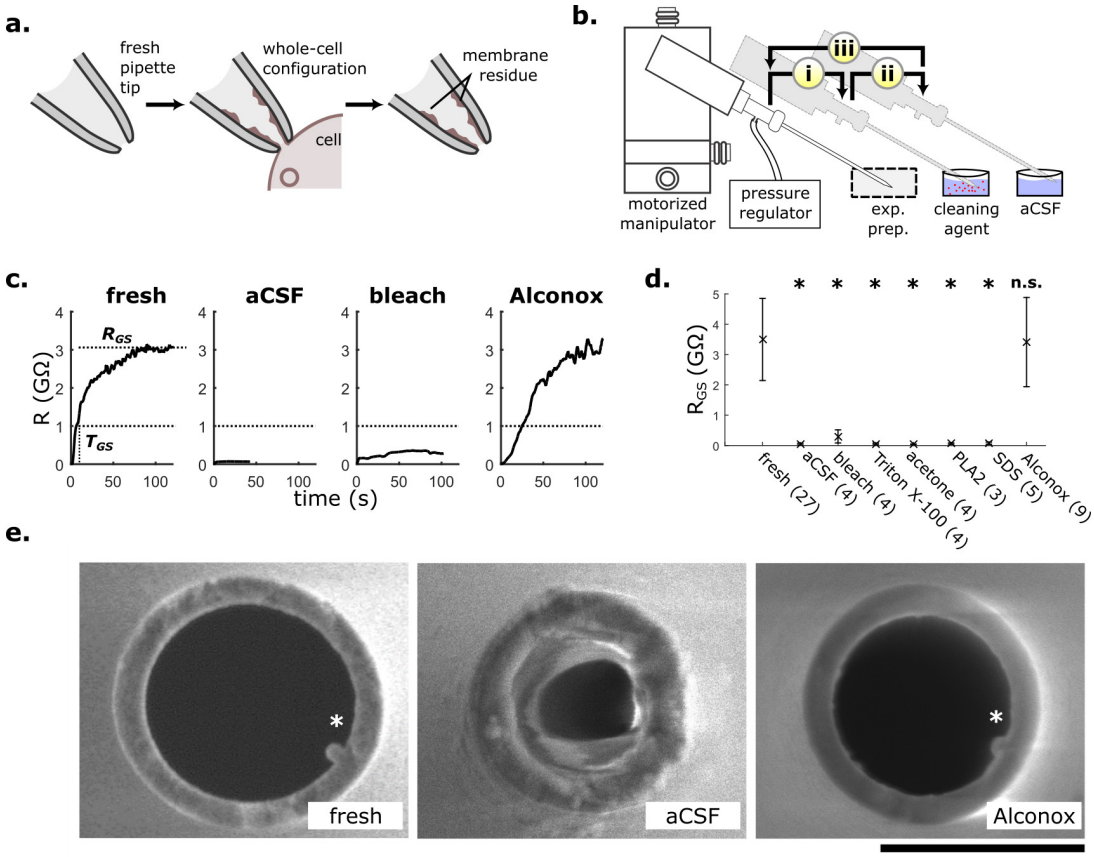

Figure 11: Cleaning patch-clamp pipettes a. During a whole-cell patch-clamp recording, cell membrane bonds to the inner walls of the pipette. After the recording is terminated, membrane residue remains, preventing the pipette from being used for subsequent recordings. b. To clean, (i) the pipette is moved from the experimental preparation to a wash bath where a cleaning agent is cycled within the tip, (ii) then to a rinse bath where the remaining cleaning agent is expelled into aCSF, (iii) and returned back to the experimental preparation. c. Representative gigaseal formation traces. When using contaminated pipettes cleaned with Alconox, a multi-GΩ seal forms reliably, as would be expected when using a fresh pipette. On the other hand, cleaning with aCSF (artificial cerebrospinal fluid) and bleach does not result in gigaseal formation. R_{GS}: maximum gigaseal resistance, T_{GS}: time (s) to reach 1 GΩ (horizontal dashed line) d. Of the six tested detergents and aCSF, only Alconox reliably achieved gigaseal resistances comparable to those of fresh pipettes ($p<0.001$; one-way ANOVA with Dunnett's post-hoc test. *: $p<0.001$; n.s.: not significant, $p>0.9$). Data shown as mean ± s.d.; n for each cleaning agent is shown in parentheses. PLA2: Phospholipase A2; SDS: Sodium Dodecyl Sulfate. e. Scanning Electron Microscopy (SEM) images of pipette tips. The Alconox-cleaned pipette tip resembles that of the fresh pipette. The pipette tip cleaned with aCSF is visibly contaminated with cell membrane residue. Pipette filament denoted with *. Scale bar: 1 μm.

3 nL of the cleaning agent. After this initial uptake, the cleaning agent is pneumatically cycled within the pipette tip (-300 mBar, +1,000 mBar for 1s each, 5 repetitions total) to physically agitate glass-adhered tissue. To expel the original cleaning agent volume (3 nL) out of the pipette at 1,000 mBar, only 1.3 s are theoretically required. We add a ~10x safety factor to ensure the removal of cleaning agent molecules that may have diffused further up the pipette. We thus expel the fluid for 10 s. In the second step of pipette cleaning (Figure 11b, step ii), the pipette is moved from the cleaning bath to a bath containing standard artificial cerebro-spinal fluid (aCSF). Any remaining cleaning agent in the pipette is expelled (+1,000 mBar for 10s). Lastly (Figure 11b, step iii), the pipette is moved back to the experimental preparation. Pipettes can then be immediately reused for a subsequent patch-clamp attempt. Refilling a pipette with internal solution is unnecessary because pipettes are commonly filled with enough solution for hundreds of attempts. All moving and cleaning steps together require 60 seconds.

Alconox was the only cleaning agent that enabled pipettes to be reused. We performed whole-cell patch-clamp recordings on human embryonic kidney (HEK293T) cells using fresh (previously unused) pipettes, cleaned them with one of six different commonly available glassware cleaning agents (see Appendix B for detergent list) as well as a control solution (aCSF), and attempted to patch another cell with the same pipette. On the second attempt, pipettes cleaned with Alconox, but not with any other cleaning agent, produced gigaseal resistances (R_{GS}) that were not significantly different from those produced by fresh pipettes (Figure 11c,d). Successful whole-cell recording rates were not different between fresh and Alconox-cleaned pipettes (fresh = 92.6%, Alconox-cleaned = 88.9%, p=0.87, Fisher's exact test; other detergents and aCSF = 0%). Gigaseals were held for 1-2 min to

ensure stability. No gigaseals were spontaneously lost during this time in either fresh or Alconox-cleaned pipettes. When using Alconox-cleaned pipettes, an outside-out patch reliably formed after withdrawing the pipette from the cell, as would be expected if using fresh pipettes (Hamill et al., 1981). Using scanning electron microscopy (SEM), we confirmed that the tip of the pipettes was being cleaned using Alconox but not aCSF (Figure 11e). Further, pre-cleaning fresh pipettes in Alconox had no effect on gigaseal formation (Figure 12). Unless stated otherwise, all subsequent experiments used Alconox.

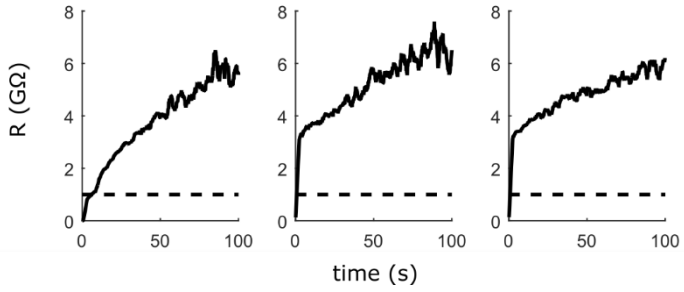

Figure 12: Three representative gigaseals obtained with fresh pipettes that were pre-cleaned in Alconox. Pre-cleaning did not hinder the formation of stable gigaseals.

Pipettes could be reused 10 times consecutively with no degradation in recording quality if they were cleaned between each patch-clamp attempt (Figure 13a). We successfully patched 84 HEK293T cells (of n=88 attempts including 1 fresh and 10 reuses; success rate = 95%) using 8 pipettes, and found no effect of the number of reuses on gigaseal resistance (R_{GS}), the time to reach 1 GΩ (T_{GS}), and the access resistance of the patched cell (R_a) for each trial (one-way repeated-measures ANOVA with number of reuses (1-10) as predictor; R_{GS}: $F_{10,40}$=0.99, p=0.46, n=8; T_{GS}: $F_{10,40}$=0.36, p=0.96, n=5, R_a: $F_{10,40}$=0.72, p=0.70, n=5).

Notably, even when pipettes failed to reach a gigaseal (e.g., R_{GS} < 1 GΩ on third, fourth reuse in Figure 13a), they were successfully cleaned and reused again, suggesting that gigaseal failures did not irreversibly contaminate the pipette tip.

Electrical resistance is commonly used to estimate pipette tip opening size prior to performing the patch-clamp recording. Higher resistances indicate a smaller opening. Therefore, increases in electrical resistance could be caused by obstructions on the pipette tip. To assess whether cleaning reduced the amount of obstructions, we measured resistance twice: once immediately after completing a whole-cell recording (before cleaning) and once more after cleaning. As expected, pipette resistance before cleaning was higher than after (Figure 13b; before: median = 5.93 MΩ, range: 4.49 to 15.0 MΩ; after: median = 5.77 MΩ, range = 4.46 to 6.28 MΩ; $p<0.05$, Wilcoxon signed-rank test). Over 10 reuses, the resistance of the pipette did not change significantly (Figure 13c; $p\geq0.19$ for 1^{st} -10^{th} reuse, n=8, Wilcoxon signed-rank test). Together, these results suggest that cleaning eliminates residue obstructions on the pipette tip over ten reuses.

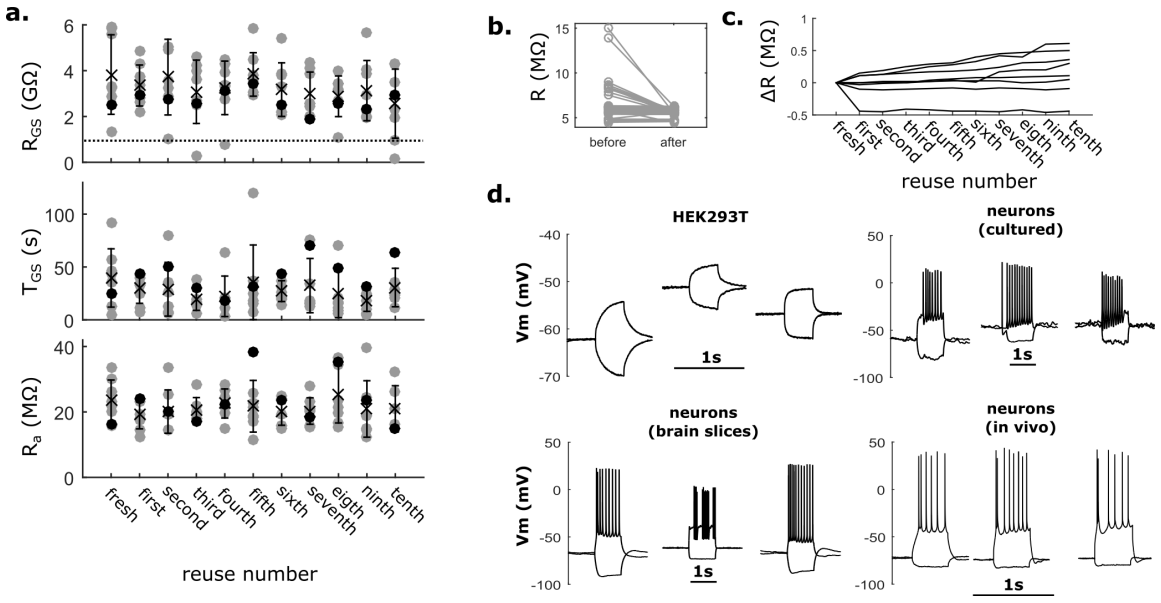

Figure 13: Pipettes can be successfully reused ten times. a. Recording quality parameters R_{GS}, T_{GS} (defined in Fig. 1c) and R_a (whole-cell access resistance) do not decrease over ten reuses of the same pipette (n=8 pipettes). Dashed line: 1 GΩ (threshold for gigaseal). Gray circles: individual trials; black circles: representative experiment with a single pipette. Data shown as mean ± s.d. b. Pipette resistance before and after cleaning with Alconox (n=88 pairs, 8 pipettes). c. Change in pipette resistance from first to tenth reuse. After 10 reuses, resistance changed (ΔR) by median: 0.175 MΩ, max: 0.61 MΩ, min: -0.44 MΩ from fresh pipette. d. Representative whole-cell responses to step current injections in different experimental preparations. Recordings from HEK293T cells were obtained from the representative experiment (black circles) in a. In each set, a single pipette is used for all three whole-cell recordings. In all preparations pipettes were reused up to ten times.

Using a single pipette for each experimental preparation, we were able to repeatedly patch-clamp in neuron cultures, acute brain slices, and *in vivo* (Figure 13d). Cleaning did not visibly alter action potential generation in these experiments. In brain slices, successful gigaseals and successful whole-cell recordings were attained at similar rates between fresh and cleaned pipettes (gigaseals: fresh=14/18 (78%), cleaned=38/46 (82%), p=0.73; whole-cell recordings: fresh=7/18 (39%), cleaned=22/46 (48%), p=0.58, Fisher's exact test). In slices, we recorded from neurons for 20 min, and found that the access resistance, input resistance, and holding current remained stable in most cells across that time (Appendix C), indicating that whole-cell recordings obtained using cleaned pipettes are stable over the duration of a typical experiment. In a separate round of experiments, we verified that the morphology of neurons can successfully be recovered and does not worsen as the pipette gets reused (Figure 14). *In vivo*, we used the Autopatcher (Kodandaramaiah et al., 2012) to patch-clamp repeatedly with the same pipette in mouse barrel cortex (depths: 400-600 um). Beyond 10 reuses, we did not perform a systematic study of pipette longevity; however, a pilot experiment in HEK cells confirmed our suspicion that pipettes could not be reused indefinitely, when three consecutive failed patch-clamp attempts occurred after 26 reuses (Figure 15). Further developments of the pipette cleaning technique are addressed in Appendix D.

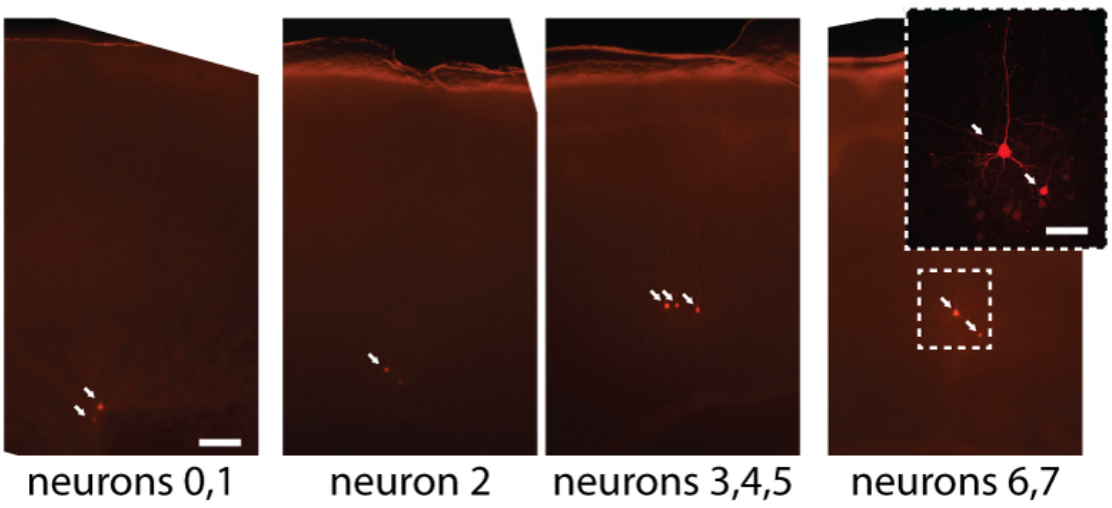

Figure 14: Histology of cells patch-clamped with the same pipette (arrows). All four slices were imaged with the same parameters (light level, exposure) for consistency. Inset: fine dendritic morphology of neurons 6,7 is visible, indicating that pipette cleaning is compatible with morphological reconstructions. Scale bar: 100 µm in four main panels, 50 µm in inset. Images courtesy of Sofia Switzer.

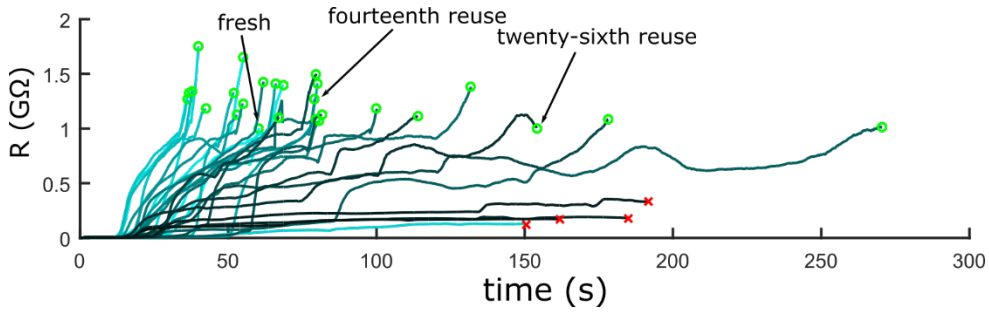

Figure 15: Gigaseal resistances of thirty reuse attempts with a single pipette. The pipette was successfully reused twenty-six times (green circles: R > 1 GΩ). The pipette did not reach a gigaseal on the fifth reuse, and consecutively on twenty-seventh through thirtieth reuse (red circles: R < 1 GΩ). Gigaseal attempts are color-coded from light to dark indicating the number of times the pipette was used. After approximately fourteen reuses, the time to form a gigaseal increases.

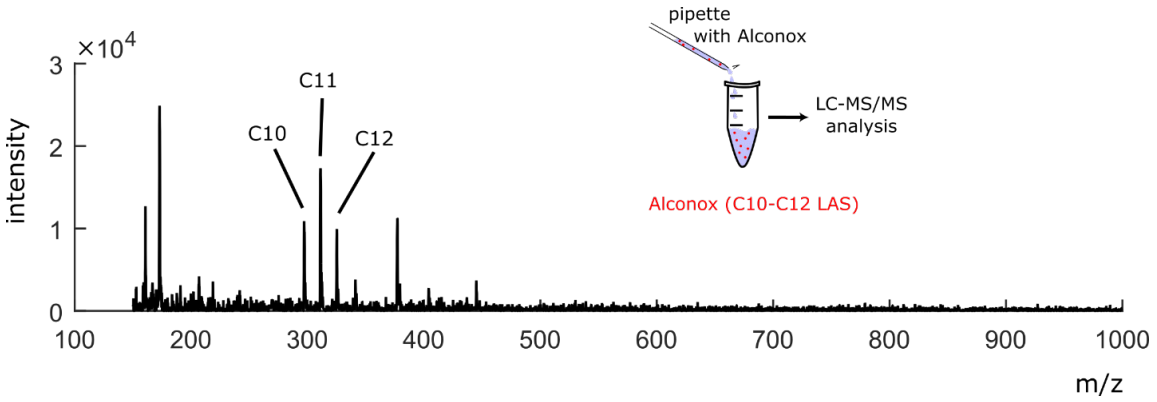

Figure 16: ESI-MS spectrum characterization of pipettes containing 67 µg/ml Alconox dissolved in DI water. The main cytotoxic components of Alconox, C10-C12 LAS compounds were identified in the solution (C10: expected m/z: 297.1, found: 297.1; C11: expected m/z: 311.2, found: 311.1; C12: expected m/z: 325.2, found: 325.2).

3.3.2 Verifying detergent removal after pipette cleaning

A major concern of using Alconox to clean pipettes is that residual surfactants in the pipette could damage the cell or affect its normal biophysical activity during a patch-clamp recording. Alconox is composed of 33-43% sodium bicarbonate, 10-20% sodium (C10-C16) linear alkylbenzene sulfonate (LAS), 5-15% sodium tripolyphosphate, 5-15% tetrasodium pyrophosphate, 1-10% sodium carbonate, and 1-5% sodium alcohol sulfate. We chose LAS, a commonly-used surfactant, as a proxy for measuring Alconox concentration remaining after rinsing.

We measured the amount of Alconox remaining after cleaning using electrospray ionization mass spectrometry (ESI-MS). Only C10-C12 LAS was found in significant quantities in the Alconox solution (Figure 16), so we focused our analysis on this family of compounds (Figure 17a). We found no traces of LAS in pipettes cleaned once or ten

times (Figure 17b, c top, middle), while the instrumentation detection limit was found to be 174 ng/mL (c (bottom)). Thus, less than 174 ng/mL of Alconox remained in the pipettes after the cleaning procedure. As a control, we ensured that LAS could still be detected using ESI-MS when purposefully introduced in small concentrations into the pipette (Figure 16).

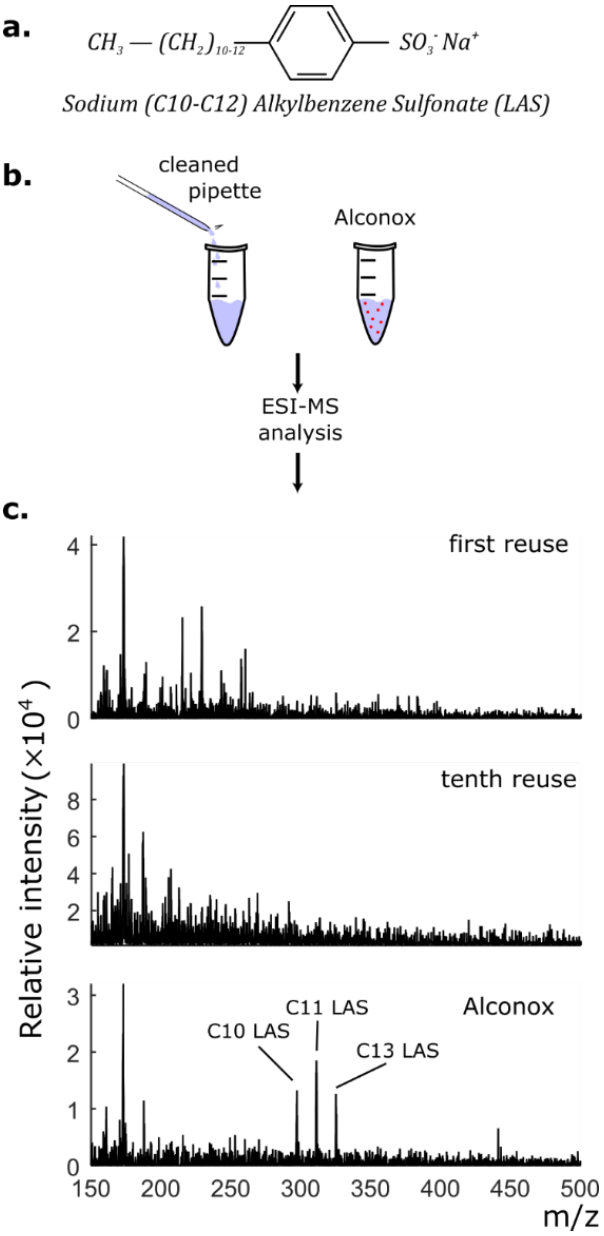

Figure 17: Detection of linear alkylbenzene sulfonate (LAS) in cleaned pipettes using electrospray ionization mass spectrometry (ESI-MS). a. LAS is the prevalent cytotoxic ingredient in Alconox. Alconox is composed of LAS with carbon chains lengths 10-12 (C10-C12). b. The contents of cleaned pipettes were collected in vials after either one or ten reuses. Known amounts of Alconox were analyzed to find the detection limit. c. ESI-MS spectrum. C10-C12 LAS is not detectable in pipettes reused once or ten times (top, middle) but is detected in an Alconox solution (174 ng/mL Alconox in DI water, bottom), indicating that less than 174 ng/mL of Alconox remains in the pipettes after cleaning. C10: expected m/z: 297.1, found: 297.3; C11: expected m/z: 311.2, found: 311.2; C12: expected m/z: 325.2, found: 325.1.

Any effect of trace amounts of Alconox in cleaned pipettes on cell receptor pharmacology would be highly undesirable. Residual LAS could disrupt gigaseal formation, thus decreasing signal quality or, more subtly, interact with amphipathic allosteric modulatory pockets on receptors, thus covertly compromising pharmacological experiments. The γ-aminobutyric acid type A Receptor ($GABA_AR$) is highly sensitive to extracellular application of surfactants (Yang and Sonner, 2008), including LAS (Machu et al., 1998); however, its intracellular effects have not been thoroughly studied. Nevertheless, we reasoned that $GABA_AR$ could serve as an indicator of adverse effects of Alconox. We used HEK293T cells expressing $GABA_AR$ as a model system to verify that cleaned pipettes are pharmacologically inert. We whole-cell patch-clamped using fresh and cleaned pipettes, and fit the measured whole-cell current responses to increasing concentrations of GABA (O'Toole and Jenkins, 2012) to the Hill equation (Figure 18a). Neither the peak evoked current (I_{pk}), the Hill's coefficient (h), nor the half maximal effective concentration (EC_{50}) metrics changed as a function of reuses (linear regression model, H_0: slope $\neq$ 0; I_{pk}: p=0.998, 95% CI: -318 to 317 pA; h: p=0.719, 95% CI: -0.065 to 0.093; EC_{50}: p=0.751, 95% CI: -6.75 to 4.90). This finding demonstrates that GABA concentration-response curves of the patch-clamped cells do not change on a population level as a function of the number of times a pipette has been reused (Figure 18b, c). Overall, pharmacology results obtained using fresh pipettes were indistinguishable from those obtained using cleaned pipettes, suggesting no effect of trace amounts of Alconox on normal receptor function of $GABA_ARs$.

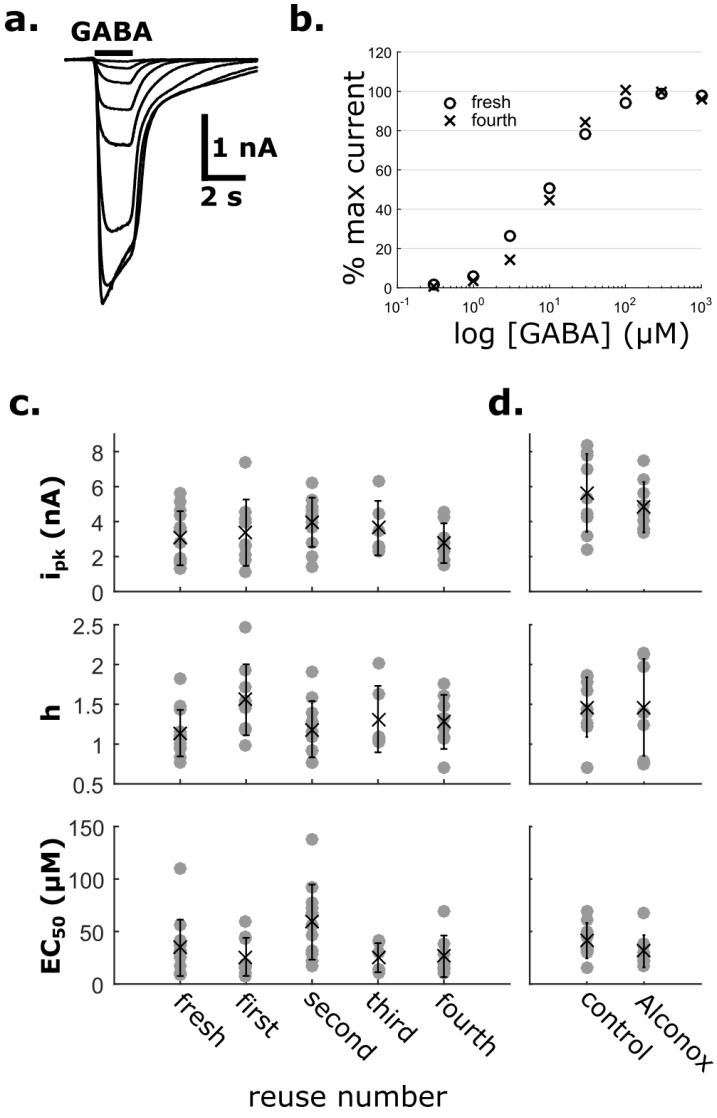

Figure 18: Pipette cleaning in conjunction with $GABA_AR$ pharmacology. a. Representative current traces recorded by whole-cell patch-clamp recording of HEK293T cells transfected with α1β2γ2s $GABA_ARs$. Black bar denotes GABA application b. Representative normalized peak current responses to different GABA concentrations. The response captured with a fresh pipette is similar to that captured with a used pipette (fourth reuse). c. Dose response characteristics of cells patched with fresh and reused pipettes. i_{pk}: peak evoked current; h: Hill coefficient; EC_{50}: half-maximal response concentration. No change in the three characteristics is observed over four reuses. d. A low dose of Alconox (67 μg/mL, or equivalently, 385× the detection limit of remaining Alconox in the pipette after cleaning) in the internal solution does not affect dose response characteristics. Data collection was performed in collaboration with Olivia Moody (Emory University).

We also found that even if small amounts of Alconox remain in the pipette after cleaning, they do not impact gigaseal formation or $GABA_AR$ pharmacology. When 67 μg/mL of Alconox (385× the ESI-MS detection limit) was intentionally dissolved in the pipette internal solution, gigaseals were still reliably achieved in all tested pipettes (n=9). No pharmacological difference between these pipettes and fresh ones was detected (Figure 18d; I_{pk}: p=0.37; h: p=0.99; EC_{50}: p=0.19). On the other hand, when a much larger dose, 10 mg/mL Alconox (0.5× the concentration in the wash bath) was added to the pipette, gigaseals did not form and the targeted cell exhibited clear apoptotic blebbing (Figure 19).

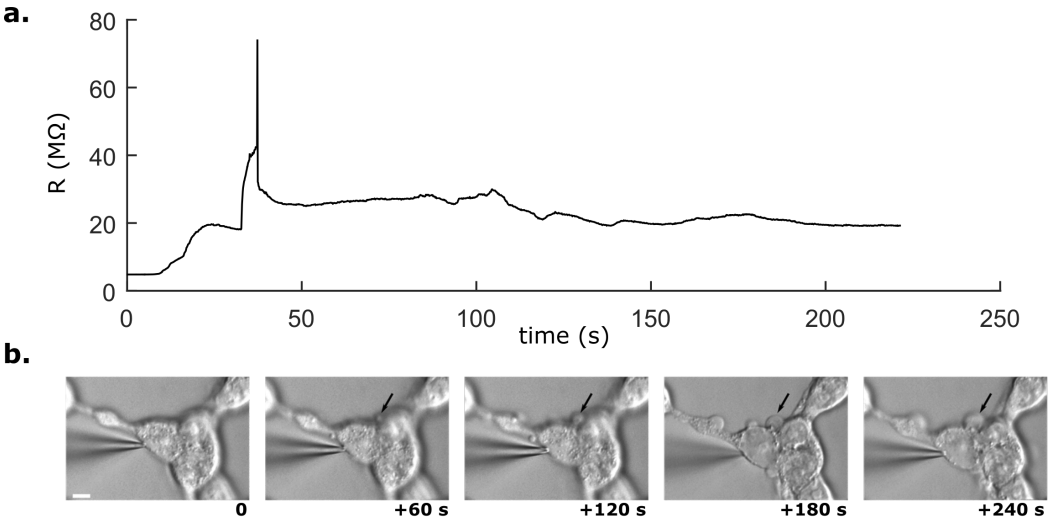

Figure 19: A pipette containing a high dose (10 mg/mL) of Alconox damages the target cell during a patch attempt. a. A gigaseal fails to form after >3 min, suggesting that Alconox is destroying cell membrane. b. Cell apoptosis during the gigaseal process is evident. Arrow indicates blebs forming on the cell. Scale bar: 10 μm.

3.4 Discussion

Discovering that pipettes could be reliably cleaned and reused multiple times was surprising given the dogmatic, decades-long practice of replacing pipettes after each patch-clamp attempt. Our simple, fast, and automated procedure consists of dipping pipettes into a commercially-available detergent, Alconox, followed by rinsing in aCSF. We demonstrated the effectiveness of this cleaning method by reusing pipettes 10 times, with no decrease in whole-cell recording quality in cultured cells, acute brain slices, and in vivo. After cleaning, the residual Alconox mass concentration in the pipettes was quantified to be less than 174 ng/mL, and shown to have no pharmacological effect on $GABA_ARs$. Since pipette cleaning is automatic, we integrated it into the Autopatcher to perform unattended, sequential patch-clamp recordings on HEK293T cells in vitro and neurons in vivo.

Alconox is composed of a surfactant, emulsifier and water softener, and in solution, it interacts with cell membranes bound to the glass pipette tip. These three ingredients solubilize adhered lipids, stabilize the lipid micelles in solution, and enhance surfactant effectiveness, respectively. After testing various cleaning agents, we chose Alconox based on empirical observation; it was not evident from chemical principles why only Alconox sufficiently cleaned pipettes to enable their reuse. Interestingly, Kao et al. used bleach to successfully clean planar borosilicate patch-clamp chips up to five times for whole-cell recording (Kao et al., 2012); yet in our experiments using conventional pipettes, bleach did not work, suggesting that the geometry of the experimental preparation may influence cleaning effectiveness. Overall, the precise mechanism of how cell membranes bond with glass during a gigaseal is still not understood despite notable efforts (Milton and Caldwell, 1990; Suchyna et al., 2009), making it difficult to devise a cleaning strategy from basic

principles. Indeed, our cleaning procedure, while functional, was not thoroughly optimized to minimize cleaning time and maximize the number of reuses. A detailed biochemical study of gigaseal formation could greatly inform such optimization efforts.

While we have demonstrated that cleaning does not affect the ion channel pharmacology of $GABA_ARs$, we have not exhaustively tested the method in cells expressing other proteins. While several studies have characterized the effects of extracellularly applied detergents on various receptors (Berger, 2016; Machu et al., 1998; Oz et al., 2004), the intracellular effect of LAS in small concentrations is not well-understood. Thus to verify general applicability, the method should be validated using more channels, receptors, and cell types.

For many patch-clamp experiments, pipette internal solution contains ingredients that degrade over time if not refrigerated (e.g. Adenosine 5′-triphosphate magnesium salt, Guanosine 5′-triphosphate sodium salt hydrate, phosphocreatine); thus, we would expect that pipettes after multiple cleanings will have reduced concentrations of these ingredients. We hypothesize that maintaining a chilled (i.e., 4°C) environment for pipette and internal solution, or devising a method for replacing internal solution after every trial could mitigate this deleterious effect.

The cleaning process is typically faster than manually swapping pipettes (i.e., 1 min versus approximately 2 min) and does not depend on operator experience, dexterity, or fatigue level. It requires no complex hardware additions to existing electrophysiology setups and no expensive or caustic reagents. Therefore, it can be readily integrated into different experimental preparations and coupled with existing techniques that complement patch-

clamp such as extracellular stimulation (Edwards et al., 1989), two-photon microscopy (Kitamura et al., 2008), and optogenetics (Boyden et al., 2005). Pipette cleaning also facilitates experiments requiring specialized pipette tips. Various tip polishing techniques (using heat, pressure (Benedusi et al., 2011; Goodman and Lockery, 2000), or focused ion beam (Malboubi et al., 2010)) and coatings (Andrásfalvy et al., 2014; Ishikawa et al., 2010) can improve the ability to obtain recordings and their quality; however, these techniques are typically too time-consuming to be routine. Cleaning could also greatly facilitate simultaneous multi-patch (i.e. dual, quadruple, octuple, etc.) experiments that have been instrumental in elucidating single-cell connectivity patterns in the brain. Since cleaning is faster than manual pipette replacement and requires no human intervention, it could increase the number and duration of simultaneous recordings.

CHAPTER 4. WALK-AWAY AUTOMATION OF IN VITRO PATCH-CLAMP ELECTROPHYSIOLOGY

4.1 Introduction

The study of neuronal structure and function on a single-cell level is critical to understanding the brain. Much of the complexity associated with the brain is generated on the single-cell level: the diversity in neuronal morphology, electrical firing patterns, and connectivity eventually gives rise to emergent network phenomena such as consciousness. However, neuronal diversity presents a major technical challenge: namely, because there are dozens of distinct brain areas with many cell types, and low inter-neuronal connection probabilities, hundreds to thousands of cells must be systematically sampled to reach conclusions about neuronal structure and function.

The whole-cell patch-clamp recording technique (Hamill et al., 1981) has been utilized to discover fundamental properties of neuronal cell types and connections (Jiang et al., 2015; Markram et al., 1997). However, the technique is typically performed manually, resulting in low throughput. To profile single cells using whole-cell recording, electrophysiologists control micromanipulators to steer pipettes to cells of interest, apply suction (typically, by mouth) to form a seal with the cell membrane, and replace the pipette after every attempt. If a study of connections is required, multiple whole-cell recordings must be performed simultaneously, with as many simultaneous recordings as possible to maximize the number of sampled connections (Perin and Markram, 2013; Wang et al., 2015). This increases the

complexity of the experiment because investigators can only control one manipulator at a time, making multi-patch experiments significantly more time-consuming, and technically difficult than single-patch experiments.

Several parts of the whole-cell patch-clamp technique have been automated by us and other groups; meanwhile, other steps in the process have evaded automation efforts. Perin and Markram created the first computer-assisted system that enabled them to patch-clamp up to 12 neurons simultaneously (Perin and Markram, 2013). The system automated pressure control, aspects of manipulator positioning, and microscope stage focusing to enable one user to control up to 12 manipulators easily. Our group has previously developed the Autopatcher, a robotic system for blind patch-clamp in-vivo (Kodandaramaiah et al., 2012, 2016). We have also adopted it to work in brain slices (Wu and Chubykin, 2017; Wu et al., 2016). However, in these solutions and others (Campagnola et al., 2014; Suter et al., 2010), some portions of the patch-clamp experiment are not automated. Notably, a trained user still needs to be always present at the electrophysiology rig to conduct portions of the experiment: to guide the pipette to the cell, to find the next cell, and to replace the pipette at the end of the trial.

Accordingly, we have devised an approach that enables automation of whole-cell recordings that is “walk-away”. In contrast to previous methods, which have automated portions of a single trial, our robotic system, called “patcherBot”, performs patch-clamp sequentially on multiple cells, without human intervention. This enables unattended operation for 45 minutes or more. We leveraged machine vision techniques for automated cell detection, tracking, and pipette identification, enabling the automation of the final, most difficult manual aspects of patch-clamp recording. The system was validated by

performing the first sequential patch-clamp of multiple cultured cells adherent on a cover slip, as well as neurons embedded in brain tissue slices without human intervention. We also demonstrate the ability of the system to perform multi-patch studies for studying neuronal connectivity.

4.2 Methods

4.2.1 Hardware

The robotic system was based on a conventional electrophysiology rig, as in our previous publications (Wu et al., 2016). Briefly, the electrophysiology rig was based on the SliceScope Pro 3000 (Scientifica Ltd). We performed two main modifications to enable full automation. First, we built a custom multi-channel pressure controller that can set pressure on up to four pipettes. For each pipette, pressure was controlled by a -10 to +10 psi regulator (part #: QPV1TBNEEN10P10PSGAXL, ProportionAir) using an analog (0-10 V) control signal. The control signal for each regulator was generated by a microcontroller (Arduino Uno, Arduino) via a digital-to-analog controller (MAX539, Maxim Integrated). Individual pressure regulators for each pipette were necessary to ensure that different pressures could be maintained on each pipette, e.g. if one pipette is forming a seal (atmospheric or negative pressure), and another is approaching a neuron (positive pressure). Second, we custom-machined an electrophysiology chamber (Figure 20) with small side chambers for cleaning and rinsing solutions. The chamber could be used for up to four pipettes.

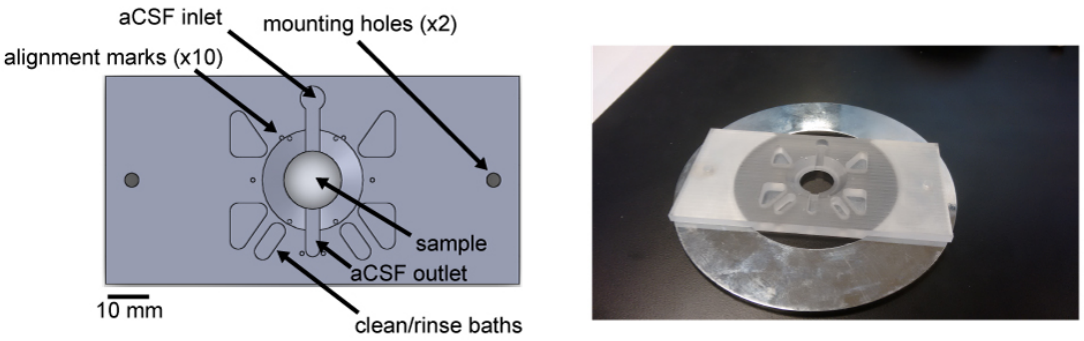

Figure 20: In-vitro electrophysiology chamber for cleaning. a. Computer-aided design (CAD) mockup of the chamber (top view). The sample (brain slice or cover slip with cultured cells) is placed in the center chamber, perfused by aCSF flowing from the inlet to the outlet. The six clean/rinse baths around the main chamber are filled with the cleaning solution (Alconox) or the rinse solution (aCSF). Only six chambers are necessary for four pipettes because the dish is made such that all manipulators can share one cleaning dish. b. Manufactured electrophysiology chamber (polycarbonate, ProtoLabs) mounted on a metal ring that will be mounted on a motorized stage.

4.2.2 Software

A finite state machine architecture was implemented to repeatedly patch-clamp user-selected cells (Figure 21). The overall steps in the block diagram were unchanged between HEK cell preparations and brain slice preparations; however, specific details of various steps were different and will be addressed. In this chapter, specific attention will be paid to the new "initialize", "calibrate" and "approach cell" states; however, a brief discussion of the other states will be presented.

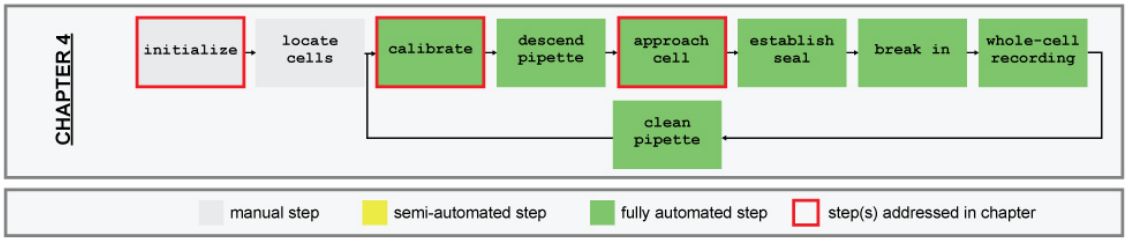

Figure 21: Top-level state machine architecture of the patcherBot. The major advances in this chapter will be the manual "initialize" state, and the automated "calibration" and "approach cell" states.

4.2.3 Initialization

The patcherBot software includes a graphical user interface (GUI) (Figure 22) where the user performs an initialization procedure consisting of a manual calibration step and a target selection step. The initial calibration steps must be performed only once for every pipette. They involve first, centering the pipette under the objective to relate the coordinate system of the pipette to that of the stage. At this time, patcherBot also stores an image of the pipette to be used for machine vision. Second, the user moves the pipette to a "HOME" position outside the bath and then to the clean and wash baths. These steps are necessary for every pipette due to inter-pipette differences in taper and tip geometry. The pipette is subsequently returned to the "HOME" position.

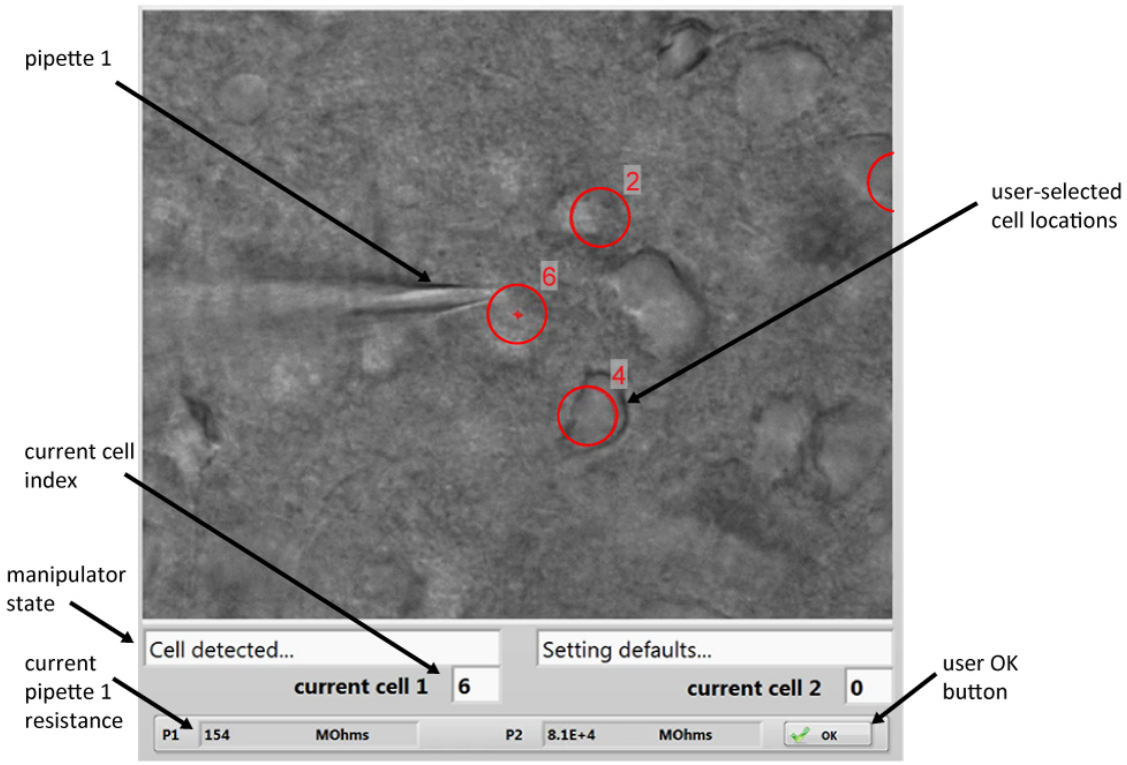

Figure 22: patcherBot GUI. Crosshair denotes camera center point. Circles with numbers denote user-picked cell locations (0, 1, 2, …) in x,y (cell 2 is not visible because it is out of focus in the z plane). In this experiment, pipette 2 was not used; thus the manipulator state did not advance. Since the pipette was not in the bath, its resistance is that of an open circuit. Red circle diameter = 10 µm for scale.

The user then chooses a "parking plane", an XY plane normal to the slice surface defined by $z = z_{park}$ where z_{park} is ideally 20-50 µm above the tissue. Pipettes will "park" on this plane prior to patching in order to perform auto-calibrations. Finally, the user picks any number of cells (up to 10 per pipette for best results, Figure 22). Selected cells are outlined with a red circle and an index number. When a cell is picked, the program stores the coordinates of each cell as well as an image of the cell (200 x 200 pixels) for later

machine vision use. Overall, the initialization procedure takes ~5 min for single-manipulator operation and ~8 min for dual-manipulator operation.

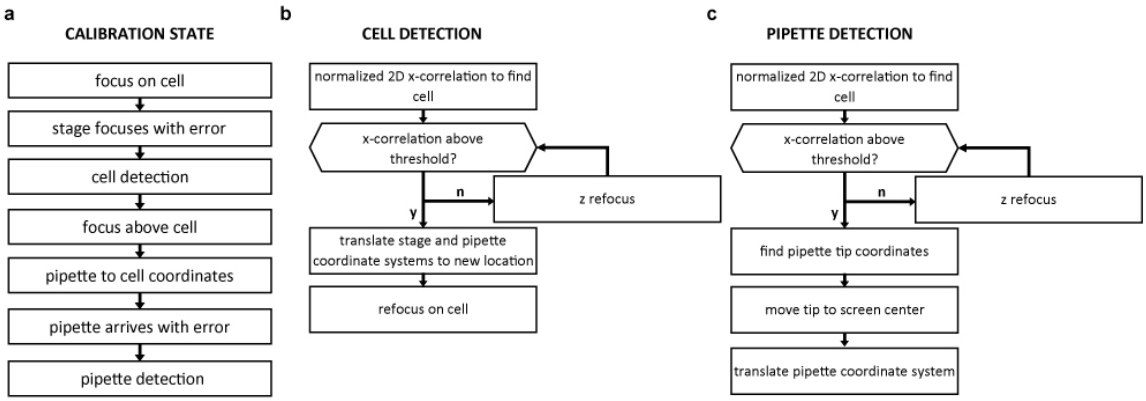

Figure 23: Automated calibration procedure. a. Outline of the "calibration" state that is performed automatically before every patch-clamp attempt. b. Cell detection state used to perform stage calibration. c. Pipette detection state used to perform pipette calibration.

4.2.4 Operation

Once the patcherBot is initialized, the entire process is free of human intervention. The subsequent steps will be performed once for every patch-clamp attempt. First, an automated calibration is performed (Figure 23a) When the stage focuses on a target cell, there is error (0-10 μm) that is caused by one or more of the following factors: (1) drift of cell in the tissue slice or on the cover slip, (2) mechanical drift in the optical system, (3) imprecision in the stage actuation and (4) inaccuracies in the manual calibration. We utilized machine vision to correct for these errors in three dimensions by refocusing on the

correct position of the target cell (Figure 23b). The originally-selected cell is found using normalized 2D cross-correlation. If the cell is not found in the field of view (no r value above threshold), the focusing plane is changed in 2 μm step increments over 20 μm. When the cell is found, the coordinate system of the stage and every active pipette undergo a translation by $(x_{found} - x_{orig}, y_{found} - y_{orig}, z_{found} - z_{orig})$ where $(x_{found}, y_{found}, z_{found})$ are the coordinates of the detected cell and $(x_{orig}, y_{orig}, z_{orig})$ are the original coordinates where the cell was expected to be. After the coordinate transform, the stage is focused on the true position of the cell. If the cell is not found in any plane, the stage returns to the original expected coordinates of the cell $(x_{orig}, y_{orig}, z_{orig})$.

The stage subsequently focuses on $(x_{found}, y_{found}, z_{park})$, directly above the cell, in the "parking plane" the user selected earlier. The pipette moves to those coordinates, typically with error (typically, 0-20 μm away from true location). This is due to two major factors: (1) micromanipulator drift or low repeatability and (2) calibration-based errors. The calibration-based errors stem from unavoidable angular inaccuracies of the initial manual calibration step: namely, small inaccuracies in the calibration angle are magnified if a target is located far away from the calibration point. We utilize machine vision to correct for these errors (Figure 23c). The pipette tip is found using machine vision, moved to the true $(x_{found}, y_{found}, z_{park})$ location, and the coordinate system of the manipulator is adjusted to reflect the true pipette position. If the pipette is not found in any plane, the pipette returns to the original pre-detection coordinates.

In HEK cell experiments, typically performed on a monolayer of cells adherent to a glass cover slip, the pipette subsequently descends to 15 μm above the target cell ("gross

approach" state), at which point, a "blind" cell approach algorithm is engaged (Figure 24a). The pipette then moves down in 1 μm steps until the targeted cell is encountered, based on a three-step resistance-based threshold, similar to the original Autopatcher algorithm (Kodandaramaiah et al., 2012). In slice experiments, the pipette instead first moves in the XY plane above the slice such that it can approach the cell on a trajectory parallel to the pipette axis. The trajectory is planned such that the pipette arrives 15 μm above the target cell in the brain slice. As the pipette arrives, it deforms the surrounding brain tissue both due to mechanical insertion and due to pressurized intracellular solution being ejected from the pipette. In previous patch-clamp automation efforts, any such deformation would result in a failed attempt because the algorithm had no way of determining in which direction the cell moved. Here, the patcherBot engages image-guided approach (Figure 24b). The algorithm utilizes an advanced machine vision algorithm (*Cell Membrane Tracking from Differential Interference Contrast Microscopy for Patch Clamp of Brain Slices*, J Lee, I Kolb, CJ Rozell, CR Forest, *submitted*) to detect neuron boundaries and track them in real time. The algorithm outputs the detected centroid of the neuron and moves the pipette towards the centroid (in x and y only) in 1 μm steps until the pipette tip is found to be within 2 μm (in x and y) of the cell centroid. Once the pipette is aligned with the cell in x and y, it moves down in 1 μm steps until the neuron is detected with a resistance-based method. If the cell centroid moves at any time, the algorithm re-aligns the pipette with the cell centroid.

After the target cell is detected, sealing and break-in algorithms are engaged, largely based on our previous work (Wu et al., 2016). In this iteration of the sealing algorithm, pressure application is based on the slope of the resistance. Once the measured resistance reaches 1 GΩ, the algorithm waits (5 s) and proceeds to the break-in state. Break-in is accomplished by short pulses of suction (100-1,000 ms, -400 mBar). A successful break-in is detected

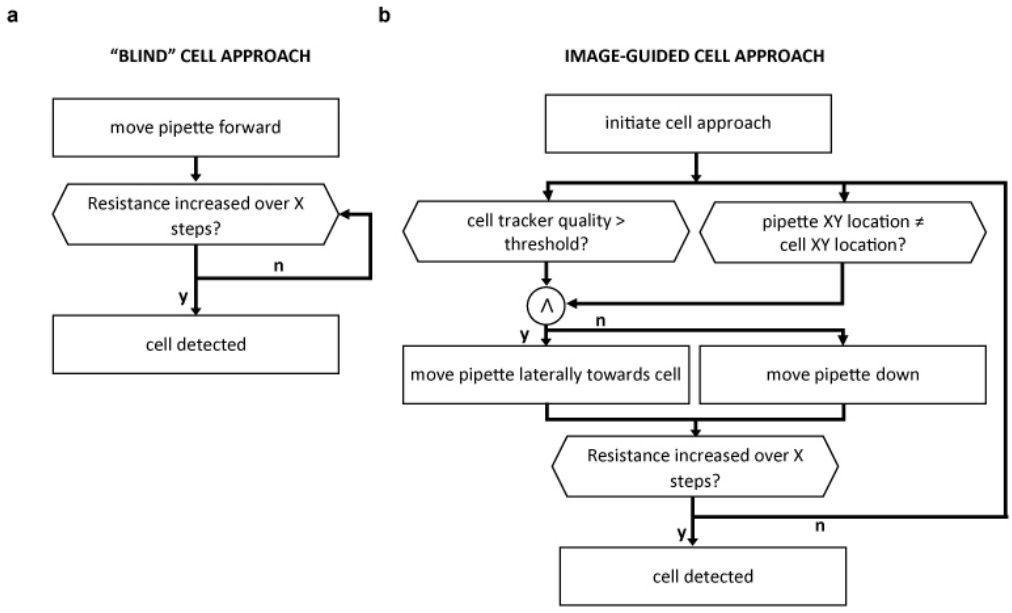

Figure 24: Automated cell approach options. a. "Blind" approach, similar in logic to the original Autopatcher software and Autopatcher IG. Pipette moves down until a resistance increase over 5 consecutive steps is detected, indicative of a cell. b. Image-guided approach, wherein the cell tracker is used to detect the centroid of the target cell. If the pipette xy position is not within 2 μm of the cell centroid, the pipette is moved laterally (1 μm steps) until the XY coordinates are aligned. If the coordinates are aligned, the pipette is moved down. Throughout this process, resistance is continually monitored to detect the cell.

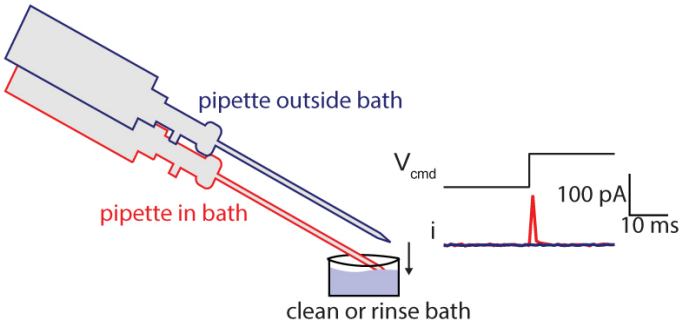

Figure 25: Pipette cleaning with closed-loop bath detection. Once the pipette is moved above the bath, a command voltage square wave (V_{cmd}) is initiated, and current (i) is simultaneously measured. Simultaneously, the pipette starts moving down (in the Z direction) into the clean or rinse bath. When the pipette touches the surface of the bath, its capacitance increases, which results in a transient peak in current (red peak). This peak is detected in software which sends a signal to the manipulator to stop moving down.

when the pipette resistance drops to under 800 MΩ and the holding current at -70 mV remains low (> -200 pA). In these experiments, the whole-cell recording state consists of a voltage clamp protocol where cell parameters (access resistance, membrane resistance, holding current) are measured as well as a current clamp protocol (0 pA for 1 s, -300 to +300 pA step for 1 s, 0 pA for 1 s).

Pipette cleaning is performed as previously described (Kolb et al., 2016). We improved the existing algorithm to account for fluid evaporation (measured to be 23 µL/hr) in a closed-loop fashion. The XY position of the clean and rinse baths are still identified by the user in the manual calibration step but the Z position is automatically determined by detecting an increase in pipette capacitance that occurs when the pipette touches fluid (Figure 25).

4.2.5 Dual patch operation

We made several changes to the single-cell patcherBot algorithm to enable it to be used for dual patching. First we reduced manipulator and stage speed from ~3,400 μm/s to ~400 μm/s to eliminate movement-induced vibration. Second, a "pick cell" state was added. In single-patch trials, cells are patch-clamped in the order in which they were picked by the user; however, for dual patch, this could lead to pipette collisions. For example, if a user selects cell 1 and cell 2 such that cell 1 is closer to manipulator 1 and cell 2 is closer to manipulator 2, during the course of the experiment, it is possible that manipulator 1 will patch-clamp cell 2 and manipulator 2 will patch-clamp cell 1. This could result in manipulator 2 colliding with manipulator 1 on the way to cell 1. To avoid this, the "pick cell" state ensures that each manipulator is assigned to the cell closest to its home position from an array of un-patched cell indices. For more than two manipulators, a more complex algorithm that predicts pipette trajectories and detects possible collision paths would need to be devised. The third addition to the dual patch algorithm is "microscope reservation" feature which ensures that each manipulator can "reserve" the microscope stage and imaging system for the pick cell, calibration, pipette descent, and cell approach states. It is essential that each manipulator has complete control over the microscope during these steps since they rely on camera output. If a manipulator is ready for the "pick cell" stage, but the microscope is reserved by the other manipulator, it must wait until the microscope is unreserved.

The patcherBot can operate in two modes: "independent" mode where both manipulators patch-clamp cells as quickly as possible, and "synchronized" mode where manipulators act in concert to maximize the number of simultaneously patch-clamped cells. The changes

described above were implemented to realize independent operation. However, to maximize the number of simultaneous whole-cell recordings, "synchronized" mode must be used, which required two additional steps. After one manipulator forms a gigaseal, the algorithm waits for the other to form a gigaseal as well. If the first gigaseal worsens ($R < 900$ MΩ), it aborts the trial, cleans the pipette and starts over. If the second gigaseal forms successfully, both manipulators attempt to break in simultaneously. When a successful whole-cell configuration is established on both manipulators, a dual recording protocol is started to test for monosynaptic connections between the patch-clamped cells (2 nA for 2 ms injected at 0.1 Hz 20 times, (Jiang et al., 2015)).

The patcherBot software is written in LabVIEW (National Instruments). The software interfaces with the MATLAB-based cell tracking algorithm, communicates with the stage, manipulators, and pressure control system with a serial interface, and communicates with the patch-clamp amplifier (Multiclamp 700b, Molecular Devices) using an ActiveX interface.

4.2.6 Culture and brain slice preparation

Human embryonic kidney (HEK293T) cells (American Type Culture Collection, Manassas, VA) were cultured as previously described (Chapter 2). All animal procedures were in accordance with the US National Institutes of Health Guide for the Care and Use of Laboratory Animals and were approved by the Institutional Animal Care and Use Committee at the Georgia Institute of Technology. Brain slices were cut and prepared as

previously described (Wu et al., 2016). Recordings were performed in mouse area VI, hippocampal CA3, and thalamus.

4.2.7 Statistics

Data are presented as mean ± standard deviation unless otherwise stated. Data normality was assessed using the Anderson-Darling test. The success rate of the patcherBot as a function of (1) number of performed cleans, (2) lateral displacement, (3) cell area, (4) image quality, and (5) cell depth was assessed using a logistic regression model. An odds ratio (OR) was calculated for each category. An odds ratio can be interpreted as the odds of success improving given a 1-unit increase in the category; for example, a cell area OR of 1.5 indicates that the likelihood of the formation of a successful gigaseal or whole-cell increases by 1.5 with every 1 μm^2 added to the cell area. Other statistical tests are reported in the results.

4.3 Results

4.3.1 Single-patch electrophysiology performance

We used the patcherBot to perform single-manipulator whole-cell recording in adherent HEK cells and neurons in acute brain slices. In both preparations, up to 10 cells were manually selected based on perceived cell health. After the calibration and cell selection steps, the patcherBot was engaged with no further experimenter intervention. In HEK cells

we used 7 pipettes to patch-clamp 54 cells of 70 attempts, (overall whole-cell success rate: 77%). In brain slices, we used 22 pipettes to patch-clamp 93 cells of 161 attempts (success rate: 58%) in cortical and sub-cortical areas (Figure 26). See Table 2 for further performance statistics. The success rate of the patcherBot in cortical neurons was higher than in subcortical areas CA3 and thalamus (cortical whole-cell success rate: 76/121=63%; subcortical whole-cell success rate: 17/40=43%). Recordings in the thalamus exhibited expected characteristics of neurons associated with that region (Figure 26): bursting, sag current, and after-hyperpolarization bursts (Leist et al., 2016; Pape, 1996; Pape and McCormick, 1989).

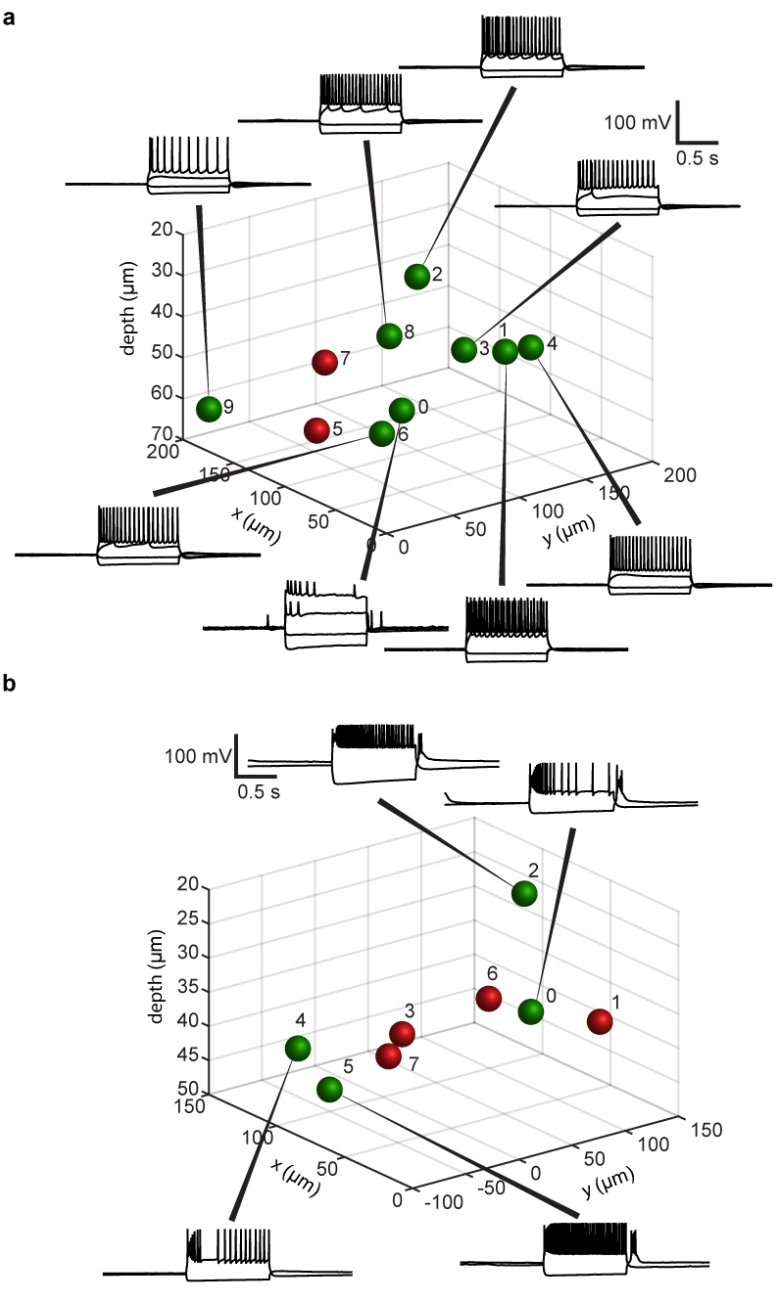

Figure 26: Representative whole-cell recordings obtained using the patcherBot. Green spheres represent successful whole-cell recordings, red spheres represent failed attempts. Cells are shown in a coordinate system that depicts their centroid location in the slice. The (0, 0, 0) point corresponds to the location where manual calibration was performed. Numbers represent order in which cells were picked and patched (0 ,1, 2, …) a. Recordings obtained from mouse cortical VI. Cell 0 had poor spike amplitude, likely due to an unhealthy cell or incomplete break-in. b. Recordings obtained from mouse thalamus. Stimulation pulse: 0 for 1 s, +250 or -200 for 1 s, 0 for 1 s.

We first benchmarked the performance of pipette cleaning to ensure that using cleaned pipettes does not decrease the likelihood of obtaining whole-cell recordings. The pipette cleaning algorithm enabled the reuse of a single pipette up to 10 times with no degradation in recording quality (Figure 27a). Disabling the cleaning algorithm prevented seal formations (Figure 27b). The number of performed cleans was not a significant factor in determining whether a particular trial will be successful (HEK cells: odds ratio, OR = 1.17, P=0.12, CI: [0.13 1.18]; neurons: OR = 1.05, P=0.47, CI: [0.92 1.19]), suggesting that there was no degradation in performance over the 10 attempts per pipette (Figure 27c,d).

Table 2: Performance results of single-manipulator patcherBot in HEK cells and brain slices.

	Adherent HEK cells	**Brain slices**
Unattended operation time	45±6 min (n=7 pipettes with 10 picked cells)	43±5 min (n=5 pipettes with 10 picked cells)
Average time per attempt	4.5 min (70 total attempts)	3.9 min (161 total attempts)
Number of cells picked per pipette	10 (n=7 pipettes)	7.3±1.9 (min: 3, max: 10) (n=22 pipettes)
Worst whole-cell success rate in experiment	6/10 (60%)	Cortex: 3/7 (43%) Subcortical: 1/5 (20%)
Best success rate in experiment	10/10 (100%)	Cortex: 6/7 (86%) Subcortical: 5/7 (71%)

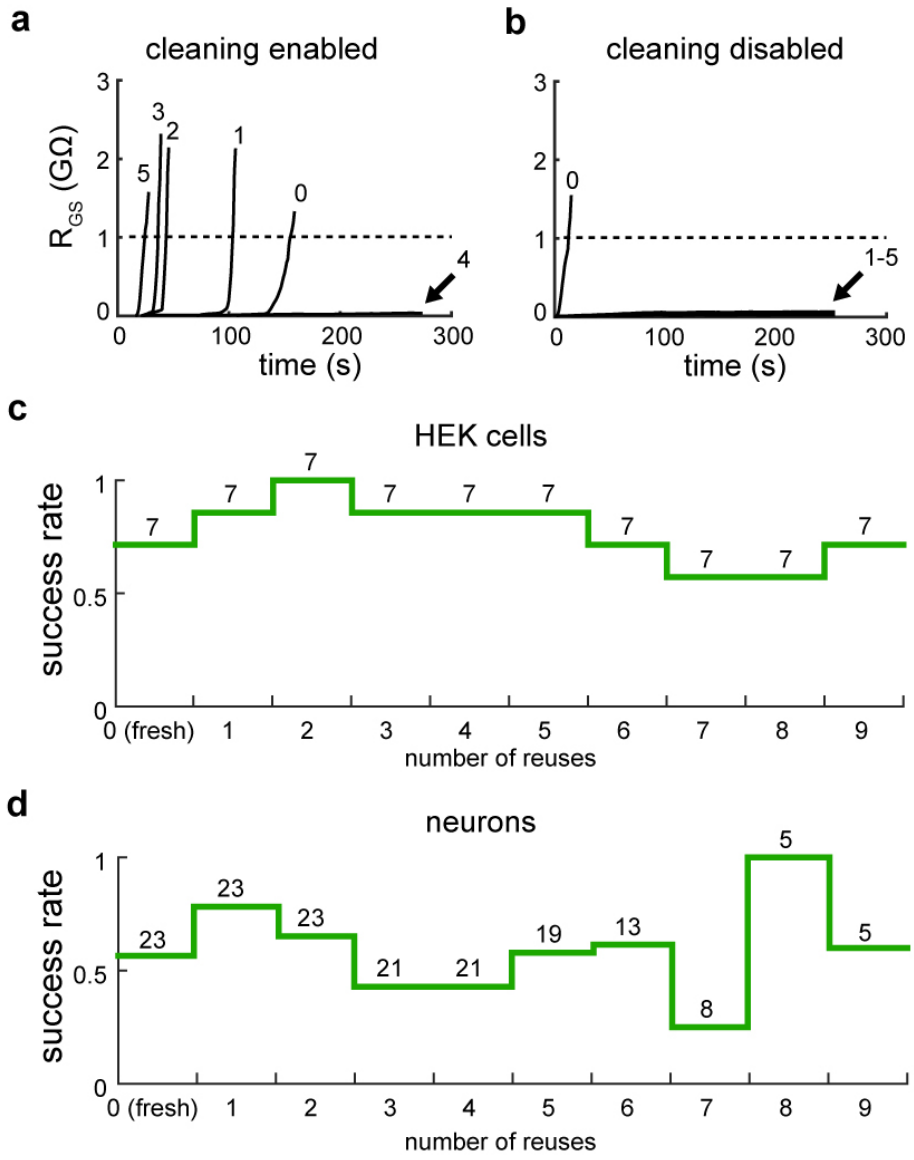

Figure 27: Automated pipette cleaning is necessary for patcherBot performance. a. In a representative experiment in brain slices with 6 selected cells, when cleaning is enabled, a pipette can achieve successive gigaseals ($R_{GS} \geq 1G\Omega$) on multiple cells (0-5, except 4) successively. b. When cleaning is disabled, a gigaseal is obtained with a fresh pipette (0) but not on any other attempt with the same attempt (1-5). c. Whole-cell success rate of pipettes over 10 trials (9 reuses) in HEK cells. d. Success rate in brain slice neurons. In both c and d, no deterioration in the success rate over 10 trials is evident. Numbers above columns indicate number of trials performed at each reuse number.

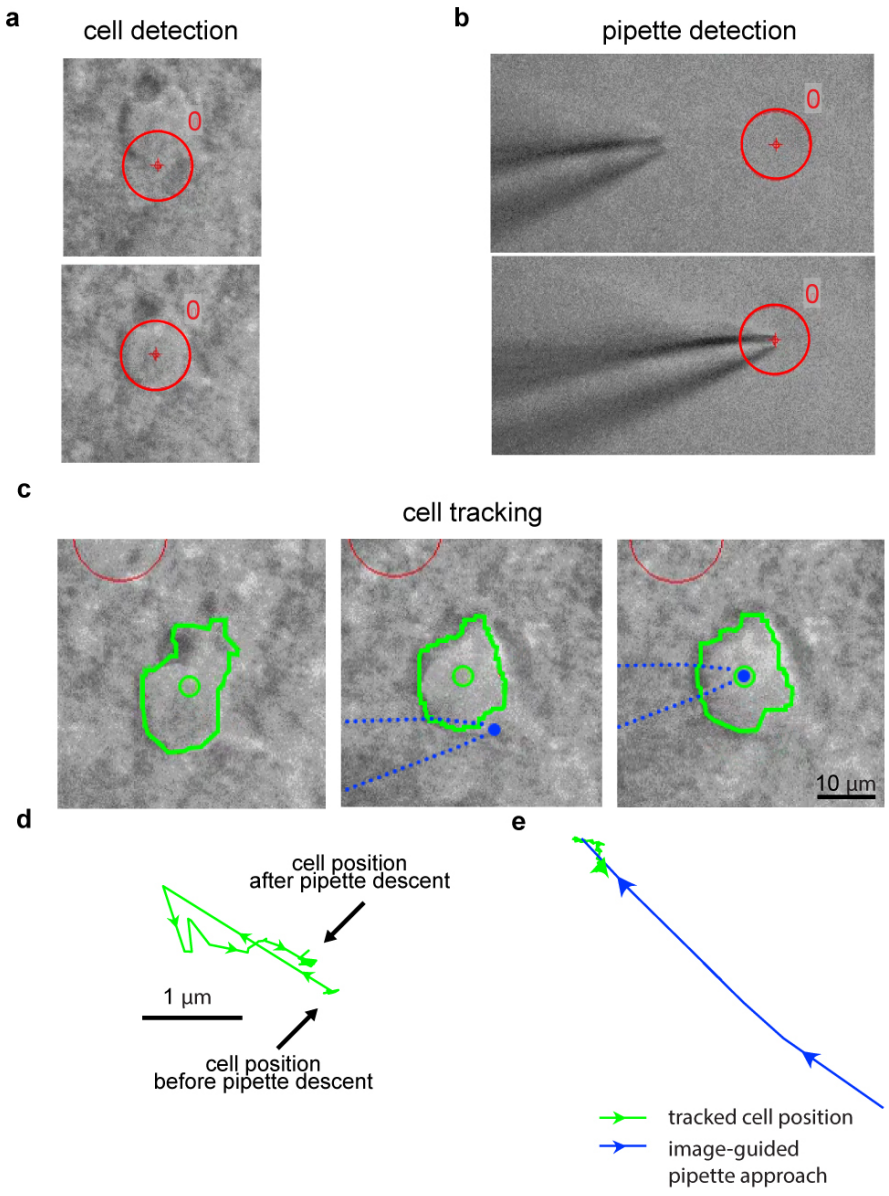

Figure 28: Representative examples of machine vision elements. a. Before (top) and after (bottom) the cell detection state. The algorithm successfully refocused on the user-selected cell. b. Before (top) and after (bottom) the pipette detection state. The algorithm successfully refocused on the pipette after it entered the field of view off-center. c. Sample cell tracking results. Cell boundaries (green outline) are automatically tracked and centroid (green circle) computed. Pipette tip location on the screen is estimated from the manipulator position (blue dot). Left: cell boundary before pipette descent. Center: Cell position and pipette position after pipette descent. Right: Cell position and pipette position after trajectory adjustment. Red circle on top left of images is a different cell. d. Cell centroid position computed by cell tracker during pipette descent. Same attempt as in c. e. Cell centroid position (green) and pipette position (blue) during the "approach cell" state. The pipette moves laterally towards the tracked cell centroid. Same attempt as in c,d.

4.3.2 Machine vision benchmarking

Machine vision was critical in achieving successful recordings in brain slices with no experimenter intervention (Figure 28). The three elements of the machine vision algorithm performed with high success rates: cell detection successfully focused on the target cell in 79% of trials (~1 μm accuracy), pipettes were detected and brought to screen center in 99% (~1 μm accuracy) and cell tracking found the cell centroid in 100% of cases (~2 μm accuracy). These three portions of machine vision were subsequently benchmarked together. We first characterized the displacement of the cells. After the pipette descended to the cell ("descend pipette" state), cells were displaced by a magnitude of 2.5±1.9 μm (N=126) in the XY plane. While the cells were also displaced in z, this displacement was not measured as it would require a manual refocusing of the microscope. Cells tended to move in the direction of pipette motion (Figure 29a), likely due to the pressure applied by the pipette on the tissue during the descent state. Depth, but not cell size was correlated with the magnitude of the displacement (depth versus displacement: r=0.35, P=0.0001; cell size versus displacement: r=-0.11, P=0.20; Pearson's *r*), indicating that cells deeper in the tissue tended to be more displaced by the pipette. Machine vision successfully compensated for the motion in 133/161 (83%) attempts, where success was defined as the pipette engaging the "establish seal" state with the target cell. The algorithm tended to perform worse with larger lateral displacements (OR = 1.3, P=0.0187, CI: [1.05 1.72]); however there were few instances of large (≥ 4 μm) displacements (Figure 29a).

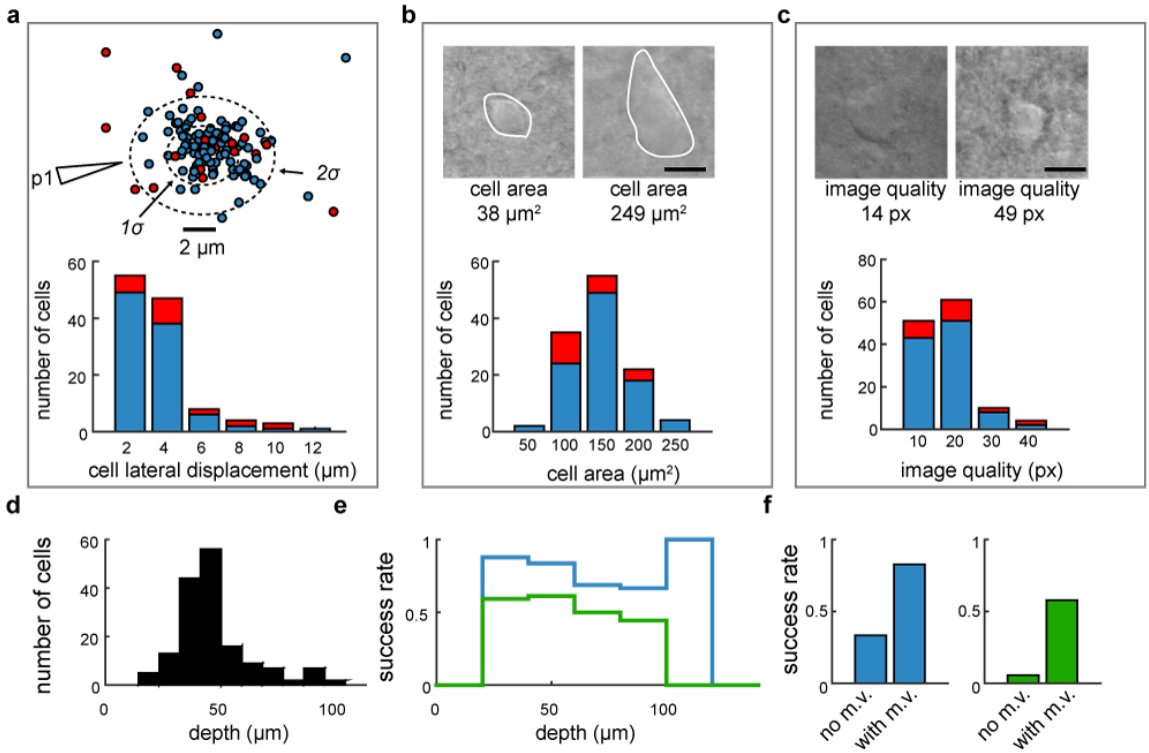

Figure 29: Benchmarking machine vision performance in brain slices. a. Top: scatterplot of cell displacement (in XY plane) after pipette descent. In this and subsequent panels (b,c), blue circles denote successful cell detection (algorithm reaching the "establish seal" state but not necessarily whole-cell), red circles denote failed detection (pipette missing the cell). "p1" shows the approximate direction of pipette 1 entering tissue. The 1σ and 2σ dotted ellipses represent 1 and 2 standard deviations of the displacements, respectively. Bottom: distribution of cell displacement. Most (87%) of cells exhibited displacements of ≤ 4 μm. b. Top: sample cell images and outlines of cells used to calculate cell area. Bottom: distribution of cell areas. c. Top: sample cell images showing poor (left) and good (right) image quality. Image quality was defined as the number of unique pixels in the image. Bottom: distribution of image quality values. d. Distribution of the depths from slice surface of user-selected cells. e. Success rates of cell detection (blue) and whole-cell recording (green). f. Success rate with and without machine vision (abbreviated m.v. in figure).

Cell size and image quality vary dramatically across brain regions; we therefore targeted cortical and subcortical regions to confirm the generality of our machine vision algorithms. Cells are typically larger in the cortex and smaller in subcortical regions and image quality is higher in cortical regions due to relatively less myelination and shallower cells. We confirmed this: cells in mouse VI cortex were significantly larger, shallower, and had better image quality than cells in subcortical CA3 and thalamus (cortical area: 132 ± 36 μm^2, n=86, subcortical area: 96 ± 32 μm^2; n=40; $P=2\times10^{-7}$, Student's unpaired t-test; cortical depth: 44±12 μm, n=86, subcortical depth: 56±23 μm^2; n=40; $P=3\times10^{-5}$, Student's unpaired t-test; cortical image quality: 24±7.6 px, n=86, subcortical image quality: 18±3 px; n=40; $P=2\times10^{-6}$, Student's unpaired t-test).

We evaluated the robustness of the patcherBot with respect to cell size, image quality and depth in slice. Our machine vision algorithms did not perform significantly worse as a function of cell size (OR=0.99, P=0.11, CI = [0.97 1.00]) and image quality (OR=1.06, P=0.07, CI= [0.99 1.13], Figure 29 b,c). Similarly, the machine vision algorithms did not fail more often when patching deeper cells (OR=1.00, P=0.8, CI= [0.98 1.03], Figure 29 d,e). As expected, when all machine vision is disabled, the success rate of cell detection as well as whole-cell recording decreases significantly (cell detection: $P=2.4\times10^{-5}$, whole-cell: $P=1.7\times10^{-5}$, Fisher's exact test; Figure 29 f).

4.3.3 Dual patch recording

Profiling principles of inter-neuronal connectivity in the brain is a major goal of neuroscience but requires thousands of simultaneous patch-clamp recordings (Jiang et al.,

2013, 2015); we demonstrate the ability of the patcherBot to perform these experiments automatically. We first developed and fine-tuned an automated dual-patch algorithm on cultured HEK cells. In the individual operation mode, two manipulators patch-clamp cells as quickly as possible to maximize single-patch throughput (Figure 30 a,d). By adding a second manipulator, the average throughput increased from ~13 attempts/hr to ~22 attempts/hr. The throughput increase was less than two-fold as would be expected from a perfectly parallelized process because (1) manipulator speed was reduced (2) manipulators had to wait to reserve the stage. Due to the asynchronous operation of the manipulators, in total, only 58 s of a 27-min experiment were spent in the waiting state. Dual patch operation also required a new "pick cell" state to assign cells to pipettes so as to eliminate the possibility of collisions (Figure 30c).

For profiling connectivity in neurons, we used the synchronized patching mode to maximize the duration of simultaneous dual whole-cell recordings (Figure 30b). In a demonstration (Figure 30e), the system performed 3 dual-patch recordings (n=2 pipettes).

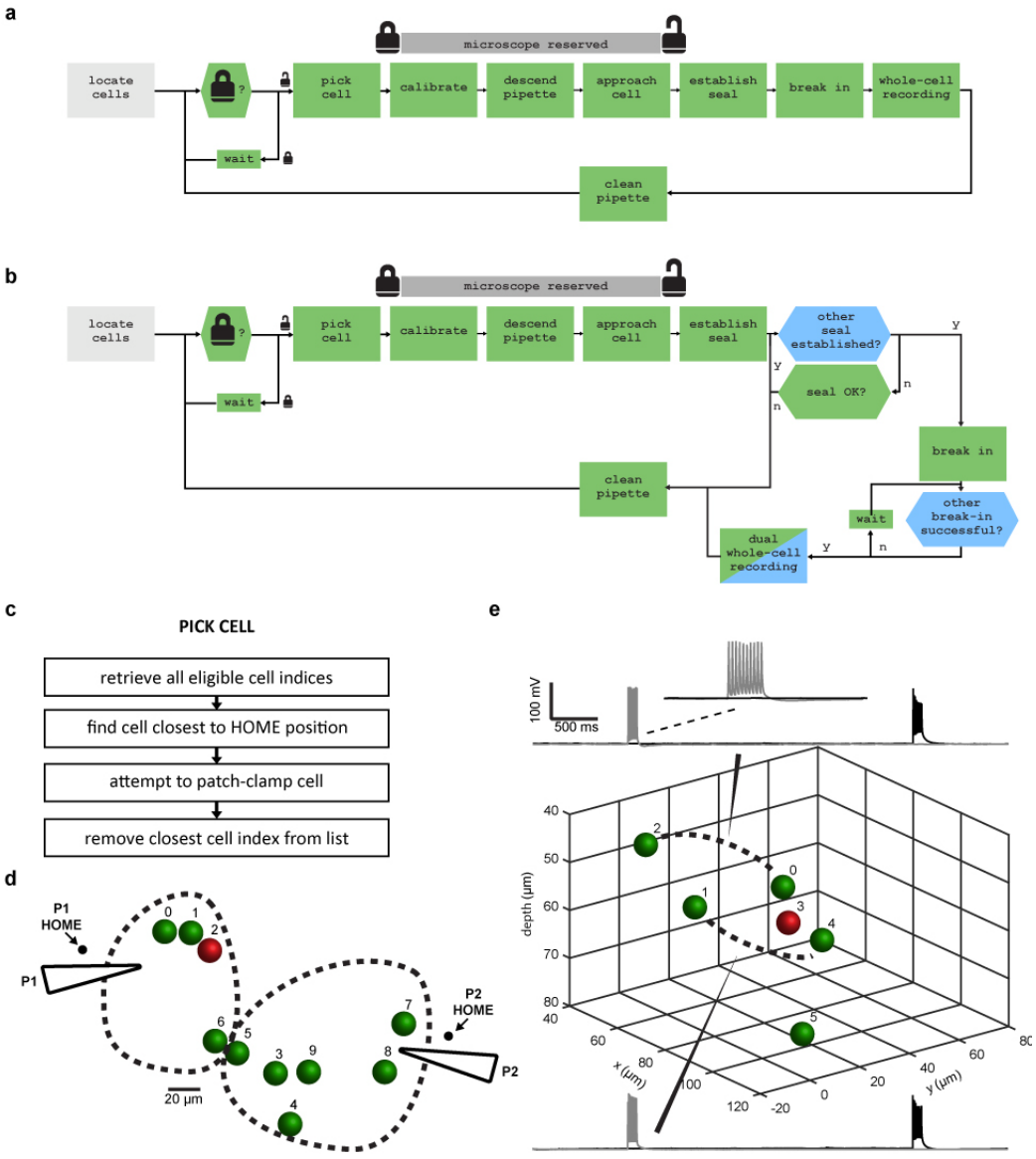

Figure 30: Dual-patch results a. State machine for individual operation, used in HEK cell dual patching. Lock symbol represents microscope reservation. Either manipulator can reserve the microscope and lock out the other manipulator from repositioning the stage. b. Dual-patch state machine for synchronized operation, used in connection profiling in brain slices. c. Description of "pick cell" state dual patch state machine. The cell closest to the manipulator HOME position is picked to prevent collisions. d. Representative dual-patch experiment (individual mode) on cultured HEK cells. Cells are shown in two dimensions instead of three as in previous figures because cultured cells are effectively in the same z plane on the coverslip. Left dashed line encircles cells patch-clamped by pipette 1 (P1); right dashed line encircles cells patch-clamped by pipette 2 (P2). Pipettes not to scale. e. Representative dual-patch experiment (synchronized mode) in brain slices. Tested connections are shown in dashed lines. Both tested pairs were not interconnected (see electrophysiology trace insets).

4.4 Discussion

We have created a system for walk-away automation of whole-cell recordings in vitro. The critical enabling techniques for this advance were machine vision and pipette cleaning. Due to its ability to perform multiple trials sequentially, the system provides an approximately ten-fold increase in unattended operation time compared to previous systems (Kodandaramaiah et al., 2012; Wu et al., 2016). The system functions with similar throughput in adherent HEK cells and mouse brain slices and is suitable for studying large-scale neuronal inter-connectivity.

In the current state, the patcherBot system can be leveraged in studies requiring high throughput. For example, to screen genetic variants of genetically-encloded Calcium indicators (GECIs), a large library of protein mutations (hundreds to thousands (Chen et al., 2013; Dana et al., 2016)) must be generated but performing whole-cell recordings on each variant to test its performance is impractical. Instead, high-throughput fluorescence-based assays are used (Wardill et al., 2013) which are not as sensitive. The patcherBot is a feasible alternative that could provide a rich dataset in less time and in a more automated way than with manual patch-calmp electrophysiology.

The ability of the patcherBot to patch-clamp in brain slices with a high success rate makes it a viable candidate to perform large-scale single-cell characterization and connectivity profiling studies in brain slices. The diversity of neuronal cell types coupled with low inter-neuronal connection probabilities make it necessary to patch-clamp thousands of cells to map a connectivity diagram of just one region of the brain with a high degree of statistical

power. The low degree of human intervention makes it possible for one trained user to operate many patcherBot devices simultaneously, increasing throughput.

Despite the advantages of our walk-away automated system, there remain some limitations. The success rate of patch-clamp of the patcherBot in adherent cell and brain slice preparations is likely lower than the most trained electrophysiologists. Further refinements are needed to close that gap, perhaps by using machine learning to derive best practices from trained electrophysiologists. Similarly, the quality of the whole-cell recordings achieved with the patcherBot may be sub-par in the current iteration of the algorithm as compared to trained investigators. Skilled users can monitor the whole-cell recording and attempt to remedy a poor recording using various, largely undocumented heuristics, such as applying high levels of suction to improve access resistance, moving the pipette after break-in to release stress on the cell membrane for improved stability, and others. These heuristics can be codified and implemented in the automated system.

The patcherBot performed patch-clamp recordings with one or two manipulators; however, adding more could dramatically improve throughput past the capabilities of even the most skilled human experimenters. Even the best human electrophysiologists can only control one manipulator at a time, so adding more manipulators will not result in an increase in single-cell patching throughput (Figure 31a). On the other hand, the patcherBot could control many manipulators, pressure lines, and command signals independently. In individual operation mode, this results in an almost linear throughput increase: that is if the throughput of one manipulator is C cells/min, with m manipulators, the theoretical throughput will approach $m\ C$ cells/min, given several assumptions: (1) a high (~80-90%) success rate, (2) similar patch times for every cell, (3) ≤ 5 manipulators (Figure 31b). In

synchronized operation mode, throughput is more difficult to estimate due to a lower success rate and human decision-making (e.g. if two of three pipettes achieved a whole-cell recording, is it better to replace the pipette and try again or just settle for a dual recording?). Nevertheless, the ability to patch-clamp multiple cells simultaneously using the patcherBot should still provide throughput improvements over manual patching (Figure 31 c,d).

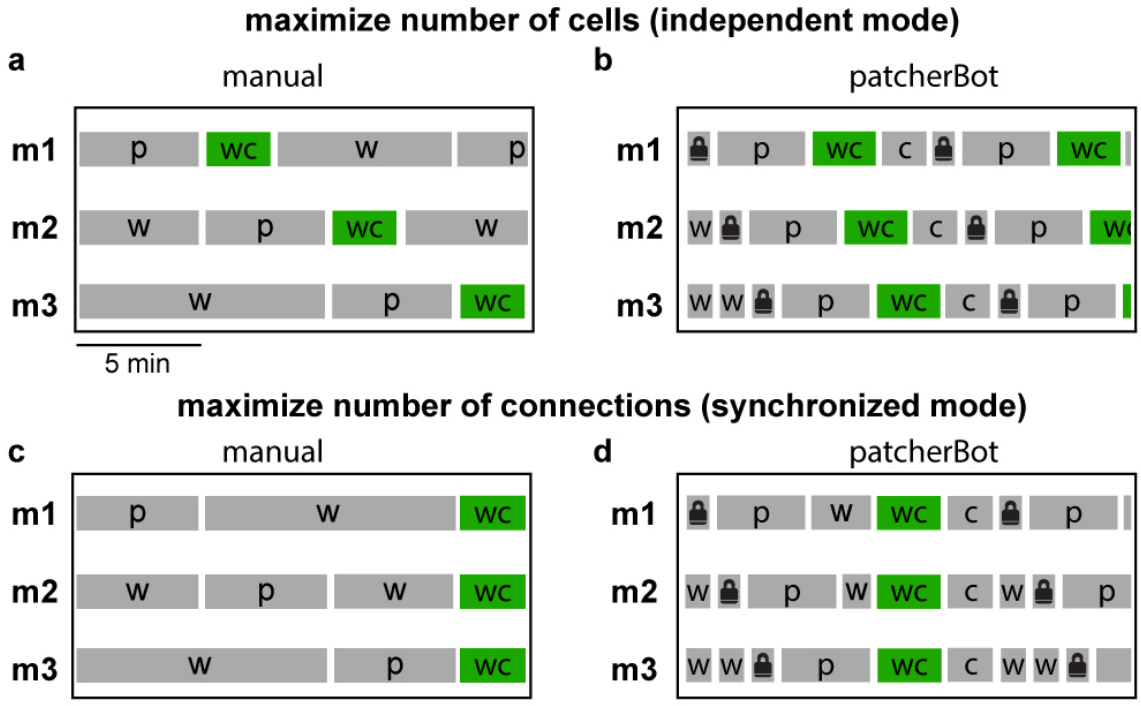

Figure 31: Theoretical throughput improvement of patcherBot with three manipulators. a. Sample timeline of manual patching when attempting to patch as many cells as possible. Additional manipulators (m2, m3) do not significantly contribute to throughput since a user can only control one manipulator at a time. b. Sample timeline of patcherBot performance in individual mode (manipulators patch-clamp cells asynchronously to maximize throughput). The ability to simultaneously attempt seals with multiple cells makes the patcherBot outperform human operators in throughput. c. Sample timeline of a manual patch-clamp experiment for probing connectivity. Cells are recorded simultaneously to maximize the number of connections that can be probed (number of possible connections = m (m-1), where m = number of manipulators). d. Sample timeline of patcherBot performance in synchronized mode. The patcherBot will outperform the throughput of human operators by a larger margin the more manipulators are added. Legend: m1-3: manipulators 1-3, p: patch-clamp attempt, w: waiting, wc: whole-cell recording, lock symbol: microscope reserved, c: cleaning.

CHAPTER 5. DISCUSSION

The study of the brain promises to be a scientifically fruitful discipline, despite the immense challenges that still remain in the field. The automated patch-clamp recording technology discussed here is particularly suited to address two major challenges in neuroscience discussed below.

The first challenge is creating a single-cell map of neurons and connections in many parts of the brain (for a review, see (Zeng and Sanes, 2017)). Dysfunctions in cell-type specific connectivity are implicated in diseases such as autism (Rinaldi et al., 2008; Silva et al., 2009), Parkinson's disease (Parsons et al., 1996; Taverna et al., 2008), and others. Discovering principles of inter-neuronal connectivity could not only begin to explain brain function, but also begin to reveal possible interventions for diseases. To do this, automated patch-clamp recording could be used in a factory-like assembly line setting. A team of surgery experts and/or machines (Pak et al., 2011) could perform initial surgery and slicing procedures, and feed resulting slices into the patcherBot, which could then work with minimal human supervision, much like a factory robot or benchtop plate reader. The standardization and automation of electrophysiology is crucial for reducing variability, enabling large-scale studies, and thus improving reproducibility of such studies.

The second challenge is molecular screening for neuronal activity monitoring. Genetically encoded Calcium indicators (GECIs) allow for simultaneous activity imaging of thousands, to, potentially, millions of neurons (Kim et al., 2016). Similarly, genetically encoded

voltage indicators (GEVIs) are promising due to their ability for direct voltage transduction (Akemann et al., 2010). However, to date, no fluorescent sensor has been discovered that has single-spike resolution, fast response time and low photobleaching rate. Further, the most advanced sensors available today were derived only after thousands of point mutations, requiring immense screening efforts (Wardill et al., 2013). Patch-clamp recording is the most sensitive measurement type to validate the performance of such indicators; yet in its current manual form it is impractical for screening large libraries. The patcherBot could thus be an effective screening tool for these molecules.

5.1 Major Contributions

The major contributions of this work include algorithm development, as well as development and validation of techniques that could be widely applicable in the neuroscience community. In this work, I

- Integrated Autopatching with pipette trajectory planning to develop Autopatcher IG (available online on www.autopatcher.org). The software package automates several parts of the patch-clamp experiment, increasing throughput.
- Developed and validated pipette cleaning, a patent-pending technique that enables patch-clamp pipettes to be reused.
- Leveraged machine vision techniques for automated cell detection, tracking, and pipette identification, enabling the automation of the final, most difficult manual aspects of patch-clamp recording.

- Built and validated the first system to perform sequential patch-clamp recording automatically without human intervention. Tested the system in adherent HEK cells and brain slices.
- Designed and validated the first system to automatically profile inter-neuronal connections.

5.2 Future Work

The Autopatcher IG software needs to undergo several software revisions to expand functionality. The Autopatcher IG still requires human intervention to perform trial-to-trial operation unlike the patcherBot; however it is not obsolete. There are still many experiments that are conducive to a medium degree of automation as opposed to full automation. For instance, in drug studies, solution cross-contamination is often so problematic as to require a fresh tissue slice for every patch-clamp recording. In this case, an investigator must be present anyway, so a human-in-the-loop approach to patching is warranted. To improve usability, the Autopatcher IG software must be made to support devices (cameras, stages, manipulators, amplifiers) from different manufacturers. This is achievableby re-writing the Autopatcher IG algorithm using functions from an existing software package. Several candidates are available which already support various electrophysiology devices: Micro-Manager (Edelstein et al., 2014), ScanImage (Pologruto et al., 2003), Acq4 (Campagnola et al., 2014), and others. Considerations such as ease of programming, user base, and support availability will be used to decide among these solutions.

The pipette cleaning technique, while potentially transformative, must be improved and tested in more preparations. Effectiveness will be improved by further examining chemical and physical methods of removing cellular debris from pipette tips. We will explore more aggressive cleaning compounds, as well as serial application of cleaning agents to increase the number of cells that a single pipette can patch. Apart from chemical cleaning techniques, we will explore physical perturbations such as high-velocity flow, sonication, and heating to mechanically destabilize cellular debris at the tip. Pipette cleaning must also be tested in more preparations: the most demanding is likely single-channel recording (Neher and Sakmann, 1976), which requires extremely high-quality, high-resistance seals. We will therefore ensure that pipette cleaning works in this experimental paradigm.

The patcherBot software can be further enhanced and modified to enable the automation of various experiments. First, the addition of more manipulators could enable faster profiling of connections. To enable this, a more advanced cell picking algorithm would need to be implemented. Instead of picking the nearest cell to the manipulator, the cell picking algorithm would need to detect potential pipette collision points and avoid them. Second, the software could be augmented to include the capability to perform patchSeq (Cadwell et al., 2016), enabling it to collect gene expression information from single cells. This would require hardware and software modifications: the cleaning chamber would need to be modified to house multiple wells with RNAse-free lysis buffer and the manipulators would need to be programmed to suck out cell contents and deposit them into the wells. Cross-contamination of samples could be a major concern; the cleaning algorithm may need to be modified to include a DNA/RNA removal step. Third, the software could be coupled with optogenetics (Boyden et al., 2005) to perform circuit discovery experiments

similar to Channelrodopsin-2-assisted circuit mapping (CRACM) (Petreanu et al., 2007). In such an experiment, a pipette would patch-clamp a cell, and candidate presynaptic cells would be optogenetically stimulated to produce post-synaptic potentials (PSPs) on neighboring cells. The cell that produces PSPs on the patched cell would be patched with another pipette, and the process repeated again, until a connected network is traced out or a dead end is reached (no presynaptic cells producing PSPs are found).

APPENDIX A. AUTOPATCHER IG USER MANUAL

A.1 Overview

The Autopatcher IG software allows the user to quickly and reliably patch-clamp neurons in acute brain slice preparations. The software, written in LabVIEW (National Instruments) controls several pieces of hardware described below

A.2 Hardware

1. Scientifica PatchStar or MicroStar micromanipulators

2. Scientifica XY stage

3. Scientifica motorized objective changer

4. Neuromatic Devices Autopatcher

5. Multiclamp 700b patch-clamp amplifier

6. Data acquisition system (optional)

A.3 Software

1. Multiclamp 700b software

2. Data acquisition software (PCLAMP, MIES, etc., optional)

A.4 Installation (EXE)

The compiled executable Autopatcher IG software can be installed from here. Source code is provided here.

First, install QImaging drivers [32-bit or 64-bit depending on your system] (http://www.qimaging.com/support/downloads/legacy_qcamdriver.php).

Unzip Autopatcher IG EXE.zip. Navigate to Autopatcher IG installer v1.000/Volume/setup.exe.

Follow the instructions on the installation prompt.

The installer will create a folder in your Program Files directory called Autopatcher IG. Navigate to that folder and start Autopatcher IG.exe.

A.5 Procedure

The program will auto-start in demo mode. Note: if the program starts with an error about not finding QCam.llb, ensure that you have downloaded and installed the QImaging drivers (previous section).

Follow the prompts in the live slice view (Figure 32) to execute the program successfully in demo mode.

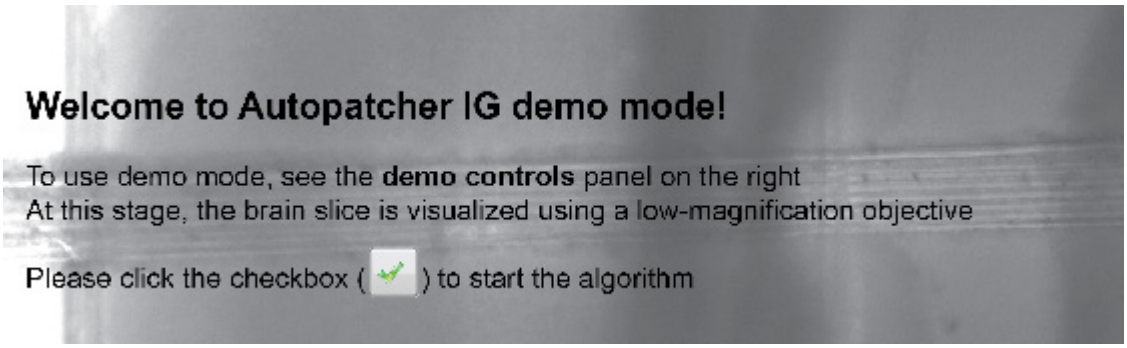

Figure 32: Autopatcher IG demo mode introduction screen.

A.6 Controls

In demo mode, all device communication with the camera, manipulator, data acquisition [DAQ] device, the pipette pressure box, and Multiclamp is disabled and instead emulated using software. To instead use one or more real devices, see the "demo controls" tab (Figure 33) in the tabbed panel on the right side of the screen.

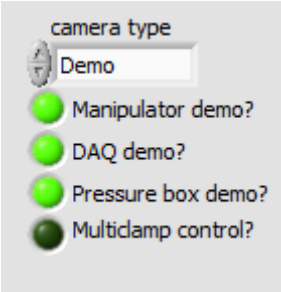

Figure 33: Demo mode control panel

Instructions to the user are shown in the instruction bar below the live view of the brain slice (Figure 34). To move ahead in the program, the user clicks the green check button on

the right. At any point, the user may exit the program by pressing the Quit button. Pipette resistance is read out to the user in the top right panel of the window (Figure 35).

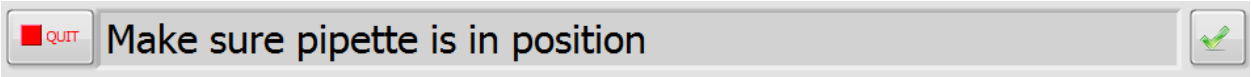

Figure 34: User instruction panel

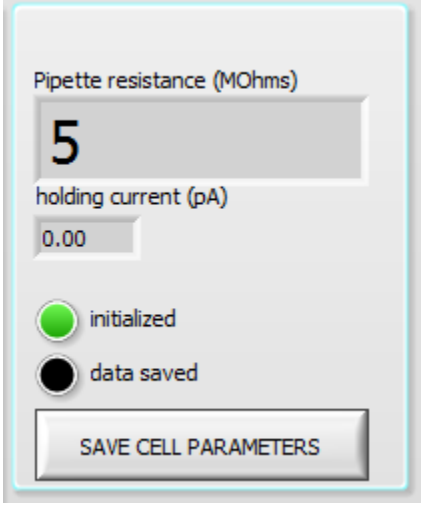

Figure 35: Operational user interface box

In experiments with real hardware, the pipette resistance is read out from the DAQ. In demo mode, the user controls the pipette resistance using the Pipette R slider (Figure 36).

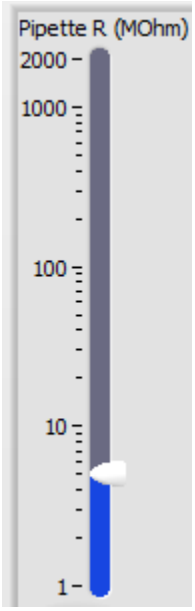

Figure 36: Pipette resistance controller for demo mode.

Try adjusting the pipette resistance. You should see the resistance reflected on the pipette resistance indicator.

The status textbox (Figure 37) shows the simulated activity of the pipette control box and manipulator, prepended with timestamps.

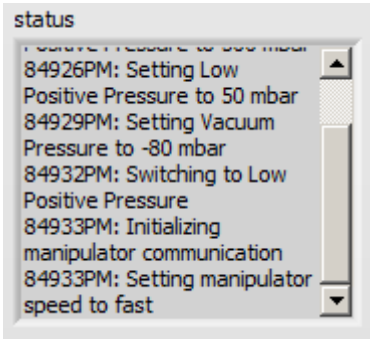

Figure 37: Status textbox shows a live-updated patch log.

The gigaseal resistance plot (Figure 38) is activated once contact with the cell is established. The plot shows the gigaseal resistance as a function of time as the algorithm attempts to form a gigaseal with the cell.

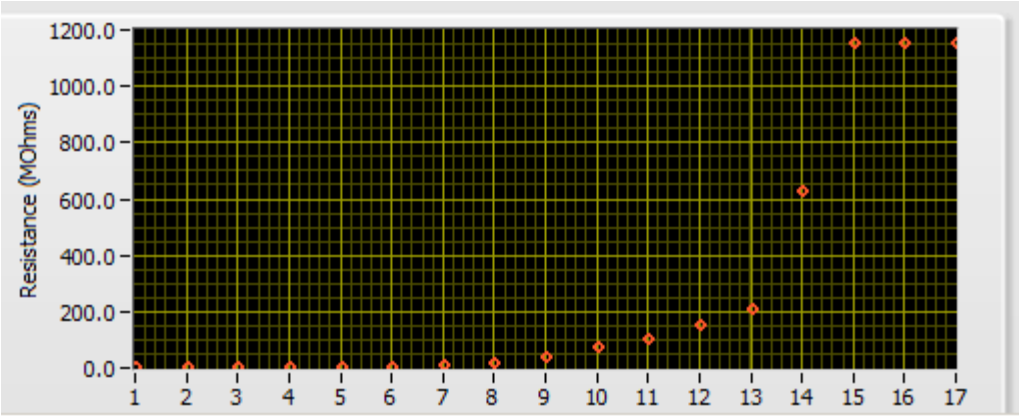

Figure 38: Sample gigaseal resistance plot.

The membrane currents plot (Figure 39) shows the instantaneous membrane current in response to a test pulse. This is equivalent to a membrane test pulse in other electrophysiology software packages such as Clampex.

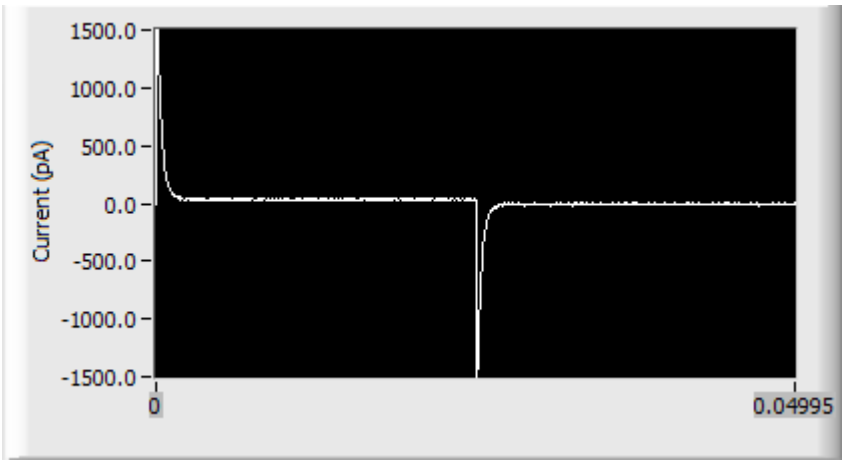

Figure 39: Membrane current plot

A.7 Troubleshooting (hardware + software)

PROBLEM: An error appears at the start of the software saying that a device (manipulator, stage, and/or Autopatcher box) was not connected even though it is.

SOLUTION: This can happen if a device was unplugged from a USB port and then plugged into another USB port.

If the device that cannot be accessed is a Scientifica device (manipulator, stage, objective changer), close slicePatch, open LinLab2, and go to Settings. Go to Devices and look at the top ribbon for tabs like SliceScope (COMX) and PatchStar (COMY) with X and Y being some number. Note down all the COM port numbers. Go back to slicePatch and scroll to the right menu for more options. Go to the tab “Options”. For the device(s) that failed to start, use the drop-down boxes to select the COM port that you noted down earlier.

After you select the correct COM port, right-click on the drop-down, go to "Data Operations" > "Use current value as default".

If the device that cannot be accessed is the Autopatcher, go to Control Panel > Device Manager. Click on the "+" next to "Ports (COM & LPT)". A menu of connected devices should pop up. One of the devices should be an Arduino. Note down the corresponding COM port. Go back to slicePatch and scroll to the right menu for more options. Go to the tab "Options". Find the COM port control corresponding to the Autopatcher. Use the drop-down boxes to select the COM port that you noted down earlier. After you select the correct COM port, right-click on the drop-down, go to "Data Operations" > "Use current value as default".

PROBLEM: Camera image looks too washed out and low-contrast.

SOLUTION: This may happen if the CameraViewer software was run prior to running slicePatch. Close slicePatch, unplug the USB and power from the camera and plug it back in. Re-start slicePatch and the image quality should improve.

PROBLEM: The pressure on the pipette is not being set properly when checked by the manometer.

SOLUTION: Ensure that house air is connected to the port in the back of the Autopatcher. Ensure that as soon as the box is turned on, the LCD screen lights up and a hissing noise comes out of the autopatcher. Ensure that the box pressure is set on "Auto" mode, as indicated by an "A" icon on the right on the LCD screen. If the box is turned to "Manual" (or "M" on the LCD screen), turn it to "Automatic" by pushing the knob on the front of the

Autopatcher box. If the pressure reading is still not correct when checked by the manometer, it could be because downstream flow is not restricted enough. Place a pipette into the pipette holder or close off the air flow using a Luer valve.

PROBLEM: Finding pipette tips under the 40x objective is difficult because pipettes do not show up onscreen immediately.

SOLUTION: This is likely because of variability in lengths of the left and right pipette. Pull a set of pipettes and inspect them by eye or using a microscope. Make sure their lengths are identical by aligning their non-sharp ends. If one pipette is longer than the other, adjust the location of the pipette stopper on the Sutter puller. It may take a few attempts to get the pipettes to be exactly the same length.

PROBLEM: Upon descending the pipette towards the cell of interest, the pipette is way off.

SOLUTION: The manipulator/stage relationship may need to be recalibrated. Contact Ilya Kolb.

A.8 Troubleshooting (patch-clamping)

This section will address problems with the process of patch-clamping, not necessarily specific to slicePatch software. These are some less well-known tricks of the trade. In general, you should achieve a gigaohm seal with your target neuron in ~80% of attempts and successfully break in ~80% of those attempts. If your success rate is significantly lower, there may be fundamental problems with your setup.

Here are some random pointers in no specific order:

- Use a low-resistance pipette but not too low. 4-6 MOhms is perfect.
- When approaching cells, make sure you use the approach axis of the pipette (approach function on Scientifica manipulators). This makes a huge difference because it improves the mechanical stability of the patch.
- Here are some things to look for when approaching a cell. That is, at what point do you release positive pressure?
    - In some preparations, you can see a "dimple" form on the cell as the pipette approaches it. In some cases, you can actually see the dimple grow. If you see this, this is the *best* indicator that you will have a good cell. Do not linger, as soon as you see the dimple, release the positive pressure. A gigaseal should form within a few seconds.
    - When you cannot see a dimple, sometimes you may see a quick "snap" of the membrane when you release positive pressure and as the pipette starts adhering to the cell membrane. This is often a good indicator that you will get a gigaohm seal.
- Ensure that the pipette spends the *minimum possible amount of time* in the tissue. As soon as the pipette is in, form the seal as quickly as you can.
- Do not move the pipette inside the tissue too much. If you see major deformation of the tissue around the shaft of the pipette, this is bad and could mean that you will not get a stable seal.
- If you are filling the cell with a dye, apply small positive pressure (5 mbar) to increase the flow of dye. The autopatcher algorithm already does this.

- Take a picture of your patched cell 5, 10, and 20 minutes after you've patched on and compare those images to the patchedCell.png image that is generated by the software. Does the pipette seem to have drifted from its original position at all? If so, this is a major problem that could manifest itself in shortened recordings due to cells sealing back up or leaky cells. To fix this, make sure all bolts on the rig are fastened tight, the air table is floating, and the cables are not taut and are not tugging at any part of the rig.
- If you see your image under 40x "jitter" back and forth at a high frequency when you stomp your foot on the ground, there is a problem with the mechanical isolation of the air table. If you see the same jitter in your pipette, this could ruin your seals.
- Spend a lot of time looking for the *best possible* cell to patch. It is better to spend 3 minutes looking for a good cell and have it yield great data than to spend 30 seconds per trial going for less optimal cells and having to do many more attempts.

APPENDIX B. CLEANING SOLUTIONS

Table 3: Solutions tested for pipette cleaning.

Cleaning solution	Source	Reference/Protocol
Bleach (8.25% Sodium hypochlorite)	The Clorox Company	(Kao et al., 2012)
Triton X-100	X100-5mL (Sigma-Aldrich)	(Koley and Bard, 2010)
Acetone	BDH1101 (VWR)	(Jamur and Oliver, 2010)
Phosopolipase A_2 (PLA, 0.0001% w/v in 10 mM HEPES buffer)	P7778 (Sigma-Aldrich)	(Beneš et al., 2004)
Sodium Dodecylbenzenesulfonate (SDS, 1% w/v)	TCD0990 (VWR)	(Kinoshita et al., 2009)
Alconox (2% w/v)	Alconox Inc.	Alconox User Manual – Alconox Inc.

APPENDIX C. SLICE RECORDING CHARACTERISTICS

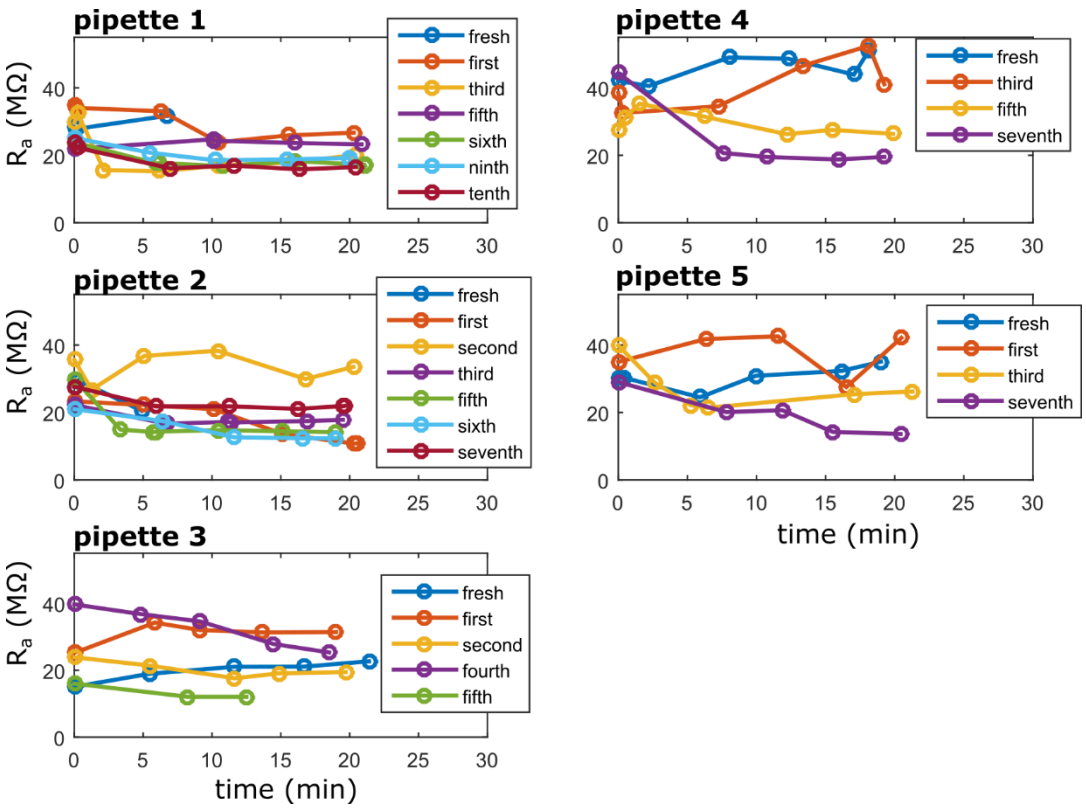

Figure 40: Access resistance of neurons in brain slices. For each plot, a single pipette was used. Only successful attempts (resulting in whole-cell recordings) are shown. Cells were held for ~20 minutes. Access resistance did not increase for fresh pipettes as well as for pipettes reused 1-10 times, indicating stable whole-cell recordings.

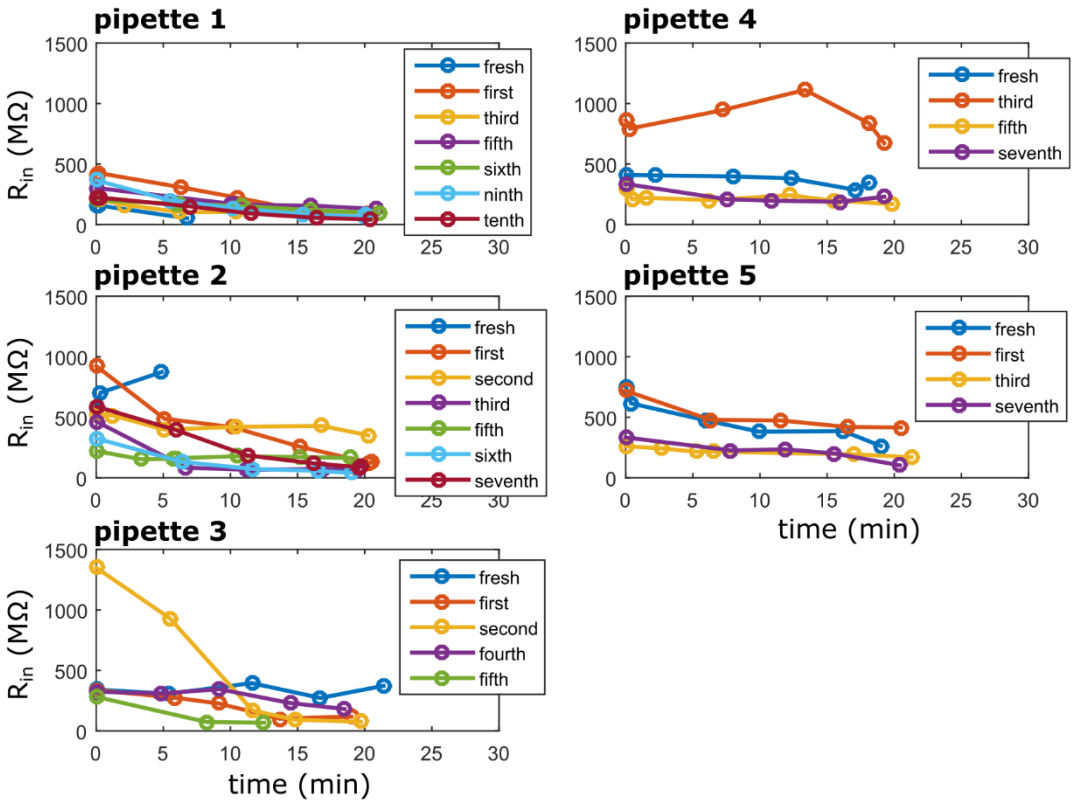

Figure 41: Input resistance of neurons in brain slices. In most cases input resistance did not change dramatically over time for fresh pipettes as well as for pipettes reused 1-10 times, indicating stable whole-cell recordings.

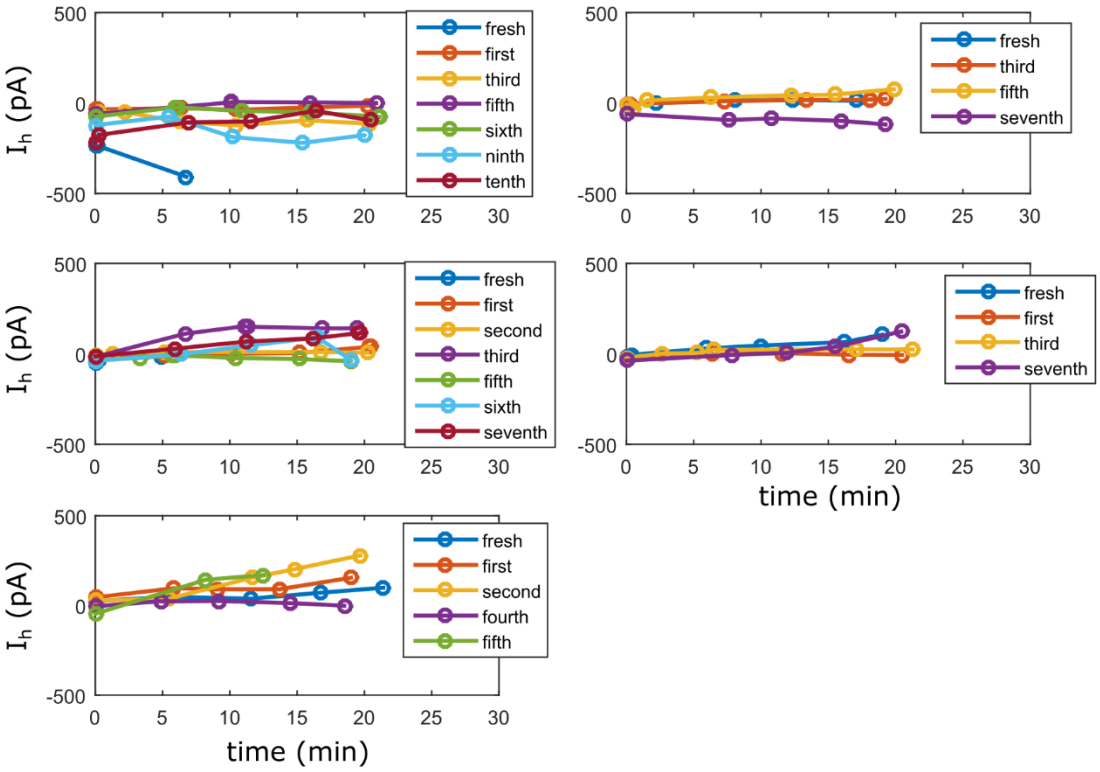

Figure 42: Holding current of neurons in brain slices. In most cases the holding current did not change dramatically over time for fresh pipettes as well as for pipettes reused 1-10 times, indicating stable whole-cell recordings.

APPENDIX D. FUTURE DIRECTIONS OF PIPETTE CLEANING

D.1 Cleaning limitations

In Chapter 2, pipette cleaning with Alconox was shown to be a reliable technique for achieving multiple whole-cell recordings with the same pipette. However, there are limitations to the effectiveness of the cleaning procedure, suggesting that Alconox may not fully remove contaminants from the pipette tip on every clean. We support this hypothesis with two pieces of experimental evidence.

First, in HEK cells (and likely in other preparations), pipettes could only be reused 10 times. Indeed, we showed that after ~14 attempts to patch with the same pipette, the time to attain a gigaseal lengthened irreversibly, and after 26 attempts, seals no longer formed (Figure 15). This suggests that the pipette was not sufficiently cleaned. Second, we tested the ability of pipettes to perform single-channel recordings (as opposed to whole-cell). These types of recordings require high seal resistances (3-10 GΩ compared to ~1 GΩ for whole-cell recordings) and are essentially the most sensitive measurements that can be taken with a patch-clamp electrode. We therefore asked: how well does pipette cleaning work for this demanding application? In preliminary trials, high-resistance (3-10 GΩ) seals resulting in single-channel recordings could not be obtained after two cleans, suggesting an incomplete clean (Figure 43). Third, the ability of cleaned pipettes to attain gigaseals was dependent on the apparent health of cultured cells; that is, cleaned pipettes worked better in healthy cells than in unhealthy ones. Meanwhile, this was not the case for fresh

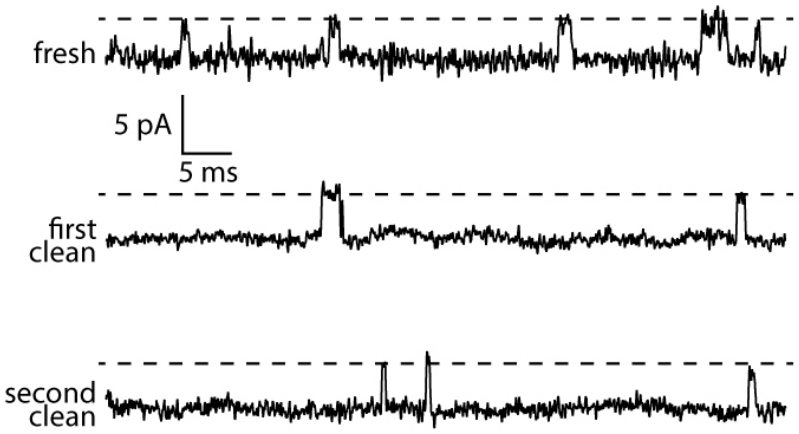

Figure 43: Single-channel recordings with pipette cleaning in adherent N2A (mouse neuroblastoma) cells. Dashed line shows approximate open-state currents in each recording.

pipettes. Together, these findings led us to conclude that the cleaning protocol must be further optimized to improve performance. Given these limitations to pipette cleaning with Alconox, we endeavored to (1) determine why Alconox works as a cleaning agent better than other tested detergents and (2) develop a more effective cleaning solution.

D.2 Why Alconox works

We looked for a mechanistic understanding of how cleaning works by independently testing the cleaning action of the constituent components of Alconox. The major (highest

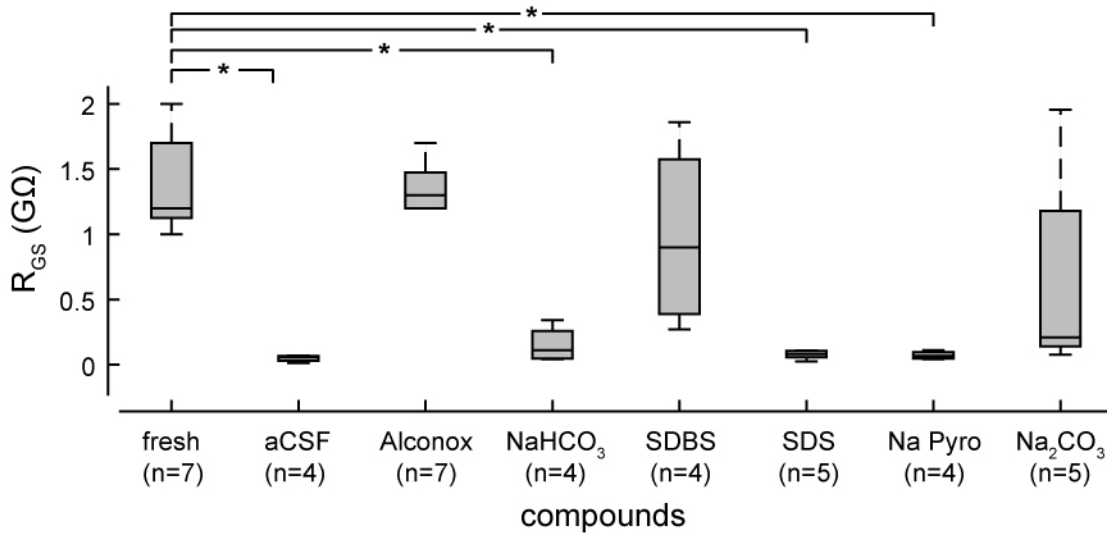

Figure 44: Testing the cleaning effectiveness of constituent components of Alconox. Alconox is made up of $NaHCO_3$, SDBS, Na Pyro, Na_2CO_3. The compound SDS was tested to compare its effectiveness to that of SDBS. * $P<0.05$, one-way ANOVA ($F_{7,32} = 11.33$) followed by Tukey's Honest Significant Difference test ($\alpha=0.05$). Abbreviations: aCSF: artificial cerebro-spinal fluid, SDBS: Sodium Alkylbenzene Sulfonate, SDS: Sodium Dodecyl Sulfate, Na Pyro: Sodium Pyrophosphate.

weight percentages) components of Alconox are: Sodium Bicarbonate ($NaCO_3$, 33-43%), Sodium Alkylbenzene Sulfonate (SDBS, 10-20%), (Tetra)Sodium Pyrophosphate ($Na_4P_2O_7$, 10-30%) and Sodium Carbonate (N_2CO_3, 1-10%) (Alconox Inc, 2017). We tested the ability of these compounds to clean pipettes by themselves in approximately the same concentrations as they are found in Alconox. The cleaning ability of the compounds was evaluated by measuring the attained gigaseal resistance as before (Figure 11 d). As a positive control, we tested fresh pipettes and as a negative control, pipettes that were rinsed in aCSF. In addition, we tested Sodium Dodecyl Sulfate (SDS), a compound similar to SDBS. We found that SDBS (and to a lesser extent, Na_2CO_3) recapitulated the cleaning

effectiveness of Alconox (Figure 44). The success of SDBS is unsurprising given that it is a detergent, which binds to and solubilizes cell membranes. However, Na_2CO_3 is a water softener with no inherent detergency; the chemical basis of Na_2CO_3 successfully cleaning pipettes is unclear. Nevertheless, both chemicals were not as effective by themselves as Alconox. This is likely due to the fact that the other chemicals such as $NaCO_3$ and $Na_4P_2O_7$, while not effective by themselves, act as water softeners to increase the detergency of SDBS. We therefore conclude that the detergent action of SDBS is the key component to the effectiveness of Alconox as a pipette cleaning solution; however, other components are required to optimize the performance of the detergent. This information can be used in the future to design improved cleaning solutions.

D.3 Improving cleaning

We will improve the effectiveness of the cleaning algorithm by further exploring chemical and physical methods of removing cellular debris from pipette tips. On the chemical side, we will first explore more aggressive cleaning compounds (e.g. sodium dichromate, Nochromix [Godax Inc]), while still ensuring a thorough washout of the chemical after cleaning. While even more aggressive cleaning agents are available such as Piranha solution (boiling sulfuric acid with hydrogen peroxide), they are too caustic and dangerous to be used in the experimental preparation. There is thus a tradeoff between cleaning effectiveness and safety that must be considered.

We will also serially apply previously-tested compounds to increase pipette longevity. The enzyme Phospholipase A2 (PLA2) hydrolyses glycerophospholipids in the cell membrane which are not explicitly targeted by Alconox. Similarly, Triton X-100 (0.2 mM) disrupts

hydrogen bonds in the lipid bilayer. Because they clean differently, serially applying these chemicals to the pipette after cleaning with Alconox may increase its longevity. On the physical side, we will explore perturbations such as high-velocity flow, sonication, and heating to mechanically destabilize cellular debris at the tip. Pipette longevity will be defined as the average number of cleaning cycles after which a significant change in recording quality parameters (gigaseal resistance, time to form gigaseal, and whole-cell access resistance) is observed. As before, we will periodically confirm this using Scanning Electron Microscopy (SEM) images of the pipette tip.

D.4 Application to planar patch-clamp

The cleaning technique has successfully been applied to patch-clamp pipettes (Figure 45 a). We therefore reasoned that the principle could be applied to planar patch-clamp arrays (Fertig et al., 2002). In planar patch-clamp recording, cells suspended in solution on a cartridge are released to flow over a planar array of glass micro-apertures that trap the cell and form the seal with the cell membrane (Figure 45 b,c). This allows the simultaneous recording 12-384 cells using commercially-available systems such as Ionworks HT (Molecular Devices) and QPatch (Sophion). A key drawback of planar patch chips is that the microfluidic aperture chips are single-use—cell debris irreversibly binds to the glass. Because of this, drug screening requires hundreds to thousands of chips, and due to the complexity of creating microfluidic chips, the consumable costs add up: one can expect to spend ~$200-$600 per day on single-use chips for a single planar patch clamp system (Comley, 2006; Milligan et al., 2009). In fact, in a 2003 survey, the high cost of planar patch clamp consumables was the leading restrictive factor limiting the use of automated

patch-clamp systems (Comley, 2006). A planar patch clamp system with an ability to reuse chips would have significant impact on the high throughput screening field.

We performed initial proof-of-principle tests to determine whether the cleaning technique can be used in this context in partnership with Dr. Carlos Vanoye and Dr. Alfred George (Northwestern University). Preliminary results show that after a 2-hr rinse in Alconox, 57 of 384 wells (15%) in the chip are usable for patch-clamp recording. These results can likely be improved by (1) ensuring that the micro-apertures remain wet so as to prevent adhesion of organic matter (2) pneumatically forcing fluid through the micro-apertures instead of passively washing them and (3) maintaining the chip in a dust-free environment for the duration of the cleaning procedure.

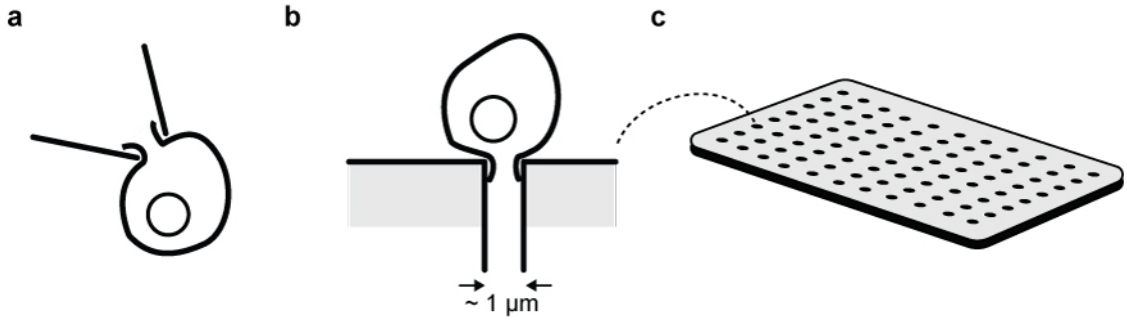

Figure 45: Schematics of conventional and planar patch-clamp techniques. a. Conventional (pipette-based) patch-clamp recording. b. Planar patch-clamp recording. Instead of using a pipette to break in to the cell, dissociated cells are pulled to a planar surface with many (tens to hundreds of) micro-apertures in individual wells, allowing the simultaneous high-throughput patch-clamp recordings.

REFERENCES

Aitken, P.G., Breese, G.R., Dudek, F.F., Edwards, F., Espanol, M.T., Larkman, P.M., Lipton, P., Newman, G.C., Nowak Jr., T.S., Panizzon, K.L., et al. (1995). Preparative methods for brain slices: a discussion. J. Neurosci. Methods *59*, 139–149.

Akemann, W., Mutoh, H., Perron, A., Rossier, J., and Knöpfel, T. (2010). Imaging brain electric signals with genetically targeted voltage-sensitive fluorescent proteins. Nat. Methods *7*, 643–649.

Akerboom, J., Chen, T.-W., Wardill, T.J., Tian, L., Marvin, J.S., Mutlu, S., Calderón, N.C., Esposti, F., Borghuis, B.G., Sun, X.R., et al. (2012). Optimization of a GCaMP Calcium Indicator for Neural Activity Imaging. J. Neurosci. *32*, 13819–13840.

Alconox Inc (2017). Alconox, Inc. - User Manual for Critical Cleaning Procedures.

Alivisatos, A.P., Chun, M., Church, G.M., Greenspan, R.J., Roukes, M.L., and Yuste, R. (2012). The Brain Activity Map Project and the Challenge of Functional Connectomics. Neuron *74*, 970–974.

Allen Institute for Brain Science (2015). Allen Cell Types Database.

Andrásfalvy, B.K., Galiñanes, G.L., Huber, D., Barbic, M., Macklin, J.J., Susumu, K., Delehanty, J.B., Huston, A.L., Makara, J.K., and Medintz, I.L. (2014). Quantum dot-based multiphoton fluorescent pipettes for targeted neuronal electrophysiology. Nat. Methods *11*, 1237–1241.

Annecchino, L.A., Morris, A.R., Copeland, C.S., Agabi, O.E., Chadderton, P., and Schultz, S.R. (2017). Robotic Automation of In Vivo Two-Photon Targeted Whole-Cell Patch-Clamp Electrophysiology. Neuron *95*, 1048–1055.e3.

Benedusi, M., Aquila, M., Milani, A., and Rispoli, G. (2011). A pressure-polishing set-up to fabricate patch pipettes that seal on virtually any membrane, yielding low access resistance and efficient intracellular perfusion. Eur. Biophys. J. *40*, 1215–1223.

Beneš, M., Billy, D., Benda, A., Speijer, H., Hof, M., and Hermens, W.T. (2004). Surface-Dependent Transitions during Self-Assembly of Phospholipid Membranes on Mica, Silica, and Glass. Langmuir *20*, 10129–10137.

Berger, M.L. (2016). Soaping the NMDA receptor: Various types of detergents influence differently [3H]MK-801 binding to rat brain membranes. Biochim. Biophys. Acta BBA - Biomembr. *1858*, 116–122.

Bi, G., and Poo, M. (1998). Synaptic Modifications in Cultured Hippocampal Neurons: Dependence on Spike Timing, Synaptic Strength, and Postsynaptic Cell Type. J. Neurosci. *18*, 10464–10472.

Boyden, E.S., Zhang, F., Bamberg, E., Nagel, G., and Deisseroth, K. (2005). Millisecond-timescale, genetically targeted optical control of neural activity. Nat. Neurosci. *8*, 1263–1268.

Cadwell, C.R., Palasantza, A., Jiang, X., Berens, P., Deng, Q., Yilmaz, M., Reimer, J., Shen, S., Bethge, M., Tolias, K.F., et al. (2016). Electrophysiological, transcriptomic and morphologic profiling of single neurons using Patch-seq. Nat. Biotechnol. *34*, 199–203.

Campagnola, L., Kratz, M.B., and Manis, P.B. (2014). ACQ4: an open-source software platform for data acquisition and analysis in neurophysiology research. Front. Neuroinformatics *8*.

Cang, J., and Isaacson, J.S. (2003). In Vivo Whole-Cell Recording of Odor-Evoked Synaptic Transmission in the Rat Olfactory Bulb. J. Neurosci. *23*, 4108–4116.

Chemla, S., and Chavane, F. (2010). Voltage-sensitive dye imaging: Technique review and models. J. Physiol.-Paris *104*, 40–50.

Chen, T.-W., Wardill, T.J., Sun, Y., Pulver, S.R., Renninger, S.L., Baohan, A., Schreiter, E.R., Kerr, R.A., Orger, M.B., Jayaraman, V., et al. (2013). Ultra-sensitive fluorescent proteins for imaging neuronal activity. Nature *499*, 295–300.

Comley, J. (2006). Automated Patch Clamping-Setting a New Standard for Early hERG. DDW DRUG Discov. WORLD *7*, 62.

Crick, F., and Koch, C. (1990). Towards a neurobiological theory of consciousness. Semin. Neurosci. *2*, 263–275.

Dana, H., Mohar, B., Sun, Y., Narayan, S., Gordus, A., Hasseman, J.P., Tsegaye, G., Holt, G.T., Hu, A., Walpita, D., et al. (2016). Sensitive red protein calcium indicators for imaging neural activity. eLife *5*, e12727.

Deisseroth, K. (2012). Optogenetics and Psychiatry: Applications, Challenges, and Opportunities. Biol. Psychiatry *71*, 1030–1032.

Dunlop, J., Bowlby, M., Peri, R., Vasilyev, D., and Arias, R. (2008). High-throughput electrophysiology: an emerging paradigm for ion-channel screening and physiology. Nat. Rev. Drug Discov. *7*, 358.

Ebner, T.J., and Chen, G. (1995). Use of voltage-sensitive dyes and optical recordings in the central nervous system. Prog. Neurobiol. *46*, 463–506.

Edelstein, A.D., Tsuchida, M.A., Amodaj, N., Pinkard, H., Vale, R.D., and Stuurman, N. (2014). Advanced methods of microscope control using μManager software. J. Biol. Methods *1*, 10.

Edwards, F.A., Konnerth, A., Sakmann, B., and Takahashi, T. (1989). A thin slice preparation for patch clamp recordings from neurones of the mammalian central nervous system. Pflüg. Arch. *414*, 600–612.

Edwards, F.A., Konnerth, A., and Sakmann, B. (1990). Quantal analysis of inhibitory synaptic transmission in the dentate gyrus of rat hippocampal slices: a patch-clamp study. J. Physiol. *430*, 213–249.

Etkin, A., Prater, K.E., Schatzberg, A.F., Menon, V., and Greicius, M.D. (2009). Disrupted Amygdalar Subregion Functional Connectivity and Evidence of a Compensatory Network in Generalized Anxiety Disorder. Arch. Gen. Psychiatry *66*, 1361–1372.

Fertig, N., Blick, R.H., and Behrends, J.C. (2002). Whole cell patch clamp recording performed on a planar glass chip. Biophys. J. *82*, 3056–3062.

Goodman, M.B., and Lockery, S.R. (2000). Pressure polishing: a method for re-shaping patch pipettes during fire polishing. J. Neurosci. Methods *100*, 13–15.

Gradinaru, V., Mogri, M., Thompson, K.R., Henderson, J.M., and Deisseroth, K. (2009). Optical Deconstruction of Parkinsonian Neural Circuitry. Science *324*, 354–359.

Grady, C.L., McIntosh, A.R., Beig, S., Keightley, M.L., Burian, H., and Black, S.E. (2003). Evidence from Functional Neuroimaging of a Compensatory Prefrontal Network in Alzheimer's Disease. J. Neurosci. *23*, 986–993.

Gray, C.M., Maldonado, P.E., Wilson, M., and McNaughton, B. (1995). Tetrodes markedly improve the reliability and yield of multiple single-unit isolation from multi-unit recordings in cat striate cortex. J. Neurosci. Methods *63*, 43–54.

Greicius, M.D., Srivastava, G., Reiss, A.L., and Menon, V. (2004). Default-mode network activity distinguishes Alzheimer's disease from healthy aging: Evidence from functional MRI. Proc. Natl. Acad. Sci. U. S. A. *101*, 4637–4642.

Hamill, O.P., Marty, A., Neher, E., Sakmann, B., and Sigworth, F.J. (1981). Improved patch-clamp techniques for high-resolution current recording from cells and cell-free membrane patches. Pflüg. Arch. *391*, 85–100.

Harris, K.D., Hirase, H., Leinekugel, X., Henze, D.A., and Buzsáki, G. (2001). Temporal Interaction between Single Spikes and Complex Spike Bursts in Hippocampal Pyramidal Cells. Neuron *32*, 141–149.

Harris, K.D., Henze, D.A., Hirase, H., Leinekugel, X., Dragoi, G., Czurkó, A., and Buzsáki, G. (2002). Spike train dynamics predicts theta-related phase precession in hippocampal pyramidal cells. Nature *417*, 738–741.

Hodgkin, A.L., and Huxley, A.F. (1952). A quantitative description of membrane current and its application to conduction and excitation in nerve. J. Physiol. *117*, 500–544.

Hopfield, J.J. (1982). Neural networks and physical systems with emergent collective computational abilities. Proc. Natl. Acad. Sci. *79*, 2554–2558.

Hoshi, T., Zagotta, W.N., and Aldrich, R.W. (1990). Biophysical and molecular mechanisms of Shaker potassium channel inactivation. Science *250*, 533–538.

Ishikawa, D., Takahashi, N., Sasaki, T., Usami, A., Matsuki, N., and Ikegaya, Y. (2010). Fluorescent pipettes for optically targeted patch-clamp recordings. Neural Netw. *23*, 669–672.

Jaffe, D., and Johnston, D. (1990). Induction of long-term potentiation at hippocampal mossy-fiber synapses follows a Hebbian rule. J. Neurophysiol. *64*, 948–960.

Jamur, M., and Oliver, C. (2010). Permeabilization of Cell Membranes. In Immunocytochemical Methods and Protocols, C. Oliver, and M.C. Jamur, eds. (Humana Press), pp. 63–66.

Jiang, X., Wang, G., Lee, A.J., Stornetta, R.L., and Zhu, J.J. (2013). The organization of two new cortical interneuronal circuits. Nat. Neurosci. *16*, 210–218.

Jiang, X., Shen, S., Cadwell, C.R., Berens, P., Sinz, F., Ecker, A.S., Patel, S., and Tolias, A.S. (2015). Principles of connectivity among morphologically defined cell types in adult neocortex. Science *350*, aac9462.

Jiang, X., Shen, S., Sinz, F., Reimer, J., Cadwell, C.R., Berens, P., Ecker, A.S., Patel, S., Denfield, G.H., Froudarakis, E., et al. (2016). Response to Comment on “Principles of connectivity among morphologically defined cell types in adult neocortex.” Science *353*, 1108–1108.

Jonas, E., and Kording, K.P. (2017). Could a Neuroscientist Understand a Microprocessor? PLOS Comput. Biol. *13*, e1005268.

Kandel, E.R. (2001). The Molecular Biology of Memory Storage: A Dialogue Between Genes and Synapses. Science *294*, 1030–1038.

Kao, L., Abuladze, N., Shao, X.M., McKeegan, K., and Kurtz, I. (2012). A new technique for multiple re-use of planar patch clamp chips. J. Neurosci. Methods *208*, 205–210.

Kempton MJ, Salvador Z, Munafò MR, and et al (2011). Structural neuroimaging studies in major depressive disorder: Meta-analysis and comparison with bipolar disorder. Arch. Gen. Psychiatry *68*, 675–690.

Kim, T.H., Zhang, Y., Lecoq, J., Jung, J.C., Li, J., Zeng, H., Niell, C.M., and Schnitzer, M.J. (2016). Long-Term Optical Access to an Estimated One Million Neurons in the Live Mouse Cortex. Cell Rep. *17*, 3385–3394.

Kinoshita, E., Kinoshita-Kikuta, E., and Koike, T. (2009). Separation and detection of large phosphoproteins using Phos-tag SDS-PAGE. Nat. Protoc. *4*, 1513–1521.

Kitamura, K., Judkewitz, B., Kano, M., Denk, W., and Häusser, M. (2008). Targeted patch-clamp recordings and single-cell electroporation of unlabeled neurons in vivo. Nat. Methods *5*, 61–67.

Kodandaramaiah, S.B., Franzesi, G.T., Chow, B.Y., Boyden, E.S., and Forest, C.R. (2012). Automated whole-cell patch-clamp electrophysiology of neurons in vivo. Nat. Methods *9*, 585–587.

Kodandaramaiah, S.B., Boyden, E.S., and Forest, C.R. (2013). In vivo robotics: the automation of neuroscience and other intact-system biological fields. Ann. N. Y. Acad. Sci. *1305*, 63–71.

Kodandaramaiah, S.B., Holst, G.L., Wickersham, I.R., Singer, A.C., Franzesi, G.T., McKinnon, M.L., Forest, C.R., and Boyden, E.S. (2016). Assembly and operation of the autopatcher for automated intracellular neural recording in vivo. Nat. Protoc. *11*, 634–654.

Kolb, I., Stoy, W.A., Rousseau, E.B., Moody, O.A., Jenkins, A., and Forest, C.R. (2016). Cleaning patch-clamp pipettes for immediate reuse. Sci. Rep. *6*, 35001.

Koley, D., and Bard, A.J. (2010). Triton X-100 concentration effects on membrane permeability of a single HeLa cell by scanning electrochemical microscopy (SECM). Proc. Natl. Acad. Sci. *107*, 16783–16787.

Larkum, M.E., and Zhu, J.J. (2002). Signaling of Layer 1 and Whisker-Evoked Ca2+ and Na+ Action Potentials in Distal and Terminal Dendrites of Rat Neocortical Pyramidal Neurons In Vitro and In Vivo. J. Neurosci. *22*, 6991–7005.

Lazebnik, Y. (2002). Can a biologist fix a radio?—Or, what I learned while studying apoptosis. Cancer Cell *2*, 179–182.

LeCun, Y., Bengio, Y., and Hinton, G. (2015). Deep learning. Nature *521*, 436–444.

Lee, A.J., Wang, G., Jiang, X., Johnson, S.M., Hoang, E.T., Lanté, F., Stornetta, R.L., Beenhakker, M.P., Shen, Y., and Zhu, J.J. (2014). Canonical Organization of Layer 1 Neuron-Led Cortical Inhibitory and Disinhibitory Interneuronal Circuits. Cereb. Cortex bhu020.

Lefort, S., Tomm, C., Floyd Sarria, J.-C., and Petersen, C.C.H. (2009). The Excitatory Neuronal Network of the C2 Barrel Column in Mouse Primary Somatosensory Cortex. Neuron *61*, 301–316.

Leist, M., Datunashvilli, M., Kanyshkova, T., Zobeiri, M., Aissaoui, A., Cerina, M., Romanelli, M.N., Pape, H.-C., and Budde, T. (2016). Two types of interneurons in the mouse lateral geniculate nucleus are characterized by different h-current density. Sci. Rep. *6*, srep24904.

Lenschow, C., and Brecht, M. (2015). Barrel Cortex Membrane Potential Dynamics in Social Touch. Neuron *85*, 718–725.

Levis, R.A., and Rae, J.L. (1993). The use of quartz patch pipettes for low noise single channel recording. Biophys. J. *65*, 1666–1677.

Ling, G., and Gerard, R.W. (1949). The normal membrane potential of frog sartorius fibers. J. Cell. Comp. Physiol. *34*, 383–396.

London, M., and Häusser, M. (2005). Dendritic Computation. Annu. Rev. Neurosci. *28*, 503–532.

Machu, T.K., Mihic, S.J., and Dildy-Mayfield, J.E. (1998). Selective Actions of a Detergent on Ligand-Gated Ion Channels Expressed in Xenopus Oocytes. J. Pharmacol. Exp. Ther. *284*, 32–36.

Malboubi, M., Gu, Y., and Jiang, K. (2010). Experimental and simulation study of the effect of pipette roughness on giga-seal formation in patch clamping. Microelectron. Eng. *87*, 778–781.

Margrie, T.W., Brecht, M., and Sakmann, B. (2002). In vivo, low-resistance, whole-cell recordings from neurons in the anaesthetized and awake mammalian brain. Pflüg. Arch. *444*, 491–498.

Markram, H. (2006). The Blue Brain Project. Nat. Rev. Neurosci. *7*, 153–160.

Markram, H., Lübke, J., Frotscher, M., Roth, A., and Sakmann, B. (1997). Physiology and anatomy of synaptic connections between thick tufted pyramidal neurones in the developing rat neocortex. J. Physiol. *500*, 409–440.

Markram, H., Muller, E., Ramaswamy, S., Reimann, M.W., Abdellah, M., Sanchez, C.A., Ailamaki, A., Alonso-Nanclares, L., Antille, N., Arsever, S., et al. (2015). Reconstruction and Simulation of Neocortical Microcircuitry. Cell *163*, 456–492.

McIntyre, C.C., and Hahn, P.J. (2010). Network perspectives on the mechanisms of deep brain stimulation. Neurobiol. Dis. *38*, 329–337.

Milligan, C.J., Li, J., Sukumar, P., Majeed, Y., Dallas, M.L., English, A., Emery, P., Porter, K.E., Smith, A.M., McFadzean, I., et al. (2009). Robotic multiwell planar patch-clamp for native and primary mammalian cells. Nat. Protoc. *4*, 244–255.

Milton, R.L., and Caldwell, J.H. (1990). How do patch clamp seals form? A lipid bleb model. Pflüg. Arch. *416*, 758–765.

Minshew, N.J., and Williams, D.L. (2007). The new neurobiology of autism: cortex, connectivity, and neuronal organization. Arch. Neurol. *64*, 945–950.

Mohamed, A. r, Dahl, G.E., and Hinton, G. (2012). Acoustic Modeling Using Deep Belief Networks. IEEE Trans. Audio Speech Lang. Process. *20*, 14–22.

Neher, E. (1992). Ion channels for communication between and within cells. Neuron *8*, 605–612.

Neher, E., and Sakmann, B. (1976). Single-channel currents recorded from membrane of denervated frog muscle fibres. Nature *260*, 799–802.

Ohki, K., Chung, S., Ch'ng, Y.H., Kara, P., and Reid, R.C. (2005). Functional imaging with cellular resolution reveals precise micro-architecture in visual cortex. Nature *433*, 597–603.

O'Keefe, J., and Nadel, L. (1978). The Hippocampus as a Cognitive Map (Oxford: Clarendon Press).

O'Toole, K.K., and Jenkins, A. (2012). The Apparent Voltage Dependence of GABAA Receptor Activation and Modulation Is Inversely Related to Channel Open Probability. Mol. Pharmacol. *81*, 189–197.

Oz, M., Spivak, C.E., and Lupica, C.R. (2004). The solubilizing detergents, Tween 80 and Triton X-100 non-competitively inhibit α7-nicotinic acetylcholine receptor function in Xenopus oocytes. J. Neurosci. Methods *137*, 167–173.

Pak, N., Dergance, M.J., Emerick, M.T., Gagnon, E.B., and Forest, C.R. (2011). An Instrument for Controlled, Automated Production of Micrometer Scale Fused Silica Pipettes. J. Mech. Des. *133*, 061006–061006.

Pape, H.C. (1996). Queer current and pacemaker: the hyperpolarization-activated cation current in neurons. Annu. Rev. Physiol. *58*, 299–327.

Pape, H.-C., and McCormick, D.A. (1989). Noradrenaline and serotonin selectively modulate thalamic burst firing by enhancing a hyperpolarization-activated cation current. Nature *340*, 715–718.

Parsons, C.G., Panchenko, V.A., Pinchenko, V.O., Tsyndrenko, A.Y., and Krishtal, O.A. (1996). Comparative Patch-clamp Studies with Freshly Dissociated Rat Hippocampal and Striatal Neurons on the NMDA Receptor Antagonistic Effects of Amantadine and Memantine. Eur. J. Neurosci. *8*, 446–454.

Perin, R., and Markram, H. (2013). A Computer-assisted Multi-electrode Patch-clamp System. J. Vis. Exp.

Perin, R., Berger, T.K., and Markram, H. (2011). A synaptic organizing principle for cortical neuronal groups. Proc. Natl. Acad. Sci. *108*, 5419–5424.

Petreanu, L., Huber, D., Sobczyk, A., and Svoboda, K. (2007). Channelrhodopsin-2–assisted circuit mapping of long-range callosal projections. Nat. Neurosci. *10*, 663–668.

Pfeffer, C.K., Xue, M., He, M., Huang, Z.J., and Scanziani, M. (2013). Inhibition of inhibition in visual cortex: the logic of connections between molecularly distinct interneurons. Nat. Neurosci. *16*, 1068–1076.

Pologruto, T.A., Sabatini, B.L., and Svoboda, K. (2003). ScanImage: Flexible software for operating laser scanning microscopes. Biomed. Eng. OnLine *2*, 13.

Rinaldi, T., Perrodin, C., and Markram, H. (2008). Hyper-Connectivity and Hyper-Plasticity in the Medial Prefrontal Cortex in the Valproic Acid Animal Model of Autism. Front. Neural Circuits *2*.

Rye, D.B., Bliwise, D.L., Parker, K., Trotti, L.M., Saini, P., Fairley, J., Freeman, A., Garcia, P.S., Owens, M.J., Ritchie, J.C., et al. (2012). Modulation of Vigilance in the Primary Hypersomnias by Endogenous Enhancement of GABAA Receptors. Sci. Transl. Med. *4*, 161ra151-161ra151.

Sánchez, D., Johnson, N., Li, C., Novak, P., Rheinlaender, J., Zhang, Y., Anand, U., Anand, P., Gorelik, J., Frolenkov, G.I., et al. (2008). Noncontact Measurement of the

Local Mechanical Properties of Living Cells Using Pressure Applied via a Pipette. Biophys. J. *95*, 3017–3027.

Scholvin, J., Kinney, J.P., Bernstein, J.G., Moore-Kochlacs, C., Kopell, N., Fonstad, C.G., and Boyden, E.S. (2016). Close-Packed Silicon Microelectrodes for Scalable Spatially Oversampled Neural Recording. IEEE Trans. Biomed. Eng. *63*, 120–130.

Shen, H. (2016). Robots record brain activity inside neurons. Nature *532*, 135–136.

Shepherd, G.M. (2015). Foundations of the Neuron Doctrine: 25th Anniversary Edition (Oxford University Press).

Shin, L.M., Rauch, S.L., and Pitman, R.K. (2006). Amygdala, Medial Prefrontal Cortex, and Hippocampal Function in PTSD. Ann. N. Y. Acad. Sci. *1071*, 67–79.

Silva, G.T., Le Bé, J.-V., Riachi, I., Rinaldi, T., Markram, K., Markram, H., Silva, G.T., Bé, J.-V.L., Riachi, I., Rinaldi, T., et al. (2009). Enhanced long-term microcircuit plasticity in the valproic acid animal model of autism. Front. Synaptic Neurosci. *1*, 1.

Smetters, D., Majewska, A., and Yuste, R. (1999). Detecting Action Potentials in Neuronal Populations with Calcium Imaging. Methods *18*, 215–221.

Sohal, V.S. (2012). Insights into Cortical Oscillations Arising from Optogenetic Studies. Biol. Psychiatry *71*, 1039–1045.

Song, S., Sjöström, P.J., Reigl, M., Nelson, S., and Chklovskii, D.B. (2005). Highly Nonrandom Features of Synaptic Connectivity in Local Cortical Circuits. PLoS Biol *3*, e68.

Stepanyants, A., Martinez, L.M., Ferecskó, A.S., and Kisvárday, Z.F. (2009). The fractions of short- and long-range connections in the visual cortex. Proc. Natl. Acad. Sci. *106*, 3555–3560.

Stuart, G.J., Dodt, H.U., and Sakmann, B. (1993). Patch-clamp recordings from the soma and dendrites of neurons in brain slices using infrared video microscopy. Pflüg. Arch. *423*, 511–518.

Suchyna, T.M., Markin, V.S., and Sachs, F. (2009). Biophysics and Structure of the Patch and the Gigaseal. Biophys. J. *97*, 738–747.

Suk, H.-J., van Welie, I., Kodandaramaiah, S.B., Allen, B., Forest, C.R., and Boyden, E.S. (2017). Closed-Loop Real-Time Imaging Enables Fully Automated Cell-Targeted Patch-Clamp Neural Recording In Vivo. Neuron *95*, 1037–1047.e11.

Suter, B.A., O'Connor, T., Iyer, V., Petreanu, L., Hooks, B.M., Kiritani, T., Svoboda, K., and Shepherd, G.M.G. (2010). Ephus: multipurpose data acquisition software for neuroscience experiments. Front. Neural Circuits *4*, 100.

Tasic, B., Menon, V., Nguyen, T.N., Kim, T.K., Jarsky, T., Yao, Z., Levi, B., Gray, L.T., Sorensen, S.A., Dolbeare, T., et al. (2016). Adult mouse cortical cell taxonomy revealed by single cell transcriptomics. Nat. Neurosci. *19*, 335–346.

Taverna, S., Ilijic, E., and Surmeier, D.J. (2008). Recurrent Collateral Connections of Striatal Medium Spiny Neurons Are Disrupted in Models of Parkinson's Disease. J. Neurosci. *28*, 5504–5512.

Thomson, A.M., Deuchars, J., and West, D.C. (1993). Large, deep layer pyramid-pyramid single axon EPSPs in slices of rat motor cortex display paired pulse and frequency-dependent depression, mediated presynaptically and self-facilitation, mediated postsynaptically. J. Neurophysiol. *70*, 2354–2369.

Tian, L., Hires, S.A., Mao, T., Huber, D., Chiappe, M.E., Chalasani, S.H., Petreanu, L., Akerboom, J., McKinney, S.A., Schreiter, E.R., et al. (2009). Imaging neural activity in worms, flies and mice with improved GCaMP calcium indicators. Nat. Methods *6*, 875–881.

Ting, J., Daigle, T., Chen, Q., and Feng, G. (2014). Acute Brain Slice Methods for Adult and Aging Animals: Application of Targeted Patch Clamp Analysis and Optogenetics. In Patch-Clamp Methods and Protocols, M. Martina, and S. Taverna, eds. (Springer New York), pp. 221–242.

Tononi, G. (2004). An information integration theory of consciousness. BMC Neurosci. *5*, 42.

Vogelstein, J.T., Packer, A.M., Machado, T.A., Sippy, T., Babadi, B., Yuste, R., and Paninski, L. (2010). Fast Nonnegative Deconvolution for Spike Train Inference From Population Calcium Imaging. J. Neurophysiol. *104*, 3691–3704.

Wang, G., Wyskiel, D.R., Yang, W., Wang, Y., Milbern, L.C., Lalanne, T., Jiang, X., Shen, Y., Sun, Q.-Q., and Zhu, J.J. (2015). An optogenetics- and imaging-assisted simultaneous multiple patch-clamp recording system for decoding complex neural circuits. Nat. Protoc. *10*, 397–412.

Wardill, T.J., Chen, T.-W., Schreiter, E.R., Hasseman, J.P., Tsegaye, G., Fosque, B.F., Behnam, R., Shields, B.C., Ramirez, M., Kimmel, B.E., et al. (2013). A Neuron-Based Screening Platform for Optimizing Genetically-Encoded Calcium Indicators. PLOS ONE *8*, e77728.

Wehr, M., and Zador, A.M. (2003). Balanced inhibition underlies tuning and sharpens spike timing in auditory cortex. Nature *426*, 442–446.

Wood, C., Williams, C., and Waldron, G.J. (2004). Patch clamping by numbers. Drug Discov. Today *9*, 434–441.

Wu, Q., and Chubykin, A.A. (2017). Application of Automated Image-guided Patch Clamp for the Study of Neurons in Brain Slices. JoVE J. Vis. Exp. e56010–e56010.

Wu, Q., Kolb, I., Callahan, B.M., Su, Z., Stoy, W., Neve, R., Kodandaramaiah, S.B., Zeng, H., Boyden, E.S., Forest, C.R., et al. (2016). Integration of autopatching with automated pipette and cell detection in vitro. J. Neurophysiol. *116*, 1564–1578.

Yang, L., and Sonner, J.M. (2008). Anesthetic-Like Modulation of Receptor Function by Surfactants: A Test of the Interfacial Theory of Anesthesia. Anesth. Analg. *107*, 868–874.

Yuste, R., and Denk, W. (1995). Dendritic spines as basic functional units of neuronal integration. Nat. Lond. *375*, 682–684.

Zeng, H., and Sanes, J.R. (2017). Neuronal cell-type classification: challenges, opportunities and the path forward. Nat. Rev. Neurosci. *advance online publication*.